

Complex Polymer Architectures Prepared using Metal Nanoparticles as Templates

DISSERTATION

zur Erlangung des akademischen Grades eines
Doktors der Naturwissenschaften
(Dr. rer. nat.)

an der
Bayreuth Graduiertenschule für Mathematik
und Naturwissenschaften der Universität Bayreuth

vorgelegt von

Ziyin Fan

geboren in Wuxi (V. R. China)

Bayreuth, 2016

Die vorliegende Arbeit wurde im Zeitraum vom Oktober 2012 bis Dezember 2015 an der Universität Bayreuth in Bayreuth am Lehrstuhl Makromolekulare Chemie II unter der Betreuung von Herrn Professor Dr. Andreas Greiner angefertigt.

Dissertation eingereicht am: 22.04.2016

Zulassung durch das Leitungsgremium: 09.05.2016

Wissenschaftliches Kolloquium: 01.12.2016

Amtierender Dekan: Prof. Dr. Stephan Kümmel

Prüfungsausschuss:

Prof. Dr. Andreas Greiner (Erstgutachter)

Prof. Dr. Hans-Werner Schmidt (Zweitgutachter)

Prof. Dr. Ulrich Schubert (Drittgutachter)

Prof. Dr. Stephan Förster (Vorsitz)

Prof. Dr. Birgit Weber

Content

Summary	1
Zusammenfassung	3
List of Publications	6
1. Introduction	7
1.1 Gold Nanoparticles.....	7
1.1.1 Spherical Gold Nanoparticles.....	9
1.1.2 Gold Nanorods	12
1.2 Polymers for Surface Functionalization of Gold Nanoparticles .	15
1.3 Controlled Functionalization of Gold Nanoparticles	21
1.4 Discrete Assembly of Gold Nanocrystals via Functionalized Polymer	25
1.5 Thesis Objectives.....	28
2. Overview of the Thesis	38
2.1 Polymer/Nanoparticle Hybrid Material for Precise Dimensions by Size Exclusive Fishing of Metal Nanoparticles	39
2.2 Polymer Cage as Universal Tools for the Precise Bottom-up Synthesis of Metal Nanoparticles	43
2.3 Assembly of Gold Nanoparticles on Gold Nanorods using Functionalized Poly(N-isopropylacrylamide) as Polymeric “Glue”	45
3. Polymer/Nanoparticle Hybrid Material for Precise Dimensions by Size Exclusive Fishing of Metal Nanoparticles	50
4. Polymer Cage as Universal Tools for the Precise Bottom-up Synthesis of Metal Nanoparticles	81
5. Assembly of Gold Nanoparticles on Gold Nanorods using Functionalized Poly(N-isopropylacrylamide) as Polymeric “Glue”	107

6. List of Abbreviations and Symbols	128
7. Acknowledgements.....	131
8. Eidesstattliche Erklärung	133

Summary

The aim of this thesis was to develop complex polymer architectures using metal nanoparticles as templates for applications in controlling the formation and precise surface modification of metal nanoparticles. The underlying concept was to prepare a cross-linked polymer shell around the metal nanoparticles, which revealed unusual architectures after etching the nanoparticle template. Novel synthetic strategy was carried out for the cross-linking of the building blocks for the polymer shell, which were firstly immobilized on the surface of nanoparticles.

Accordingly, a globular cross-linked multi-dentate polymer otherwise known as the polymer cage was developed involving spherical gold nanoparticles (AuNPs) as template. The synthetic approach of the polymer cage was based on the “grafting-around” method for the preparation of stoichiometric functionalized metal nanoparticles. This method described the surface polymerization of vinyl-carrying ligands immobilized on the AuNP surface, which was initiated by an external functionalized initiator. The polymerization generated a cross-linked polymeric monolayer shell coating around the AuNPs and tethered with single functionality introduced by the initiator. The free-standing polymer shell, namely the polymer cage, was isolated after the gold core was etched. The polymer cage exhibited a globular shape and contained numerous thiol groups on its cross-linked backbone. Its defined structure and size were characterized by transmission electron microscopy (TEM) and its cross-linking was verified by Raman spectroscopy as well as the stability test of the cage stabilized AuNPs against the dodecanethiol.

The unique architecture granted the polymer cage the ability to precisely have control over the property of metal nanoparticles. One application was to use the polymer cage as “fishing nets” for the size-selective separation of pre-synthesized metal nanoparticles (Chapter 3). The polymer cage could selectively extract AuNPs smaller than 15 nm in diameter with high efficiency, while other non-cross-linked linear polymer systems, such as thiol-end-functionalized linear polymer and block polymer, were not able to sort AuNPs with a diameter less than 40 nm.

Besides, the polymer cage was applied as the universal template for the precise bottom-up approach for nanoparticle synthesis (Chapter 4), which denoted the preparation of mono-

Summary

functionalized nanoparticles with defined size via the in-situ reduction route. So far, metal nanoparticles, such as gold-, silver-, palladium-, and platinum nanoparticles, have been successfully prepared in the polymer cage. The polymer cage was proven to exhibit a certain capacity through a series refilling experiments of AuNPs in the polymer cage, whereas the amounts of cage versus gold in the feed varied during the bottom-up synthesis. The as-prepared AuNPs showed sudden agglomeration, as the amount of the gold exceeded the capacity of the polymer cage. In contrast, the linear diblock copolymer showed a continuous increase of the nanoparticle size with the amount of gold versus polymer. The difference in the size evolution of AuNPs in these two polymer systems confirmed the limited mobility of the polymer cage due to the cross-linking, which in turn verified the cross-linking resulted from the “grafting-around” method.

The aim of the future work is to build a cross-linked cylindrical polymer brush. For this purpose, gold nanorods (AuNRs) were selected as the template. The first step in this direction was to tether AuNRs with linear telechelic polymer through one coordinating end, while the other functional end should be used for the cross-linking. Hence, a thermoresponsive polymer α -amino- ω -mercapto-poly(*N*-isopropylacrylamide) (PNiPAM) was designed as building blocks for a smart polymer brush. The thiol-ends of PNiPAM were grafted on the AuNRs surface, while the amine-ends could be interconnected through acid-amine-coupling reaction. The distribution of PNiPAM around AuNRs were visualized with the help of AuNPs. In detail, citrate stabilized AuNPs underwent ligand exchange with the nitrogen compounds of the PNiPAM shell around AuNRs. This led to the formation of a satellite-like assembly of AuNPs around AuNRs. The AuNPs distributed around the AuNRs homogeneously confirmed that, PNiPAM covered the whole AuNR including its side and both ends. Additionally, the resulting satellite-like assembly displayed tunable optical property depending on the temperature change.

In conclusion, novel polymer architecture has been developed through the cross-linking of the building blocks on nanoparticle surface. The globular polymer cage prepared by the AuNP-guided synthesis was used for the precise control of the size and functionality of metal nanoparticles. The focus of the future work is the cylindrical polymer brush which could be achieved by involving the AuNR as template and the linear telechelic polymer as building block. So far, it has already been proven that the linear telechelic polymer distributed homogeneously around AuNRs.

Zusammenfassung

Ziel dieser Arbeit war die Entwicklung komplexer Polymer-Architekturen mittels Metallnanopartikeln als Template, für Anwendungen in denen eine Bildungskontrolle und präzise Oberflächenmodifikation von Metallnanopartikeln benötigt werden. Das zugrundeliegende Konzept basierte auf der Herstellung einer vernetzten Polymerschale um die Metallnanopartikeln, welche besondere Architekturen nach dem Ätzen der Nanopartikeltemplate zeigte. Eine neuartige synthetische Strategie wurde für die Vernetzung der Bausteine der Polymerschale entwickelt, welche zuerst auf der Oberfläche der Nanopartikeln immobilisiert wurden.

Dementsprechend wurde ein kugelförmiges, vernetztes mehrzähniges Polymer – genannt Polymerkäfig – entwickelt, wobei sphärische Goldnanopartikel (AuNP) als Template eingesetzt wurden. Die synthetische Vorgehensweise für die Polymerkäfige basierte auf einer „grafting-around“ Methode, wodurch stöchiometrisch funktionalisierte Metallnanopartikeln hergestellt wurden. Die Methode umfasst eine Oberflächenpolymerisation von Vinyltragenden Liganden auf AuNP-Oberflächen, welche durch einen spezifisch funktionalisierten Initiator gestartet wurde. Die Polymerisation generierte eine vernetzte Monolage aus Polymer, welche die AuNP einhüllte und lediglich über die Funktionalität des Initiators mit dem Nanopartikel verbunden war. Die freistehende Polymerschale (oder Polymerkäfig) wurde isoliert indem der AuNP Kern durch Ätzen entfernt wurde. Der Polymerkäfig wies eine kugelförmige Form auf und besaß mehrere Thiolgruppen im Polymerrückgrat. Diese definierten Strukturen und Größen wurden durch Transmissionselektronenmikroskopie (TEM) charakterisiert. Die Vernetzung der Polymerkäfige sowie die Fixierung der Polymerkäfigstabilisierten AuNP wurden durch Raman-Spektroskopie in Gegenwart von Dodecanthiol nachgewiesen.

Die einzigartige Architektur verlieh dem Polymerkäfig die Fähigkeit, die Größe und Funktionalität der Metallnanopartikeln präzise zu kontrollieren. Eine Anwendung war, die Polymerkäfige als „Fischernetz“ für eine größenselektive Trennung der zuvor synthetisierten Metallnanopartikeln (Kapitel 3) zu verwenden. Dabei konnten die Polymerkäfige selektiv AuNP kleiner 15 nm im Durchmesser mit hoher Effizienz extrahieren, wogegen andere unvernetzte, lineare Polymersysteme, zum Beispiel ein lineares, thiolendfunktionalisiertes

Polymer und ein lineares Blockcopolymer, nicht fähig waren AuNP mit Durchmessern unter 40 nm zu sortieren.

Außerdem wurden Polymerkäfige als universelles Templat für eine präzise bottom-up Nanopartikelsynthese eingesetzt (Kapitel 4). Dabei zeichnete sich die Synthese der monofunktionalisierten Nanopartikeln durch eine definierte Größe aus und erfolgte über eine in-situ Reduktionsroute. In dieser Arbeit wurden Gold-, Silber-, Palladium- und Platinnanopartikel erfolgreich in Polymerkäfigen verarbeitet. Die Polymerkäfige besaßen eine definierte Aufnahmekapazität, was durch eine Serie von Wiederbefüllungsexperimenten mittels AuNP nachgewiesen werden konnte. Dabei wurde in der bottom-up Synthese die Käfigkonzentration im Vergleich zu Gold variiert. Sobald die Goldmenge die Kapazität der Käfige überschritt, agglomerierten die überschüssigen AuNP sofort. Im Gegensatz dazu zeigte ein lineares Diblockcopolymer eine kontinuierliche Zunahme der Nanopartikelgrößen mit dem Verhältnis Gold zu Polymer. Die unterschiedlichen Größenentwicklungen der AuNP in den zwei genannten Polymersystemen bestätigte die limitierte Aufnahmefähigkeit des Polymerkäfigs durch die Vernetzung, was wiederum die Vernetzung, resultierend aus einer „grafting-around“ Methode, bewies.

Das Ziel einer zukünftigen Arbeit ist das Aufbauen von vernetzten zylindrischen Polymerbürste. Hierfür wurden Goldnanostäbchen (AuNR) als Templat ausgewählt. Der erste Schritt war, AuNR, ausgestattet mit einem linearen, telechelem Polymer durch ein koordinierendes Ende zu verbinden, während eine andere funktionelle Endgruppe für die Vernetzung eingesetzt werden sollte. Hierzu wurde das thermoresponsive Polymer α -Amino- ω -mercapto-poly(*N*-isopropylacrylamid) (PNiPAM) als Bausteine für eine responsive Polymerbürste eingesetzt. Die ω -ständigen Thiolenden von PNiPAM wurden auf den AuNR Oberflächen aufgepfropft, während die α -ständigen Aminenden durch eine Säure-Amin-Kupplungsreaktion miteinander verbunden werden konnten. Die Verteilung von PNiPAM um die AuNR wurde mithilfe von AuNP sichtbar gemacht. Im Detail vollziehen die citratstabilisierten AuNP einen Ligandenaustausch mit den Stickstoffverbindungen der PNiPAM-Schalen, welche um die AuNR angeordnet sind. Dies führte zu der Bildung eines Satelliten-ähnlichen Assemblies von AuNP um die AuNR. Die homogene Verteilung der AuNP um die AuNR bestätigte, dass PNiPAM die AuNR vollständig umschloß und beide Enden bedeckte. Zusätzlich zeigte das resultierende

Satelliten-ähnliche Assemblies einstellbare optische Eigenschaften, welche temperaturabhängig waren.

Zusammenfassend wurden neue Polymerarchitekturen durch eine Vernetzung von Polymerbausteinen auf einer Nanopartikeloberfläche entwickelt. Kugelförmige Polymerkäfige, welche durch eine AuNP-gesteuerte Synthese hergestellt wurden, wurden für eine präzise Steuerung der Größe und Funktionalität der Metallnanopartikel eingesetzt. Der Fokus von zukünftigen Arbeit bezieht sich auf zylindrische Polymerbürsten. Diese konnten realisiert werden, indem AuNR als Template und ein lineares, telecheles Polymer als Baustein eingesetzt wurden. Es wurde bereits nachgewiesen, dass das lineare, telechele Polymer homogen um die AuNR verteilt ist.

List of Publications

Chapter 3

- [1] Z. Fan, M. Köhn Serrano, A. Schaper, S. Agarwal, A. Greiner, *Adv. Mat.* **2015**, 27, 3888-3893.

Chapter 4

- [2] Z. Fan, X. Chen, M. Köhn Serrano, H. Schmalz, S. Rosenfeldt, S. Förster, S. Agarwal, A. Greiner, *Angew. Chem* **2015**, 127, 14747; *Angew. Chem. Int. Ed.* **2015**, 54, 14539.

Chapter 5

- [3] Z. Fan, M. Tebbe, A. Fery, S. Agarwal, A. Greiner, *Particle & Particle Systems Characterization*, **2016**, accepted.

1. Introduction

The goal of this thesis is to prepare special polymer architecture using metal nanoparticles as templates, which requires the understanding of the interaction between the metal nanoparticles and the polymers immobilized on their surfaces. This chapter will address two aspects: the metal nanoparticles and the functionalized polymers. The metal nanoparticles will focus on the gold nanoparticles including spherical nanoparticles and nanorods, which were used in this thesis as the templates. The following section will discuss the types and syntheses of the functionalized polymers, as well as their interactions with gold nanoparticles. The controlling of the functionalities on the surface of metal nanoparticles is essential to building the complex polymer architectures. Therefore, different techniques of controlled surface functionalization of metal nanomaterial will be highlighted in this chapter. Furthermore, the application of the functionalized polymer in assembling nanomaterials will be reviewed. Within this context, the *Thesis Objective* clarifies the aim of developing nanoparticle-assisted new polymer architectures.

1.1 Gold Nanoparticles

The concept of nanoscience and nanotechnology was first introduced by R. P. Feynman in 1959^[1] and since then it has attracted tremendous attention of academic researchers. Recently, nanotechnology is rapidly-developing; it has been widely applied in the chemical and pharmaceutical industries and its presence has already penetrated our daily lives. Nanoparticles are defined as particles with dimensions ranging between 1 nm and 100 nm.^[2] The colloidal gold nanoparticle (AuNP) is one of the most intensively studied metal nanoparticles. Regarding its size and shape, AuNPs exhibit unique optical and electrical features, as well as high catalytic properties that result from their high surface area to volume ratio.^[3–5] Furthermore, the surface of AuNPs is capable to being modified with ligands containing sulfur, nitrogen, and phosphorous compounds that possess high affinity to the gold surface.^[6–9] **(Figure 1.1)** AuNPs when tailored with biomolecules reveal a promising future in biomedicine, for example bioimaging, biosensors, photothermal therapy, and gene transfection.^[10–14] The outstanding electric properties of AuNPs, especially gold array/assemblies, can make them to be fabricated as nanoelectronics,^[15,16] as substrates for

1. Introduction

surface-enhanced Raman spectroscopy (SERS),^[17,18] and can be used to enhance the efficiency of photovoltaic cells.^[19] Moreover, AuNPs can be used as homogeneous^[20] and heterogeneous^[21,22] catalysts for various organic reactions, such as hydrogenation, oxidation, and nucleophilic addition.^[23–25]

Controlling the growth mechanism, AuNPs with various shapes can be achieved: spherical nanoparticles, nanorods, nanowires and cube-like, and star-like nanoparticles.^[26] Subsequently, spherical AuNPs and gold nanorods (AuNRs) will be referred to as representative metal nanoparticles to demonstrate the usability as the template for building novel polymer architectures.

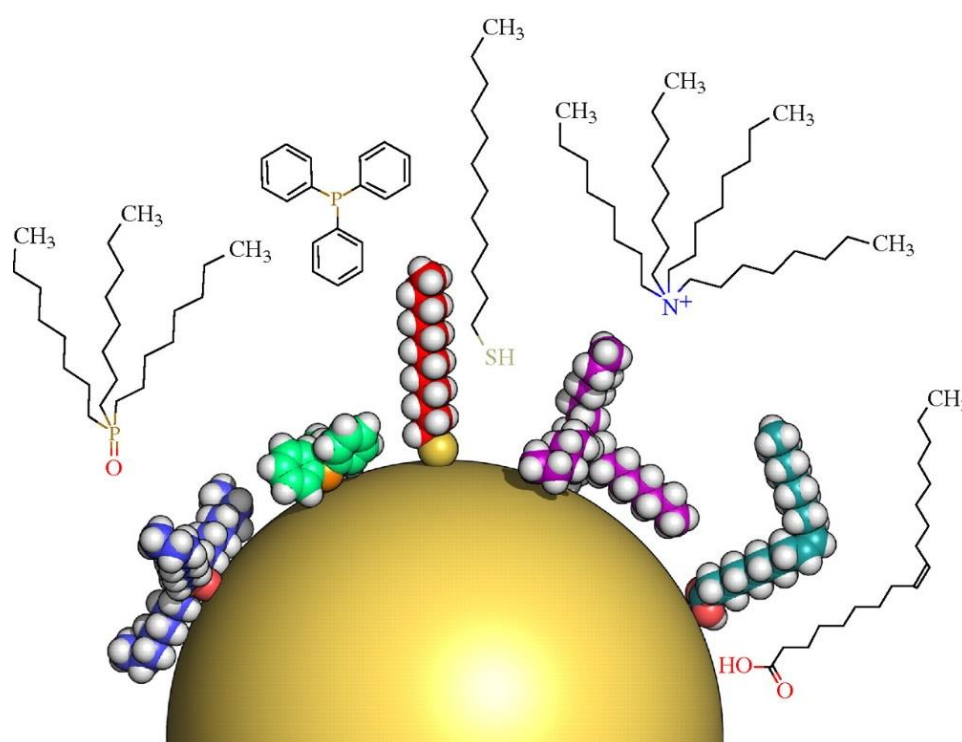


Figure 1.1. Schematic illustration of the spatial conformation of the hydrophobic ligands on a nanoparticle 5 nm in diameter depending on their chemical structures and space-filling models (drawn to scale, expect the chemical structures above). From left to right: trioctylphosphine oxide (TOPO), triphenylphosphine (TPP), dodecanethiol (DDT), tetraoctylammonium bromide (TOAB) and oleic acid (OA). © 2010, The Royal Society.^[27]

1. Introduction

1.1.1 Spherical Gold Nanoparticles

The history of AuNPs can date back to the 4th century when they were used to create the famous color-changing glass Lycurgus Cup.^[28] Generally, AuNPs can be prepared conveniently by reducing the Au^{III} derivatives as precursors with the presence of ligands in one phase.^[29,30] The most common gold precursors are chloroauric acid^[31,32] and gold phosphine complex.^[33,34] There are other precursors, such as Au(I)-glutathione polymer,^[35] and Au^I halides^[36]. The preferred options for the reducing agent are sodium borohydride (NaBH₄),^[37] superhydride,^[38,39] 9-borabicyclo[3.3.1]nonane (9-BBN),^[33,40] and hydrazine^[41] depending on the choice of the reaction medium and individual reducing rate. The stabilizing ligands play an essential role in improving the stability of the colloidal AuNPs. Through their electrostatic^[37,42] and/or steric protection,^[43,44] ligands are able to lower the surface energy of the colloidal particles. For example, citrate ions are well-known in the Turkevich method as ligands that provide the electrostatic stabilization and act as reducing agent during the preparation of colloidal AuNPs.^[45] Furthermore, they affect the solution's pH, by which the growth kinetics and eventually the size and size distribution of the AuNPs are modulated.^[46] Conventional polymeric ligands, such as polyvinylpyridine,^{[47][48]} polyvinylalcohol,^[49] polyvinylpyrrolidone,^[50] can offer nanoparticles sufficient steric hindrance to prevent agglomeration.

Despite the one-phase synthesis, colloidal AuNPs can be prepared in a biphasic system, which is known as the Brust-Schiffrin method.^[51,52] This method broadens the scope of the applicable ligands in the organic phase by using a phase transfer catalyst that transfers either the chloroauric acid or the ligand into the same phase. A typical Brust-Schiffrin synthesis involves tetraoctylammonium bromide (TOAB) (a quaternary ammonium salt) as the phase transfer catalyst and alkanethiol as the ligand. In a water/toluene biphasic system, Au^{III} is reduced to Au^I by alkanethiol (R'SH) after being transferred to the organic phase by TOAB and then forms tetraalkylammonium complex.^[53] Meanwhile, alkanethiol is oxidized to disulfide (R'SSR'). Different species of Au^I complexes are formed depending on the molar ratio of gold-to-ligand. The detailed reaction mechanism is shown in **Figure 1.2**.

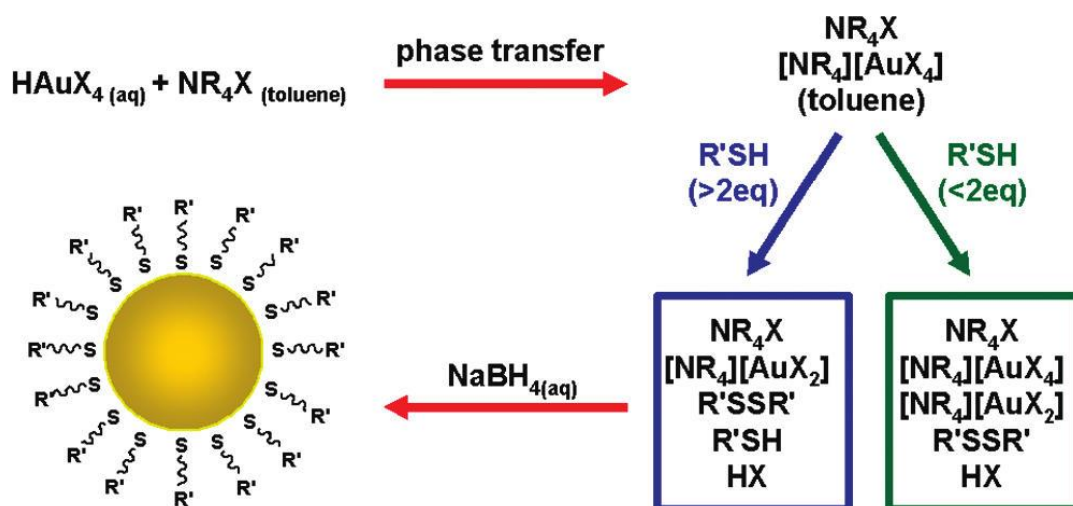


Figure 1.2. Schematic illustration of the biphasic Brust-Schiffrin synthesis of colloidal AuNPs. (HAuX₄: gold halide, NR₄X: tetraalkylammonium halide, R'SH: alkanethiol.)^[53] Reprinted with permission from Ref [53]. © 2010 American Chemical Society.

The thiol-ligands form a self-assembled monolayer (SAM) around the AuNP surface. The understanding of the thiolate-gold interaction plays a vital role in the controlled functionalization of gold nanomaterials.^[54] The bond between gold and thiolate exhibits a predominant covalent nature, which is mostly generated through the interaction of the gold with thiols and disulfides. For the formation of thiolate-gold bonds, the thiols are firstly deprotonated into a thiol radical and subsequently form a SAM on the AuNPs surface. Disulfides undergo the dissociation mechanism forming directly strong thiolate bond to gold surface.^[55]

Colloidal AuNPs are colorful as they can absorb and scatter light.^[56] Excited by an incident electromagnetic radiation with a specific wavelength, the conductive electrons of the nanoparticles oscillate collectively around the positively charged metal core at a certain frequency, which is defined as the surface plasmon resonance (SPR).^[57] (**Figure 1.3**)

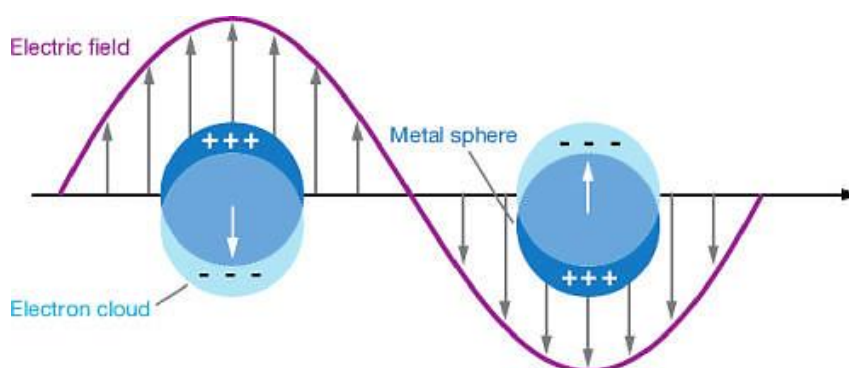


Figure 1.3. Schematic illustration of the principle of surface plasmon resonance.^[58] Reprinted with permission from Ref [58]. © 2007, Annual Reviews.

1. Introduction

For example, the absorption band of spherical AuNPs with a mean diameter of 15 nm is located in the range of visible light around 520 nm^[59] which results in a wine-red color of the AuNP dispersion. The optical properties of colloidal AuNPs can be tuned by their size, shape and local refractive index affected by the surrounding medium, type of ligands, and temperature. Typically, the absorption maximum of AuNPs is red-shifted with their size growth.^[60,61] (Figure 1.4) The scattering effect becomes more dominant when the diameter of the nanoparticles reaches 40 nm. AuNPs are developed as substrates for SERS based on their plasmonic properties and they can enhance the Raman scattering on the surface.^[17]

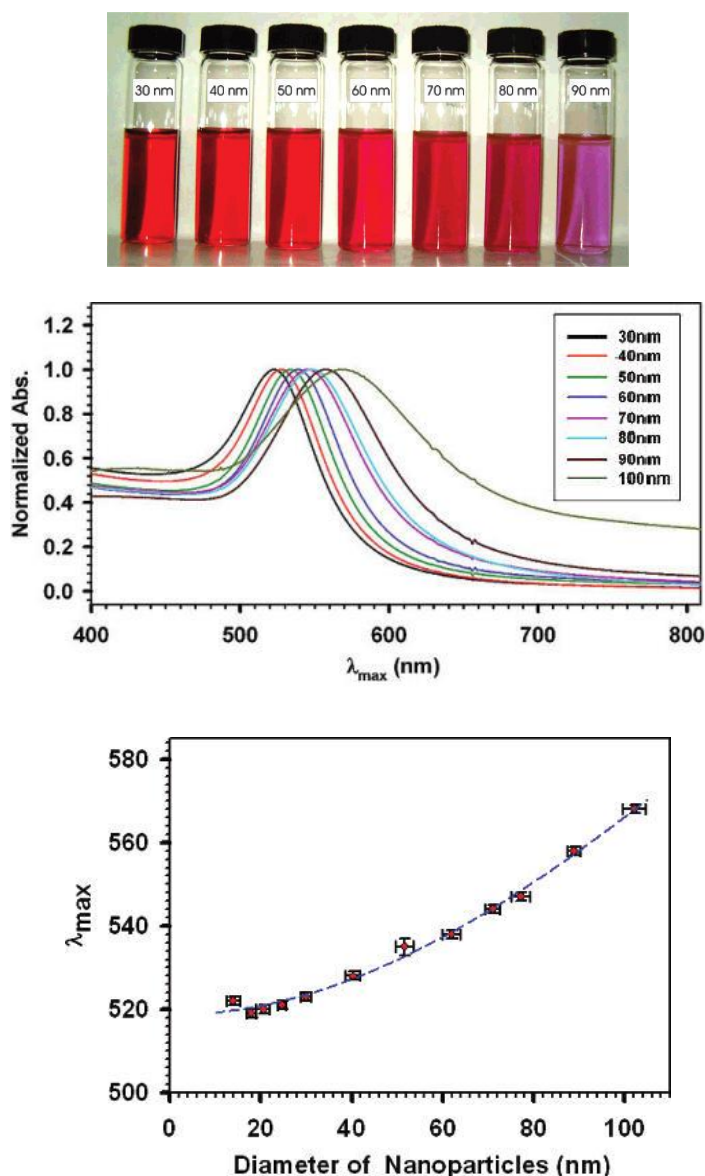


Figure 1.4. Photos showing the color change of AuNPs with their sizes (top). UV-vis spectra of gold nanoparticles with different diameters in aqueous medium (middle). Plot of the absorption maxima (λ_{max}) of the plasmonic band depending on the diameter of the AuNPs (bottom). Reprinted with permission from Ref [58]. © 2007 American Chemical Society.

1. Introduction

A variety of techniques can be applied to characterize the AuNPs. According to the UV-vis spectra, the number density of the particles N can be calculated from Equation (1) based on the absorption at the wavelength of 450 nm (A_{450}) and the diameter d of gold nanoparticles in nanometers.^[62]

$$N = \frac{A_{450} \times 10^{14}}{d^2 \left[-0.295 + 1.36 \exp \left(- \left(\frac{d-96.8}{78.2} \right)^2 \right) \right]} \quad (1)$$

Fluorescence spectroscopy can be used to determine the size and concentration of the colloidal gold dispersion.^[63] Dynamic light scattering (DLS),^[64] small angle X-ray scattering (SAXS),^[45,65] asymmetrical flow field-flow fractionation^[66,67] and gel electrophoresis^[68] provide information about the size and size distribution of the AuNPs. A direct observation of AuNPs can be achieved by various imaging techniques. The most popular methods are transmission electron microscopy (TEM),^[69–71] scanning electron microscopy (SEM)^[72,73] and atomic force microscopy (AFM).^[72,74,75]

The ligands on the AuNP surface can be qualitatively and quantitatively analyzed by nuclear magnetic resonance spectroscopy (NMR),^[76] electrophoresis, thermal gravimetric analysis (TGA),^[77] X-ray photoelectron spectroscopy (XPS),^[78] mass spectroscopy (MS),^[79] and inductively coupled plasma optical emission spectroscopy (ICP-OES).^[80] Scanning tunneling microscopy (STM) is a powerful tool to characterize the ligand monolayer shell around AuNPs.^[81] When the AuNPs (<5 nm) are coated in a monolayer consisting of binary ligands, the arrangement of the ligands can be derived in combination with NMR analysis.^[82,83] Electron paramagnetic resonance (EPR) spectroscopy provides further insight into the aging mechanism of thiolate-protected gold nanoparticles through the ligand exchange reaction with disulfide.^[84]

1.1.2 Gold Nanorods

The gold nanorods (AuNRs) when compared to spherical AuNPs reveal unique optical, electronic, and catalytic properties due to their anisotropic property.^[26] The seed-mediated approach is the most popular way to prepare it and this can be further fused using photochemistry, ultrasound, and template-mediated synthesis.^[85] The seed-mediated approach involves two steps: the seed formation and the successive growth process. (**Figure**

1. Introduction

1.5) In a typical approach, small nanoparticle seeds (about 4 nm) are prepared through the reduction of HAuCl_4 by NaBH_4 in the presence of sodium citrate (NaCt) or cetyltrimethylammonium bromide (CTAB) as protecting ligands. The citrate reduction generates gold seeds in multiply-twinned crystalline while the gold seeds capped with CTAB are single-crystalline. Therefore, CTAB shows a better performance in the yield and polydispersity of the gold nanorods than the citrate. The following step enables the gold seeds to grow step-by-step in a controlled manner by adding the gold seeds to the growth solution containing HAuCl_4 , CTAB for structure-directing, silver nitrate for controlling the aspect ratio and ascorbic acid.^[86] During the growth process, Au^{III} is reduced to Au^{I} with the help of the mild reducing agent ascorbic acid and further reduced to Au^0 using the gold seeds as the catalyst. CTAB attaches preferentially on the gold $\{110\}$ facet, which allows the nanorod to grow along the $\{110\}$ instead of the $\{100\}$ direction. Eventually, CTAB forms a bilayer on the longitudinal side of the AuNRs.^[87] The silver ions react with CTAB forming $[\text{AgBr}]$ ion pairs. This step contributes to the formation of a CTAB bilayer, controlling the reduction rate of the gold ions and forming single-crystalline AuNRs. The size, shape and aspect ratio of AuNRs rely on the nature and the molar ratio of the gold precursor, the reducing agent and the capping agent.

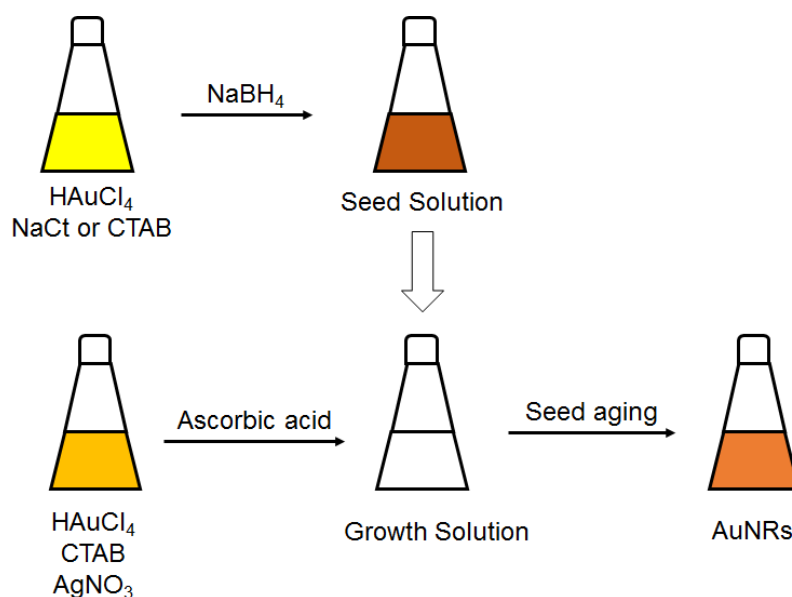


Figure 1.5. Schematic illustration of the seed-mediated synthesis of AuNRs.

The AuNRs exhibit distinctive optical properties^[60] when compared to the spherical AuNPs. They have two distinct surface plasmon bands: one transverse surface plasmon resonance (TSPR) located around 520 nm in the visible region and one longitudinal surface plasmon resonance (LSPR) that appears in the near-infrared (near-IR) region. TSPR and LSPR result from

1. Introduction

the oscillation of the electron cloud perpendicular to and along the long axis, respectively.^[88] LSPR is red-shifted with the increase of the aspect ratio. (**Figure 1.6**) Also, LSPR is highly sensitive to the change in the dielectric constant of the surroundings of AuNRs. For example, solution medium and ligands results in a shift of the LSPR band and intensity degradation. The strong absorption in the near-IR region and enhanced electric field on their tips make AuNRs extraordinary substrates for Raman spectroscopy.

AuNRs are widely applied as sensors in the detection of heavy metals, such as Hg^I, Cu^{II}, Cr^{IV}, and Pb^{II}.^[89,90] In the field of biosensing, and biorecognition of biomolecules, numerous applications for AuNRs were discovered through the modification with specific biotags.^[91,92] In biomedicine, AuNRs have not only been used as a contrast agent and in photothermal therapy for cancer treatment,^[93,94] but have also been used in drug- and gene-delivery.^[95–97]

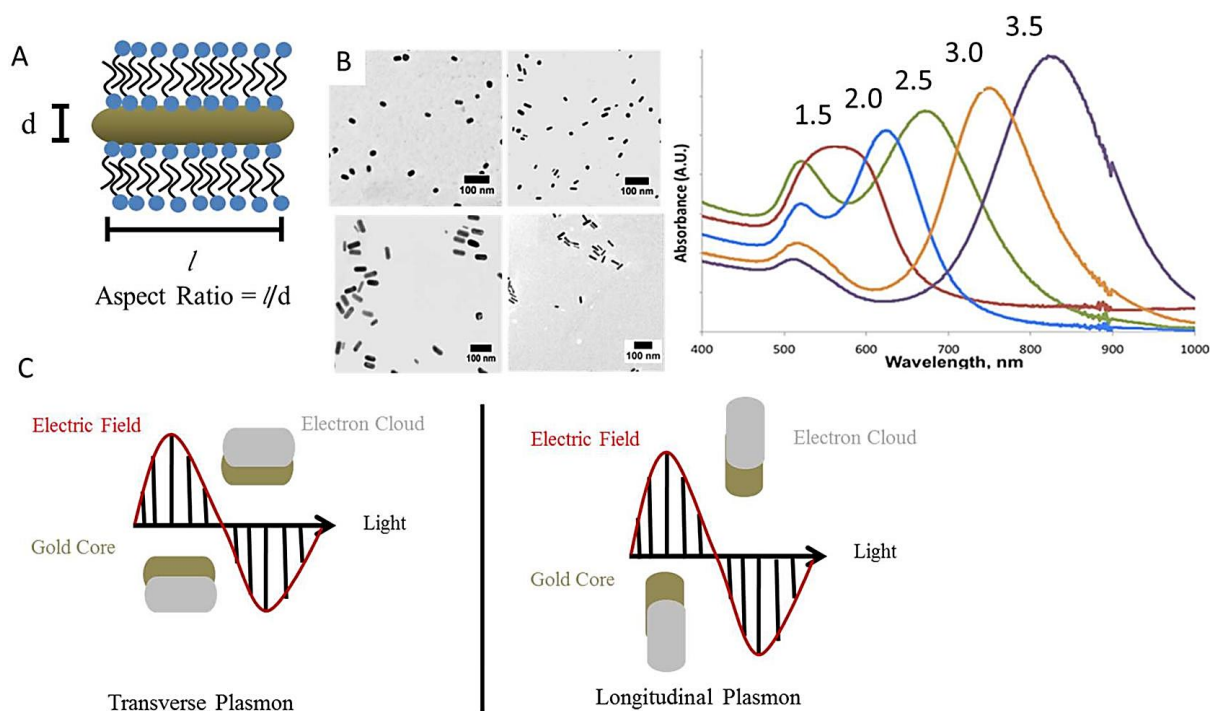


Figure 1.6. A: Schematic illustration of the structure of the CTAB stabilized AuNRs (d : width, l : length). B: The evolution of AuNRs characterized by TEM and UV-vis spectroscopy. The LSPR band is red-shifted with the aspect ratio. C: Schematic illustration of the principle of the transverse (left) and longitudinal (right) plasmon resonance.^[60] Reprinted with permission from Ref. [60]. © 2013, American Chemical Society.

1.2 Polymers for Surface Functionalization of Gold Nanoparticles

The immobilization of functionalized polymers on the surface of AuNPs has created numerous novel hybrid materials for applications in biomedicine, electronics, and optic devices and as catalysts.^[98–100] Generally, polymers are bound to the surface of the AuNPs through specific functionalities called anchor groups. They contain sulfur, nitrogen, and phosphorous that exhibit high affinity to the gold surface. The representative anchor groups are thiol,^[101] disulfide, dithioester, trithiolcarbonate,^[102] thiophene,^[103] amine,^[104] pyrrole,^[105] and pyridine.^[106]

The interplay between the polymer architecture and the nanoparticles has profound impact on the surface properties of the resulting metal nanomaterials. Polymer architectures can be categorized based on the branching of the polymer segments on the backbone. In addition to the linear polymer, complex polymer architectures like star polymer, comb polymer, dendrimer and polymer brush have been prepared via the living polymerization combined with other techniques.^[107–110] In addition, template polymerization also generates special cross-linked polymer structures with controllable size.^[111] For example, two-dimensional (2D) polymeric layer was achieved by the Langmuir-Blodgett technique.^[112] Three-dimensional (3D) cross-linked polymer structure could be prepared using the spherical AuNPs as templates.^[113–115] The polymerization could also be conducted on the surface of the AuNRs coated by the vinyl-functionalized CTAB ligands.^[116] However, the independent structure of the polymeric shell without the support of the template was not studied yet.

Subsequently, the basics of the preparation of the polymer grafted AuNPs will be introduced. As illustrated in **Figure 1.7** (the left half of figure 1.7, indicated by the green arrows), the pre-synthesized functionalized polymers can be immobilized onto the AuNP surface through the “grafting-to” approach. Depending on their architecture and allocation of the functional groups, three mechanisms of the “grafting-to” approach are depicted: wrapping, plug in, and folding. The wrapping mechanism is suitable for the linear homopolymers and the linear block copolymers that are composed of monomers containing the anchor groups. AuNPs coated with end-functionalized polymers present a core-corona structure. Only the functional chain end undergoes the ligand exchange, whereas the rest of the polymer chain is not involved in the direct stabilization of the nanoparticles. This mechanism is therefore described as “plug in”. The folding mechanism is applied to the non-linear polymers, such as the polymer cage

and dendrimer with limited chain mobility.

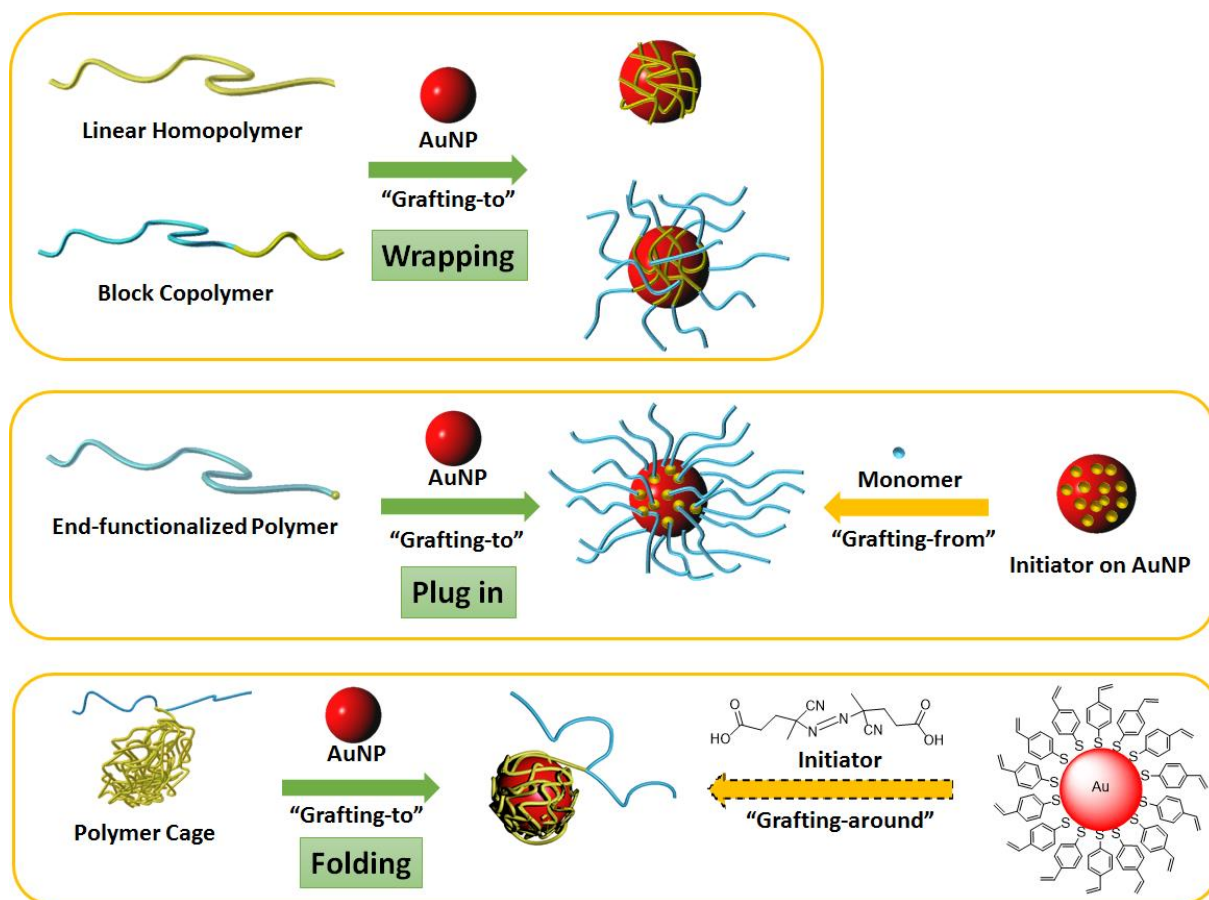


Figure 1.7. Schematic presentation of the mechanisms of the immobilization of different types of pre-synthesized polymers onto the AuNP surface ("grafting-to", the left half, green arrow) as well as the alternative approaches to the same type of polymer coated nanoparticles ("grafting-from" and "grafting-around", the right half, yellow arrow, dashed arrow for "grafting-around" indicates that several synthetic steps are not shown).

The "grafting-to" approach can be further split into the in-situ reduction route and the ligand exchange route. As mentioned in Section 1.1.1, the in-situ route generated the polymer protected AuNPs through the reduction of the gold salts in a solution containing the polymer ligands and the reducing agent. The in-situ reduction route offers a straightforward method to prepare polymer-stabilized AuNPs. AuNPs can also be prepared using the polymer as the reducing agent. For instance, PVP reduced the Au^I precursor at high temperature while serving as the protecting ligand.^[117] The size and the size distribution of the prepared AuNPs are highly dependent on the relative concentration of the polymers.

The ligand exchange reaction is meant to immobilize the functionalized polymers on the pre-prepared AuNP surface based on the coordination strength of the anchor group. Ligand exchange reaction can be carried out in the one-phase as well as the biphasic system depending on the solubility of the polymers. In the one-phase system, for instance, poly(*N*-

1. Introduction

acryloylglycinamide) (PNAGA), an upper critical solution temperature (UCST)-type polymer soluble in water, can undergo a ligand exchange reaction with Ct@AuNPs in aqueous phase.^[118] In the biphasic system, the phase transfer reaction only occurs at the interface. In order to enlarge the interface and accelerate the reaction rate, a phase transfer catalyst or sonication^[119] is required. The ligand exchange offers the possibility to pre-determine the nanoparticle size while the coated polymer shell improves their stability and compatibility.^[120] The photos in **Figure 1.8** show the versatility of the ligand exchange reaction.

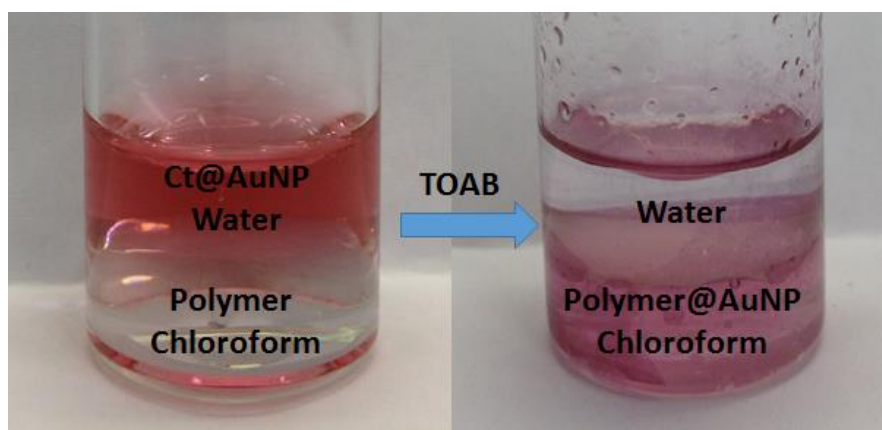


Figure 1.8 Photos showing a typical biphasic ligand exchange reaction. Hydrophobic functionalized polymer was dissolved in the chloroform phase, while the citrate-stabilized AuNPs (Ct@AuNP) were prepared in the aqueous phase (left). The phase transfer occurred after adding TOAB as a phase transfer catalyst. The AuNPs were transferred from the aqueous phase to the organic phase through the indication of the color transfer (right).

Homopolymers that contain coordinating monomers wrap around the AuNP surface through the coordination of the main chain. Typical conventional vinyl-polymers used for wrapping of AuNPs are polyvinylalcohol,^[121] PVP,^[122] and polyvinylpyrrolidone.^[123] Conjugated polymers, such as polypyrrole,^[124] and polythiophene,^[125] were used to embed AuNPs in order to study the interface of the conducting polymer with metal electrodes. Unlike the homopolymer, the block copolymer is attached to the gold surface partially through the coordinating block, for example the PVP block of poly(styrene-*block*-4-vinylpyridine) (PS-*b*-PVP), while the non-coordinating block (the polystyrene block) provides additional steric stabilization as the outer shell for the nanoparticles. The nature and the length of the polymeric blocks have a large impact on the self-organization and location of the AuNPs in polymer matrices.^[126,127]

The end-functionalized polymer can graft onto the AuNPs, thereby forming hairy core-corona colloidal nanoparticles. Various methods have been developed for the end-capping of the different polymers (**Figure 1.9**). One typical method is anionic polymerization which is

1. Introduction

terminated by a proper end-capping agent during the living polymerization. For instance, ethylene sulfide was used to generate the thiol-end-capped polystyrene^[119] (Figure 1.9 A). Controlled radical polymerization offers a wide range of monomers and end-capping methods. Polymers for example are terminated with thiolate and were often prepared by atom-transfer radical-polymerization (ATRP)^[128,129] or reversible addition-fragmentation chain-transfer (RAFT) polymerization. For ATRP, disulfide moieties were usually introduced into the center of the polymer by the disulfide functionalized alkyl halide initiator, like bis[2-(2-bromoisobutyryloxy)ethyl]disulfide] ((BiBOE)₂S₂) (Figure 1.9 B).^[110] The RAFT polymerization involves chain transfer agents (CTA) containing dithiolester and trithiolcarbonate, which can be directly utilized as the anchor groups for metal nanoparticles.^[102] Furthermore, using NaBH₄^[130] and hydrazine-1-hydrate^[131] as an example, the thiol-terminated RAFT polymer can be prepared by reducing the dithiolester or trithiolcarbonate end using (Figure 1.9 C). Through the study of the interaction of poly(*N*-isopropylacrylamide) (PNiPAM) with gold surface, it was discovered that the ω -endgroup of PNiPAM has a greater impact on the nanoparticle growth and stabilization than the molar mass, while the xanthate group showed a better performance than thiolate in improving the stability of the nanoparticles.^[132]

Polymer cages and dendrimers with limited chain mobility collectively change their conformation and undergo the folding mechanism as they graft onto the AuNPs. The unique structure of this type of polymers helps to control the growth of the metal nanoparticles. The size and size distribution of the AuNPs prepared for example in the poly(amidoamine) (PAMAM) dendrimer can be monitored by the dendrimer generations.^[133] The polymer cage exhibits a certain capacity, which allowed the nanoparticles to grow under excellent size control. The detailed preparation and application of the polymer cage will be briefly explained in this section and further expatiated on in Section 1.3.

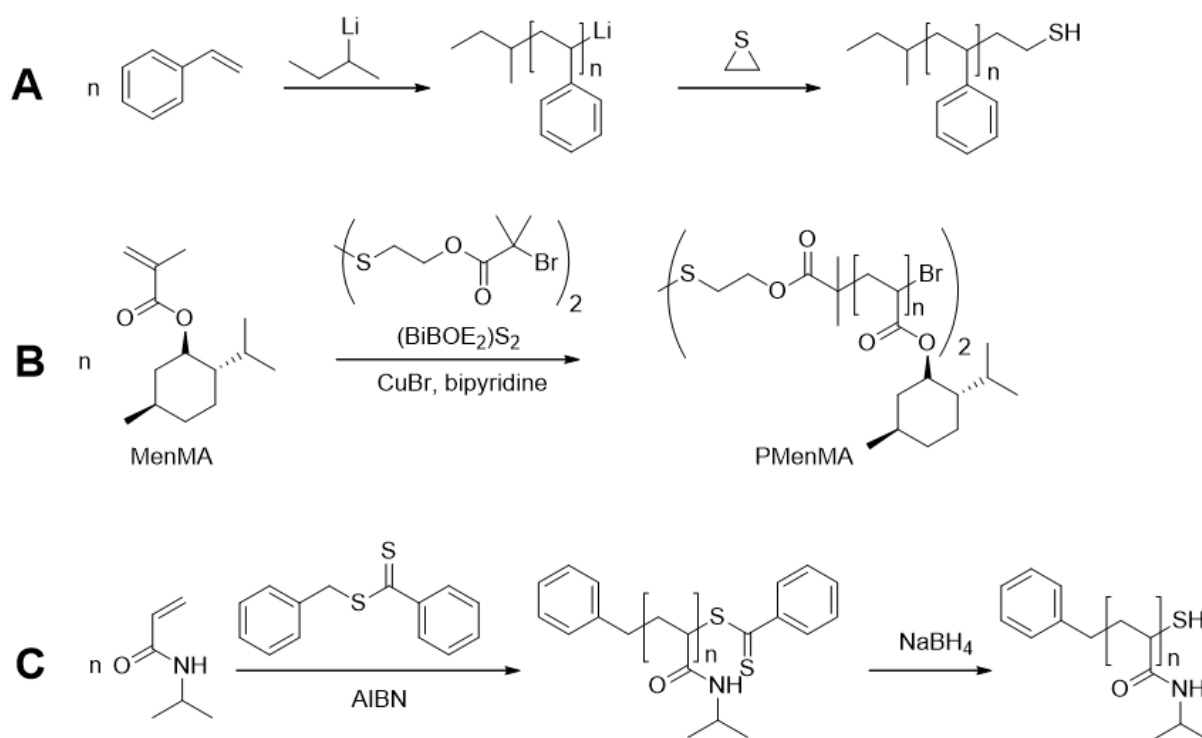


Figure 1.9. Examples of three typical synthetic procedures preparing end-functionalized polymers for the surface modification of AuNPs. A: Thiol-end-capped polystyrene was prepared by anionic polymerization with subsequent termination using ethylenesulfide.^[119] B: Poly(L-menthyl methacrylate) (PMenMA) was synthesized by ATRP of methyl L-mentholacrylate (MenMA) using $(\text{BiBOE}_2)_2$ as a co-initiator.^[129] C: The RAFT polymerization generated the dithioester terminus of poly(*N*-isopropylacrylamide), which could be further reduced to thiolate.^[130]

Densely packed AuNPs with the core-corona structure can be prepared via the “grafting-from” approach, which is also known as surface-initiated polymerization. The initiation site is first immobilized on the nanoparticle and the polymer chains are propagated on the nanoparticle’s surface. In the case of AuNPs, ATRP is one of the most popular methods applied,^[134] as this living polymerization can generate a homogeneous polymer shell with controllable shell thickness and is suitable for the direct coating of nanoparticles with block copolymers. **Figure 1.10** demonstrates the “grafting-from” approach to preparing polymethylmethacrylate (PMMA) grafted nanoparticles using ATRP.^[107]

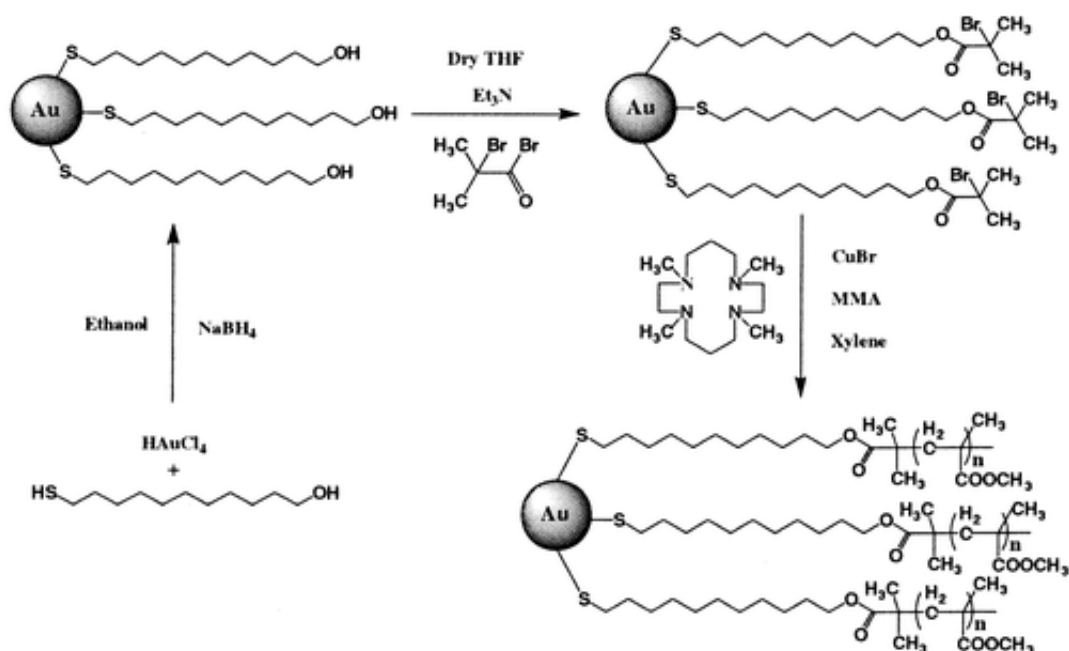


Figure 1.10. Schematic illustration of the synthetic procedure of the PMMA coated gold nanoparticles via the “grafting-from” approach. Reprinted with permission from Ref. [126]. © 2002, American Chemical Society.

The “grafting-around” method (Figure 1.7) was introduced by Prof. Dr. Andreas Greiner and his group. It generates mono-functionalized nanoparticles coated with a cross-linked polymeric monolayer. In 2008, C. Krüger designed a vinyl-containing ligand (4-vinylbenzenethiol) that was immobilized onto the surface of the AuNP using the Brust-Schiffrin method.^[135] The free radical polymerization of the vinyl ligands on the AuNP surface was initiated by an external carboxylate-functionalized azo-initiator 4,4'-azobis-(4-cyanopentanoic acid). (**Figure 1.11 A**) Since the decomposition rate of the initiator is much lower than the propagation rate, the surface polymerization should be initiated by only one radical and this leads to the formation of mono-functionalized nanoparticles. The stoichiometric functionalization was proven by the dimerization of mono-carboxylate-functionalized AuNPs with 1,7-heptandiamine (Figure 1.11 B) and the formation of the necklace-like array of AuNPs after grafting them onto the poly(allylamine) (Figure 1.11 C). This “grafting-around” approach is the foundation of this thesis and inspired the research on the precise functionalization of metal nanoparticles. The diverse applications of this technique will be discussed in Section 1.3.

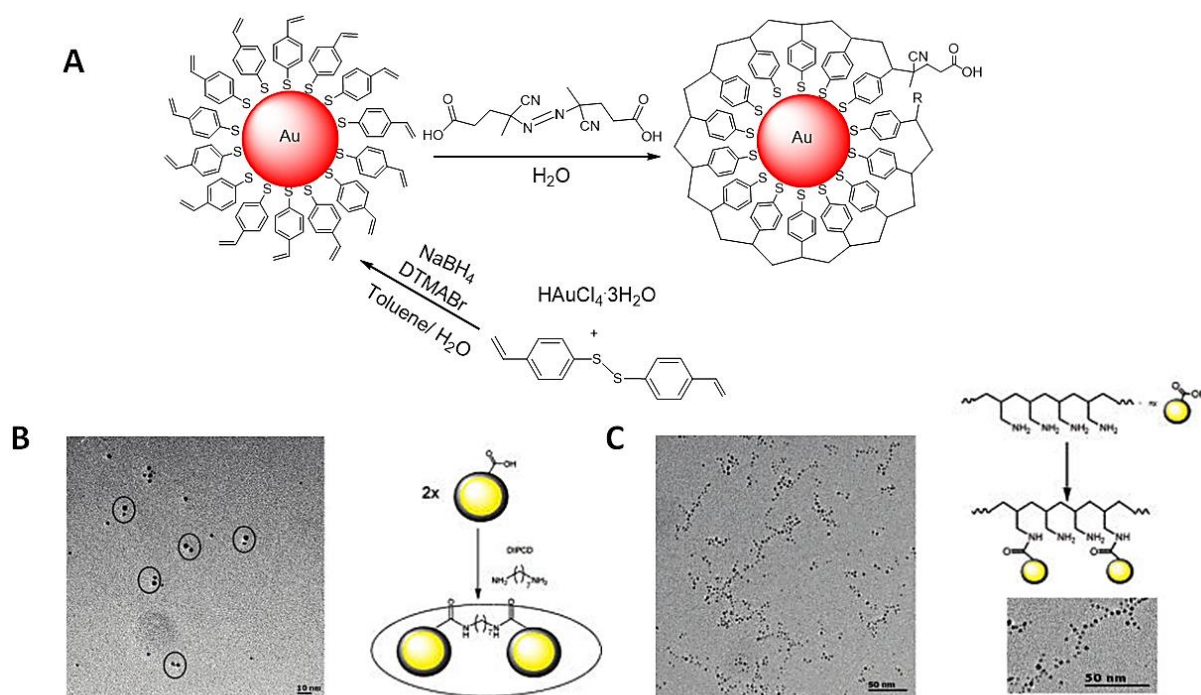


Figure 1.11. A: Schematic illustration of the “grafting-around” approach that generated mono-functionalized AuNPs. B: Dimerization of mono-functionalized AuNP using 1,7-heptadiamine. C: Mono-functionalized AuNPs formed a necklace-like array through coupling with the poly(allylamine) chain. Reprinted with permission from Ref. [127]. © 2008, American Chemical Society.

1.3 Controlled Functionalization of Gold Nanoparticles

The control over the surface chemistry of nanoparticles is becoming an increasingly dominant theme in the current research trend focusing on the need for more complex nanoparticle structures and assemblies. To this end, different methods and novel polymers have been developed, especially in response to the challenge of establishing stoichiometric control over the ligands and functionalities on the nanoparticle surface.

Generally, nanoparticles with defined composition and arrangement of mixed ligands can be achieved through interface-mediated synthesis. The underlying concept is to differentiate the nanoparticle surface regionally at the interface while involving different types of ligands at each phase for the surface modification. For instance, mono-functionalized AuNPs were prepared through the solid-phase approach (demonstrated in **Figure 1.12**). The polymer resin for the solid-phase synthesis was modified with thiolate groups that could undergo ligand exchange reaction with densely packed AuNPs. The concentration of the loaded thiol-functionality should be kept low to ensure that each nanoparticle makes contact with only

1. Introduction

one external ligand.^[136,137] As for the interface of two immiscible liquids, the mono-vinyl-functionalized AuNPs was prepared through the ligand exchange with 11-mercaptopundecyl methacrylate (MUMA) at the water/toluene interface, which could be further used as the comonomer for copolymerization with styrene.^[138] Moreover, the interface-mediated synthesis creates a variety of Janus-type nanoparticles.^[139–141] For example, the amphiphilic Janus AuNPs were prepared by grafting one side with hydrophilic poylethylenoxide (PEO) in the thiol-functionalized PEO single-crystal suspension. The opposite side of the nanoparticle was coated with a hydrophobic PMMA through the “grafting-from” approach. The single-crystal of PEO was dissolved afterward leaving the amphiphilic Janus nanoparticles behind.^[140]

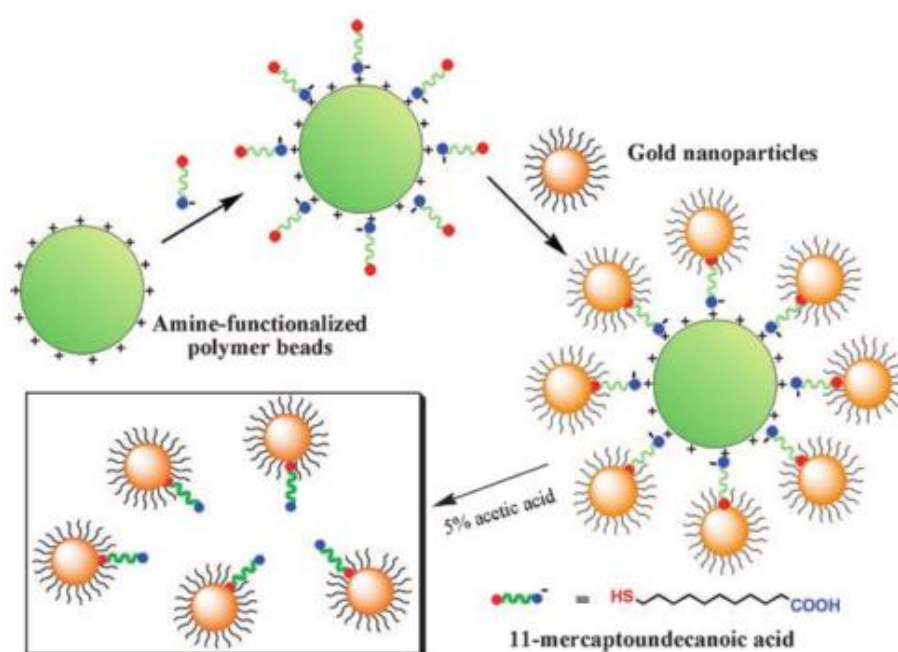


Figure 1.12. Schematic illustration of the solid-phase synthesis of mono-functionalized AuNPs. The amine-functionalized polymer beads were loaded with 11-mercaptopundecanoic acid through electrostatic attraction, which simplified the synthetic procedure for resin modification.^[136] © 2011 WILEY-VCH Verlag GmbH & Co. KGaA, Weinheim.

Instead of replacing the ligands on the nanoparticle surface with ligands located in another phase, DeVries et al. reported a precise ligand exchange at the polar defects of a monolayer protected nanoparticle, where the ligands are most likely to desorb resulting from lack the intermolecular stabilization of their neighboring ligands.^[81] The pole-functionalized AuNPs were used as building blocks to be linked through condensation polymerization, thereby forming a necklace-structure. Recently, a dynamic covalent exchange was introduced by F. della Sala et al. for the reversible control of the nanoparticle functionalization (**Figure 1.13**).^[142] The basis of this system is the monolayer of hydrazone coated on the AuNPs, which

enables a quantitative covalent exchange reaction using acid or nucleophilic as catalysts. Although the process is reversible and the composition of the ligand shell can be monitored by NMR, the location of the hydrazone exchange on a single nanoparticle is unpredictable.

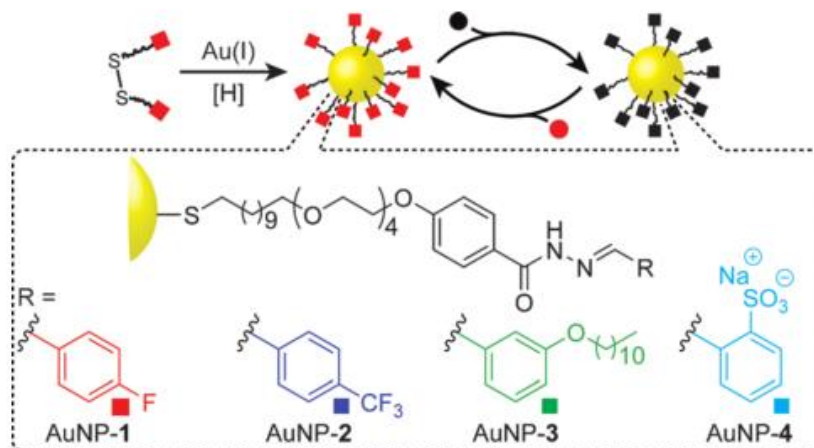


Figure 1.13. Schematic presentation of the concept of reversible surface modification. The nanoparticles were coated by with *N*-aroylhydrazone monolayer, of which the hydrazone moieties underwent a reversible exchange with other functionalities. © 2015 Flavio della Sala, Euan R. Kay. Published by Wiley-VCH Verlag GmbH & Co. KGaA.

The nanoparticles can be directly prepared in a specially designed monofunctional polymer. For example, AuNPs were prepared using the in-situ method in a functional thioether dendrimer carrying single acetylene functionality. (**Figure 1.14**) The dumbbell-like dimer of the mono-functionalized AuNPs was formed through the coupling reaction of the deprotected mono-functionality. Due to the size limitation of the dendrimer, the nanoparticles prepared had a mean diameter of less than 2 nm (1.3 nm).^[143] Similar functionalized multidentate ligands were used by T. Peterle for the building of nanoparticle superstructures.^[144]

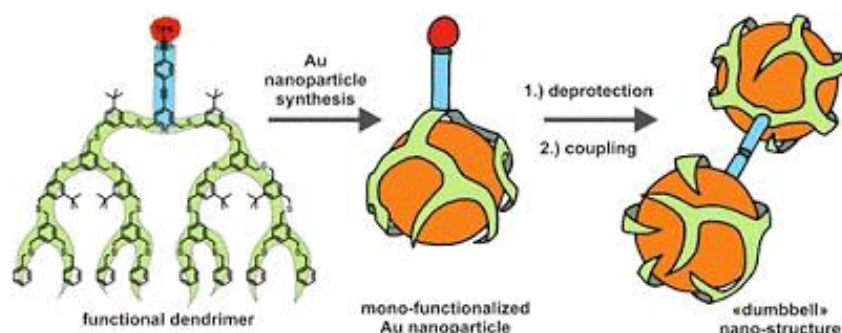


Figure 1.14. Schematic illustration of mono-functionalized AuNPs stabilized in the single dendrimer that formed a dumbbell-structure through homocoupling. Reprinted with permission from Ref. [132]. © 2012, American Chemical Society.

As earlier mentioned, the “grafting-around” method produces mono-functionalized nanoparticles simply through immobilization of vinyl-ligands and the surface polymerization.

1. Introduction

Based on this method, the AuNP carrying a single methylcoumarin moiety with a polystyrene spacer in between was developed by S. Bokern et al.^[145] and instead of using the low molecular initiator, a polystyrene macroinitiator that exhibited α,ω -methylcoumarin termini, and an azo-center was involved in the surface polymerization of the vinyl ligands (**Figure 1.15**). The unique structure of the AuNP tethered with single macromolecular chain is well-defined by gel permeation chromatography (GPC) coupled with a diode array detector (DAD), as was evident by the appearance of the peak indicating the cumulative molecular weight of the AuNP and the polystyrene bridge. The methylcoumarin moiety enabled a wide range of possibilities to couple this artificial molecule with other functional organic or bio-molecules and to build nanoparticle assemblies. Furthermore, one AuNP corresponds to one functionality, which is presented as a promising tool for sensing technique.

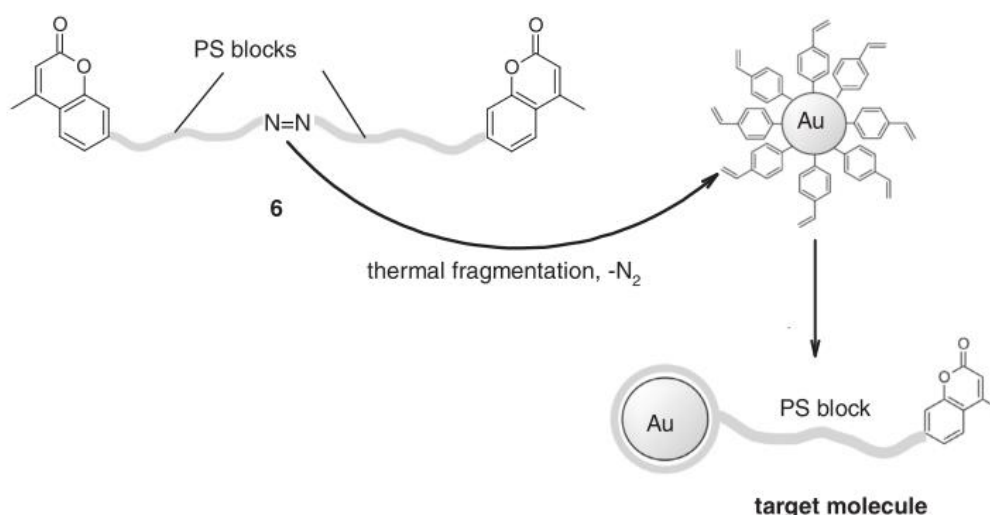


Figure 1.15. Schematic illustration of the “grafting-around” approach using a bi-end-functionalized polystyrene azo-macroinitiator. © 2011 WILEY-VCH Verlag GmbH & Co. KGaA, Weinheim.

Aside replacing the initiator, the carboxylate mono-functionality on the AuNP resulting from the original “grafting-around” approach can also be modified. As reported by K. Gries, the carboxylate group was converted to vinyl through acid-amine-coupling with 4-vinylaniline.^[146] The resulting vinyl-mono-functionalized AuNPs were utilized as an artificial monomer for copolymerization with MMA, which can be applied to the copolymerization of various mono-functionalized metal nanoparticles with vinyl monomers. (**Figure 1.16**) The successful copolymerization was characterized by DAD-GPC, TEM, AFM, and TGA.

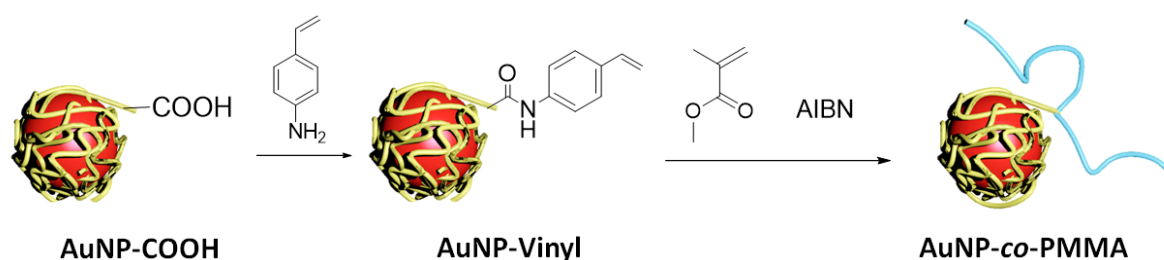


Figure 1.16. Schematic presentation of the synthetic procedure of the copolymerization of a vinyl-mono-functionalized AuNP (AuNP-Vinyl) and MMA (AuNP-co-PMMA). The mono-carboxyl-functionalized AuNP (AuNP-COOH) was reacted with 4-vinylaniline yielding viny-functionalized AuNP, which were further free radical copolymerized with MMA.

The mono-functionality chain end tailored on poly(4-vinylthiolbenzene) resulted from the “grafting-around” method. Specifically, the “grafting-around” method does not only generate mono-functionalized nanoparticles but also delivers a unique polymeric shell carrying single functionality.

Despite all the synthetic tools available, nanoparticles with a defined number of functionalities can be separated using ultracentrifugation^[147] and electrophoresis for charged colloidal particles.^[148]

1.4 Discrete Assembly of Gold Nanocrystals via Functionalized Polymer

Individual AuNPs display specific colors due to their localized surface plasmon resonance. When two AuNPs are brought closer together, near-field interaction leads to the coupling of their individual localized surface plasmon resonances, which can be observed as a shift of the plasmonic band. Meanwhile, near-field coupling generates a “hot spot” at the gap (critical distance of around 2 nm) between two nanoparticles, where the electromagnetic field is significantly enhanced. Therefore, various AuNP assemblies have been developed based on this effect in order to be exploited using SERS.

Various strategies have also been developed to prepare discrete assemblies of AuNPs. The most popular approach is to modify the nanoparticle surface using biopolymers such as DNA (deoxyribonucleic acid)^[149] and proteins (peptides). These biomolecules can be covalently grafted onto the AuNPs, thereby providing them with sufficient stability in a biological medium. Through a specific interaction, such as oligonucleotide hybridization,^[150] antigen-antibody,^[151] and biotin-streptavidin,^[152] the assembly of nanoparticles can be directed in a precisely

1. Introduction

controlled spatial position and orientation. However, this biopolymer-based approach can only operate in restricted conditions and it is therefore difficult to apply outside of the biological field. In this context, the use of a synthetic polymer (and organic molecules) expands the scope of the nanoparticle assembly. While the regioselectivity of the synthetic polymer coated nanocrystals still remains a challenge, the nanoparticle can still be assembled via polymers in different ways.

The modulation of the aggregation kinetics of the nanoparticles generates AuNP dimers that were encapsulated in polystyrene-*block*-poly(acrylic acid) (PS-*b*-PAA). As reported by X. Wang et al., the dimer were further used as the catalysts for the guided growth of the ZnO-nanowires.^[153] (Figure 1.17 A) The purpose of the PS-*b*-PAA shell here is to protect and isolate the dimers, while the individual PS-*b*-PAA coated nanoparticles were arranged into a nanoparticle chain triggered by the salt, acid or 1-(3-dimethylamino)propyl)-3-ethylcarbodiimide methiodide (EDC)^[154] (Figure 1.17 B).

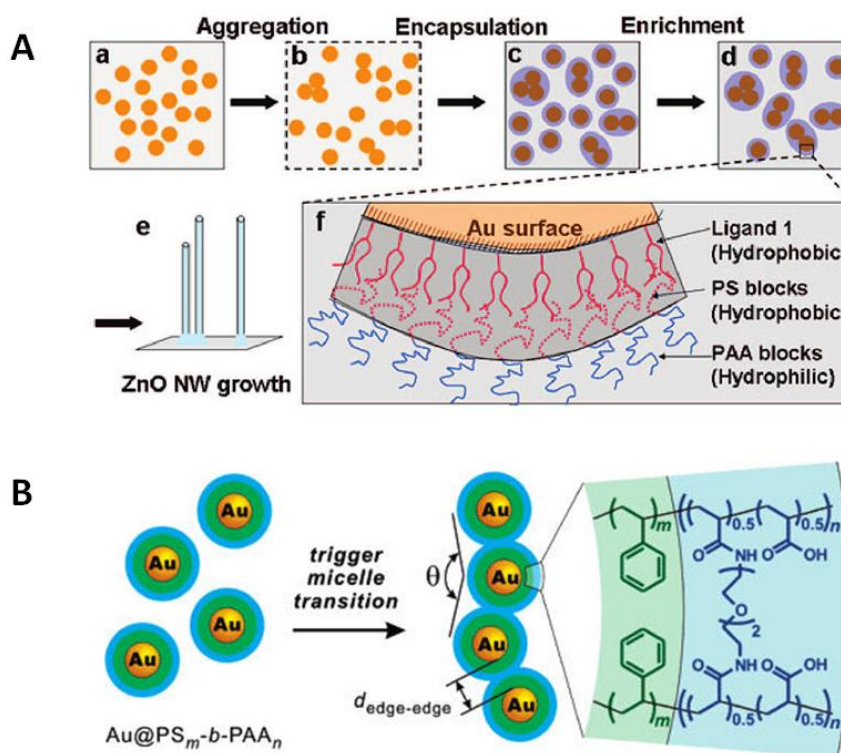


Figure 1.17. A: AuNP dimers were prepared through induced aggregation and subsequently stabilized in the PS-*b*-PAA shell, which was used to catalyze the growth of ZnO-nanowire. Reprinted with permission from Ref [145], © 2008, American Chemical Society. B: Schematic illustration of the sphere-to-string transition of the PS-*b*-PAA coated nanoparticles triggered by EDC. Reprinted with permission from Ref. [146]. © 2005, American Chemical Society.

As introduced in Section 1.3, mono-functionalized polymers offer an alternative to preparing a nanoparticle dimer through homocoupling and fascinating assembly structures can be

1. Introduction

generated using anisotropic nanoparticles, such as AuNRs. For instance, amphiphilic AuNRs with a hydrophobic polystyrene grafted to the both ends and hydrophilic CTAB-bilayer around the longitudinal side were assembled into different structures (side-to-side, end-to-end) according to the choice of solvents used (**Figure 1.18**).^[155]

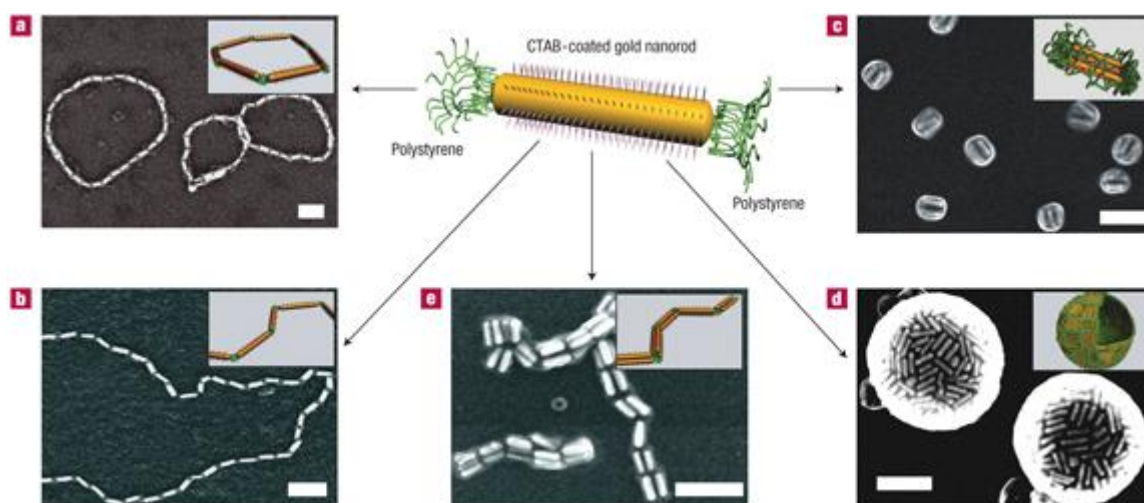


Figure 1.18. Self-assembly of amphiphilic AuNRs in different solvents. (a): ring structure: dimethyl formamide (DMF)/water (6 wt%); (b) chain structure: DMF/water (20 wt%); (c) bundles: tetrahydrofuran (THF)/water (6 wt%); (d) nanospheres: THF/water (20 wt%); (e) bundle nanorod chain: DMF/THF/water: 42.5:42.5:15. All scale bars are 100 nm. © 2007, rights managed by Nature Publishing Group.

In comparison to the homogeneous arrays, the heterogeneous array reveals a wide range of choice of building blocks when it comes to their size, shape, composition and organization.^[156] The satellite structure of nanoparticle array can be arranged through DNA^[157,158] or organic molecules,^[141,159,160] that exhibit a strong plasmon coupling effect and can be used as substrates for SERS.^[161] In addition, the dramatic change in the hydrodynamic radius of the coupled nanoparticle-nanorod assembly was used as a probe for cancer biomarker detection.^[162] Polymers that contain more than one anchor group to the gold surface can be applied to the coupling of heterogeneous nanocrystals. S. Pierrat has established a strategy to assemble AuNPs on AuNRs by stabilizing them with mono- and bifunctional polyethylene glycol (PEG)^[163] (**Figure 1.19**). AuNRs decorated with superparamagnetic iron oxide nanoparticles were prepared by R. Turby et al. via α -carboxy- ω -thiolate functionalized PEG.^[164] To explore this further, Chapter 2 will introduce a telechelic poly(*N*-isopropyl acrylamide) (PNiPAM) as a polymer glue to achieve a satellite assembly of AuNPs around AuNRs. Moreover, the coupled LSPR of the resulting satellite assembly exhibits the thermal sensitive behavior.

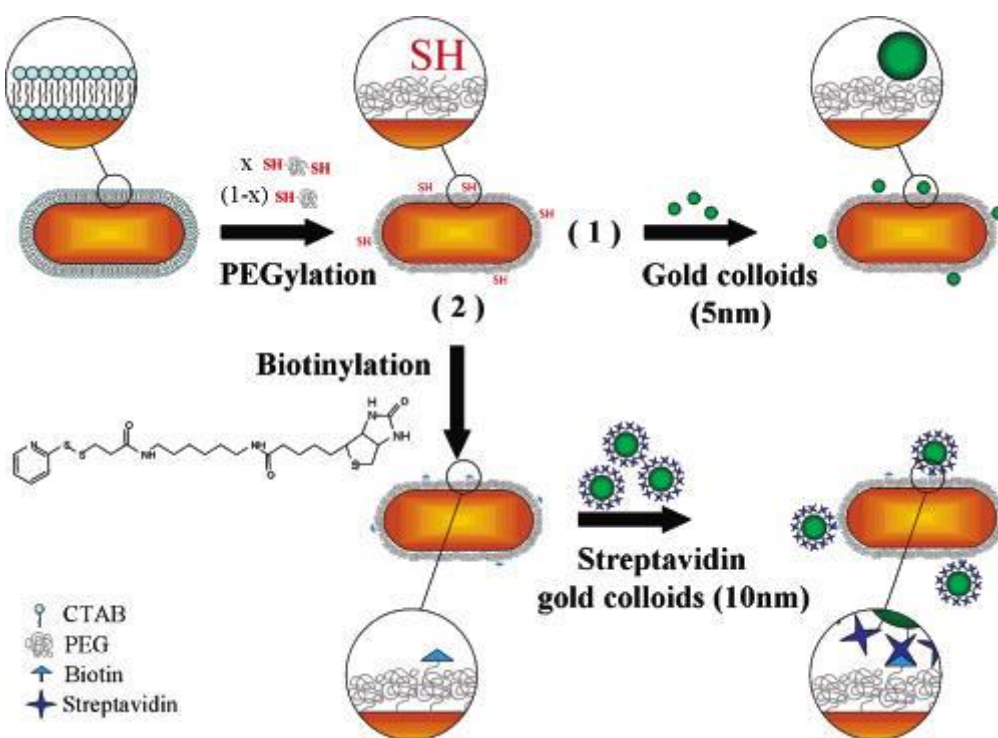


Figure 1.19. Schematic illustration of AuNP assembly around the mono- and bi-thiol-functionalized PEG protected AuNRs. AuNRs were tethered with biotin and attracted the streptavidin stabilized AuNPs. Reprinted with permission from Ref. [152]. © 2007, American Chemical Society.

1.5 Thesis Objective

The aim of this thesis is to develop novel polymer architectures using metal nanoparticles as templates. In this respect, feasible synthetic strategies would be carried out to prepare the suitable polymer building blocks (monomer or segment) for grafting on metal nanoparticles and then to cross-link these building blocks. In order to test the feasibility of the concept, spherical AuNPs would be selected as the representative template, as their preparation and surface properties were well established. If the vinyl monomers were polymerized around the globular surface of AuNPs, a cross-linked polymeric shell exhibiting a globular shape should be achieved. Moreover, the polymeric shell could be stoichiometric functionalized through an external functionalized initiator. Therefore, a ligand suitable for the surface polymerization should contain both the vinyl- and thiol-components, like 4-vinylbenzenethiol. The polymerization could be initiated by an azo-initiator tethered with carboxylate group. The resulting polymeric shell as known as the “polymer cage”, should exhibit defined size and numerous anchor groups after the gold core is etched. Taking account of this unique property,

1. Introduction

the polymer cage could be applied as confinements in the precise control over the size and functionality of metal nanoparticles.

The next step aims to prepare more complex polymer architecture: the cylindrical cross-linked polymer brush. The cylinder shape requires AuNRs as templates. As for the segments for the polymer brush, a telechelic linear polymers could be designed with one chain end grafting on the AuNRs and the other chain end for cross-linking. For this purpose, poly(*N*-isopropylacrylamide) (PNiPAM) could be functionalized with one thiol-end and one amine-end. The PNiPAM could be immobilized on AuNRs through the thiol-end, while acid-amine-coupling reaction could be carried out on the amine-ends. Meanwhile, the resulting polymer brush should be thermoresponsive due to PNiPAM. In order to identify the distribution of PNiPAM around AuNRs, AuNPs could be assembled around the PNiPAM coated AuNRs through the ligand exchange with the nitrogen-compounds of PNiPAM. Thus, the location of PNiPAM and availability of the amine-ends could be visualized with the help of AuNPs.

The next Chapter, entitled “Overview of the Thesis,” will provide a summary of the individual topics pertaining to this research, including the researcher’s motivation, conceptualization and preparation of the work, essential characterizations and the conclusion. In the subsequent chapters, the detailed experiments, analysis, and results will be presented.

References:

- [1] R. P. Feynman, *J. Microelectromechanical Syst.* **1992**, *1*, 60.
- [2] S. Horikoshi, N. Serpone, in *Microwaves Nanoparticle Synthesis: Fundamentals and Applications*, (Eds: S. Horikoshi, N. Serpone), Wiley-VCH, Weinheim, Germany **2013**, Ch. 1.
- [3] M.-C. Daniel, D. Astruc, *Chem. Rev.* **2004**, *104*, 293.
- [4] Y.-W. Lin, C.-C. Huang, H.-T. Chang, *Analyst* **2011**, *136*, 863.
- [5] W. Dong, G. B. Sukhorukov, H. Mo, *Phys. Chem. Chem. Phys.* **2003**, *5*, 3003.
- [6] R. D. K. P. D. Jazdzinsky, G. Calero, C. J. Ackerson, D. A. Bushnell, *Science* **2007**, *318*, 430.
- [7] B. M. Barngrover, C. M. Aikens, *J. Am. Chem. Soc.* **2012**, *134*, 12590.
- [8] F. Griffin, D. Fitzmaurice, *Langmuir* **2007**, *23*, 10262.
- [9] A. Dass, A. Stevenson, G. R. Dubay, J. B. Tracy, R. W. Murray, N. Carolina, *J. Am. Chem. Soc.* **2008**, *25*, 5940.
- [10] H. Jans, Q. Huo, *Chem. Soc. Rev.* **2012**, *41*, 2849.
- [11] D. Radziuk, H. Moehwald, *Phys. Chem. Chem. Phys.* **2015**, *17*, 21072.
- [12] J. N. Anker, W. P. Hall, O. Lyandres, N. C. Shah, J. Zhao, R. P. Van Duyne, *Nat. Mater.* **2008**, *7*, 443.
- [13] W. Lu, S. R. Arumugam, D. Senapati, A. K. Singh, T. Arbneshi, S. A. Khan, H. Yu, P. C. Ray, *ACS Nano* **2010**, *4*, 1739.
- [14] L. Sun, D. Liu, Z. Wang, *Langmuir* **2008**, 10293.
- [15] A. N. Shipway, E. Katz, I. Willner, *ChemPhysChem* **2000**, *1*, 18.
- [16] S. Lal, S. Link, N. J. Halas, *Nat. Photonics* **2007**, *1*, 641.
- [17] C. E. Talley, J. B. Jackson, C. Oubre, N. K. Grady, C. W. Hollars, S. M. Lane, T. R. Huser, P. Nordlander, N. J. Halas, *Nano Lett.* **2005**, *5*, 1569.
- [18] N. Pazos-perez, C. S. Wagner, J. M. Romo-herrera, L. M. Liz-marzun, F. J. G. De Abajo, A. Wittemann, A. Fery, R. A. Alvarez-puebla, *Angew. Chem.* **2012**, *124*, 12860; *Angew. Chem. Int. Ed.* **2012**, *51*, 12688.

1. Introduction

- [19] X. Chen, L. Zuo, W. Fu, Q. Yan, C. Fan, H. Chen, *Sol. Energy Mater. Sol. Cells* **2013**, *111*, 1.
- [20] Z. D. Pozun, S. E. Rodenbusch, E. Keller, K. Tran, W. Tang, K. J. Stevenson, G. Henkelman, *J. Phys. Chem. C* **2013**, *117*, 7598.
- [21] F. Mitschang, H. Schmalz, S. Agarwal, A. Greiner, *Angew. Chem.* **2014**, *126*, 5073; *Angew. Chem. Int. Ed.* **2014**, *53*, 4972.
- [22] M. Stratakis, H. Garcia, *Chem. Rev.* **2012**, *112*, 4469.
- [23] A. S. K. Hashmi, *Top. Organomet. Chem.* **2013**, *44*, 143.
- [24] M. Haruta, *Gold Bull.* **2004**, *37*, 27.
- [25] P. Raffa, C. Evangelisti, G. Vitulli, P. Salvadori, *Tetrahedron Lett.* **2008**, *49*, 3221.
- [26] K. Sohn, F. Kim, K. C. Pradel, J. Wu, Y. Peng, F. Zhou, J. Huang, *ACS Nano* **2009**, *3*, 2191.
- [27] R. A. Sperling, W. J. Parak, *Philos. Trans. A. Math. Phys. Eng. Sci.* **2010**, *368*, 1333.
- [28] I. Freestone, N. Meeks, M. Sax, C. Higgitt, *Gold Bull.* **2007**, *40*, 270.
- [29] S. Eustis, H.-Y. Hsu, M. a El-Sayed, *J. Phys. Chem. B* **2005**, *109*, 4811.
- [30] T. Sakai, P. Alexandridis, *J. Phys. Chem. B* **2005**, *109*, 7766.
- [31] S. Liu, G. Chen, P. N. Prasad, M. T. Swihart, **2011**, 4098.
- [32] S. J. Barrow, X. Wei, J. S. Baldauf, A. M. Funston, P. Mulvaney, *Nat. Commun.* **2012**, *3*, 1275.
- [33] R. Sardar, J. S. Shumaker-Parry, *J. Am. Chem. Soc.* **2011**, *133*, 8179.
- [34] A. P. Kozlova, A. I. Kozlov, S. Sugiyama, Y. Matsui, K. Asakura, Y. Iwasawa, *J. Catal.* **1999**, *181*, 37.
- [35] G. Pourceau, L. Del Valle-Carrandi, P. Di Gianvincenzo, O. Michelena, S. Penadés, *RSC Adv.* **2014**, *4*, 59284.
- [36] X. Lu, H. Y. Tuan, B. A. Korgel, Y. Xia, *Chem. Eur. J.* **2008**, *14*, 1584.
- [37] V. J. Gandubert, R. B. Lennox, *Langmuir* **2005**, *21*, 6532.
- [38] C. K. Yee, R. Jordan, A. Ulman, H. White, A. King, M. Rafailovich, J. Sokolov, S. Brook, N. York, *Langmuir* **1999**, *15*, 3486.

- [39] M. K. Corbierre, N. S. Cameron, R. B. Lennox, *Langmuir* **2004**, *20*, 2867.
- [40] R. Sardar, J. S. Shumaker-Parry, *Chem. Mater.* **2009**, *21*, 1167.
- [41] G. Hou, L. Zhu, D. Chen, M. Jiang, *Macromolecules* **2007**, *40*, 2134.
- [42] S. I. Lim, C.-J. Zhong, *Acc. Chem. Res.* **2009**, *42*, 798.
- [43] Y. Liu, M. K. Shipton, J. Ryan, E. D. Kaufman, S. Franzen, D. L. Feldheim, *Anal. Chem.* **2007**, *79*, 2221.
- [44] S. M. Marinakos, J. P. Novak, L. C. Brousseau III, A. B. House, E. M. Edeki, J. C. Feldhaus, D. L. Feldheim, *J. Am. Chem. Soc.* **1999**, *121*, 8518.
- [45] J. Polte, T. T. Ahner, F. Delissen, S. Sokolov, F. Emmerling, A. F. Thünemann, R. Kraehnert, *J. Am. Chem. Soc.* **2010**, *132*, 1296.
- [46] X. Ji, X. Song, J. Li, Y. Bai, W. Yang, X. Peng, *J. Am. Chem. Soc.* **2007**, *129*, 13939.
- [47] S. S. Kumar, C. S. Kumar, J. Mathiyarasu, K. L. Phani, *Langmuir* **2007**, *23*, 3401.
- [48] B. A. Rozenberg, R. Tenne, *Prog. Polym. Sci.* **2008**, *33*, 40.
- [49] P. K. Khanna, R. Gokhale, V. V. V. S. Subbarao, A. K. Vishwanath, B. K. Das, C. V. V. Satyanarayana, *Mater. Chem. Phys.* **2005**, *92*, 229.
- [50] C. E. Hoppe, M. Lazzari, I. Pardiñas-Blanco, M. A. López-Quintela, *Langmuir* **2006**, *22*, 7027.
- [51] M. Brust, M. Walker, D. Bethell, D. J. Schiffrin, R. Whyman, *J. Chem. Soc., Chem. Commun.* **1994**, 801.
- [52] L. M. Liz-Marzán, *Chem. Commun.* **2013**, *49*, 16.
- [53] P. J. G. Goulet, R. B. Lennox, *J. Am. Chem. Soc.* **2010**, *132*, 9582.
- [54] H. Häkkinen, *Nat. Chem.* **2012**, *4*, 443.
- [55] H. Gronbeck, A. Curioni, W. Andreoni, *J. Am. Chem. Soc.* **2000**, *122*, 3839.
- [56] S. Eustis, M. A. El-Sayed, *Chem. Soc. Rev.* **2006**, *35*, 209.
- [57] M. Pelton, J. Aizpurua, G. Bryant, *Laser Photonics Rev.* **2008**, *2*, 136.
- [58] K. A. Willets, R. Van Duyne, R. P. Van Duyne, *Annu. Rev. Phys. Chem.* **2007**, *58*, 267.
- [59] M. Karg, N. Schelero, C. Oppel, M. Gradzielski, T. Hellweg, R. von Klitzing, *Chem. Eur. J.*

- 2011**, 17, 4648.
- [60] S. E. Lohse, C. J. Murphy, *Chem. Mater.* **2013**, 25, 1250.
- [61] P. N. Njoki, I.-I. S. Lim, D. Mott, H.-Y. Park, B. Khan, S. Mishra, R. Sujakumar, J. Luo, C.-J. Zhong, *J. Phys. Chem. C* **2007**, 111, 14664.
- [62] W. Haiss, N. T. K. Thanh, J. Aveyard, D. G. Fernig, *Anal. Chem.* **2007**, 79, 4215.
- [63] M. A. K. Abdelhalim, M. M. Mady, *J. Nanomed. Nanotechnol.* **2012**, 03, 1.
- [64] H. Liu, N. Pierre-Pierre, Q. Huo, *Gold Bull.* **2012**, 45, 187.
- [65] H. Koerner, R. I. MacCuspie, K. Park, R. A. Vaia, *Chem. Mater.* **2012**, 24, 981.
- [66] M. Lattuada, C. Olivo, C. Gauer, G. Storti, M. Morbidelli, *Langmuir* **2010**, 26, 7062.
- [67] F. R. L. Calzolari, D. Gilliland, C. P. García, *J. Chromatogr. A* **2011**, 1218, 4234.
- [68] C. S. M. Hanauer, S. Pierrat, I. Zins, A. Lotz, *Nano. Lett.* **2007**, 7, 2881.
- [69] H. Long, Y. Jin, A. Sanders, W. Park, W. Zhang, *J. Am. Chem. Soc.* **2014**, 136, 1782.
- [70] K. Hata, H. Fujihara, *Chem. Commun.* **2002**, 2714.
- [71] J. Turkevich, P. C. Stevenson, J. Hiller, *Discuss. Faraday Soc.* **1951**, 11, 55.
- [72] S. Kraus-Ophir, J. Witt, G. Wittstock, D. Mandler, *Angew. Chem.* **2014**, 126, 300; *Angew. Chem. Int. Ed.* **2014**, 53, 294.
- [73] H. Wu, Z. Liu, X. Wang, B. Zhao, J. Zhang, C. Li, *J. Colloid Interface Sci.* **2006**, 302, 142.
- [74] K. Kim, H. Ryoo, Y. M. Lee, K. S. Shin, *J. Colloid Interface Sci.* **2010**, 342, 479.
- [75] J. Tian, L. Yuan, M. Zhang, F. Zheng, Q. Xiong, H. Zhao, *Langmuir* **2012**, 28, 9365.
- [76] R. Sharma, G. P. Holland, V. C. Solomon, H. Zimmermann, S. Schifffenhaus, S. a. Amin, D. A. Buttry, J. L. Yarger, *J. Phys. Chem. C* **2009**, 113, 16387.
- [77] J. Shan, M. Nuopponen, H. Jiang, E. Kauppinen, H. Tenhu, *Macromolecules* **2003**, 36, 4526.
- [78] M. I. Gibson, M. Danial, H.-A. Klok, *ACS Comb. Sci.* **2011**, 13, 286.
- [79] C. a Fields-Zinna, J. F. Parker, R. W. Murray, *J. Am. Chem. Soc.* **2010**, 25, 17193.
- [80] S. Elzey, D.-H. Tsai, S. a Rabb, L. L. Yu, M. R. Winchester, V. a Hackley, *Anal. Bioanal. Chem.* **2012**, 403, 145.

1. Introduction

- [81] G. A. Devries, M. Brunnbauer, Y. Hu, A. M. Jackson, B. Long, B. T. Neltner, O. Uzun, B. H. Wunsch, F. Stellacci, *Science* **2007**, *315*, 358.
- [82] A. M. Jackson, J. W. Myerson, F. Stellacci, *Nat. Mater.* **2004**, *3*, 330.
- [83] F. S. X. Liu, M. Yu, H. Kim, Marta. Mameli, *Nat. Commun.* **2012**, *3*, 1182.
- [84] Y. Ma, V. Chechik, *Langmuir* **2011**, *27*, 14432.
- [85] C. J. Murphy, T. K. Sau, A. M. Gole, C. J. Orendorff, J. Gao, L. Gou, S. E. Hunyadi, T. Li, *J. Phys. Chem. B* **2005**, *109*, 13857.
- [86] L. G. Xu, H. Kuang, L. B. Wang, C. L. Xu, *J. Mater. Chem.* **2011**, *21*, 16759.
- [87] B. Nikoobakht, M. A. El-Sayed, *Langmuir* **2001**, *17*, 6368.
- [88] Q. Li, Y. Cao, in *Nanorods* (Eds. O. Yalçin), InTech, **2005**, Ch. 8.
- [89] L. Vigdeman, B. P. Khanal, E. R. Zubarev, *Adv. Mater.* **2012**, *24*, 4811.
- [90] L. Beqa, A. K. Singh, S. A. Khan, D. Senapati, S. R. Arumugam, P. C. Ray, *ACS Appl. Mater. Interfaces* **2011**, *3*, 668.
- [91] X. Huang, S. Neretina, M. A. El-Sayed, *Adv. Mater.* **2009**, *21*, 4880.
- [92] G. J. Nusz, S. M. Marinakos, A. C. Curry, A. Dahlin, F. Hook, A. Wax, A. Chilkoti, *Anal. Chem.* **2008**, *80*, 984.
- [93] A. Agarwal, S. W. Huang, M. O'Donnell, K. C. Day, M. Day, N. Kotov, S. Ashkenazi, *J. Appl. Phys.* **2007**, *102*, 064701.
- [94] X. Huang, I. H. El-Sayed, W. Qian, M. A. El-Sayed, *J. Am. Chem. Soc.* **2006**, *128*, 2115.
- [95] Y. Xiao, H. Hong, Z. M. Vyara, A. Javadi, W. Xu, Y. Yang, Y. Zhang, J. W. Engle, R. J. Nockles, W. Cai, D. A. Steeber, S. Gong, *Theranostics* **2012**, *2*, 757.
- [96] A. M. Alkilany, L. B. Thompson, S. P. Boulos, P. N. Sisco, C. J. Murphy, *Adv. Drug Deliv. Rev.* **2012**, *64*, 190.
- [97] A. K. Salem, P. C. Searson, K. W. Leong, *Nat. Mater.* **2003**, *2*, 668.
- [98] I. T. M. Liang, I-C. Lin, M. R. Whittaker, R. F. Minchin, M. J. Monteiro, *ACS Nano* **2010**, *4*, 403.
- [99] J. Shan, H. Tenhu, *Chem. Commun.* **2007**, 4580.
- [100] A. C. Balazs, T. Emrick, T. P. Russell, *Science* **2006**, *314*, 1107.

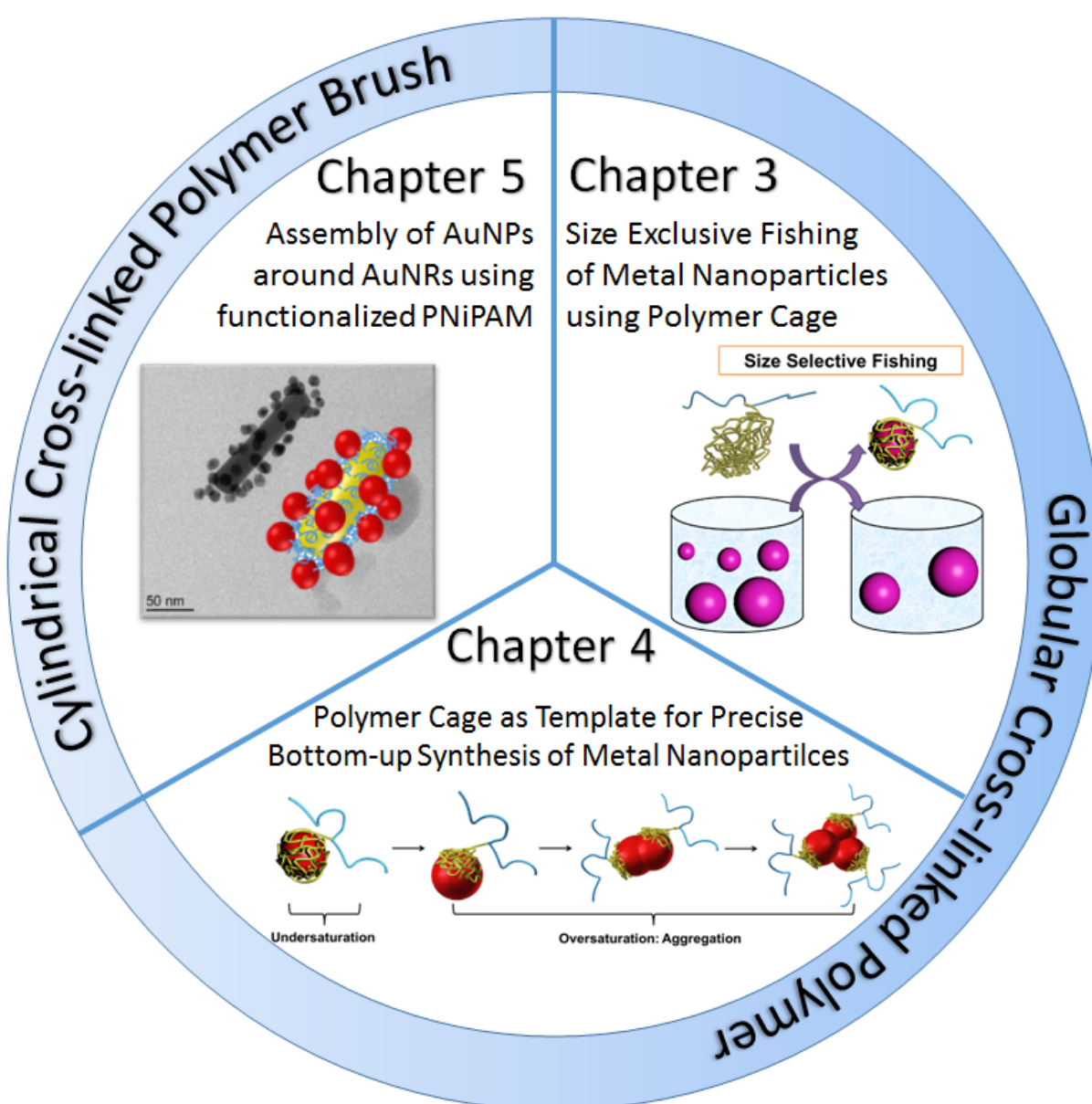
- [101] J. Tian, J. Jin, F. Zheng, H. Zhao, *Langmuir* **2010**, *26*, 8762.
- [102] A.-S. Duwez, P. Guillet, C. Colard, J.-F. Gohy, C.-A. Fustin, *Macromolecules* **2006**, *39*, 2729.
- [103] P. G. Nicholson, V. Ruiz, J. V Macpherson, P. R. Unwin, *Phys. Chem. Chem. Phys.* **2006**, *8*, 5096.
- [104] T. Nakamura, A. Tamura, H. Murotani, M. Oishi, Y. Jinji, K. Matsuishi, Y. Nagasaki, *Nanoscale* **2010**, *2*, 739.
- [105] E. Spain, T. E. Keyes, R. J. Forster, *Electrochim. Acta* **2013**, *109*, 102.
- [106] J. Q. Lu, S. S. Yi, *Langmuir* **2006**, *22*, 3951.
- [107] T. K. Mandal, M. S. Fleming, D. R. Walt, *Nano Lett.* **2002**, *2*, 3.
- [108] H. Gao, K. Matyjaszewski, *J. Am. Chem. Soc.* **2007**, *129*, 6633.
- [109] P. J. M. Stals, Y. Li, J. Burdyńska, R. Nicolaÿ, A. Nese, A. R. a Palmans, E. W. Meijer, K. Matyjaszewski, S. S. Sheiko, *J. Am. Chem. Soc.* **2013**, *135*, 11421.
- [110] K. Matyjaszewski, N. V Tsarevsky, *Nat. Chem.* **2009**, *1*, 276.
- [111] R. Saito, *Polymer* **2008**, *49*, 2625.
- [112] J. van Heijst, M. Corda, O. Lukin, *Polymer* **2015**, *70*, 1.
- [113] S. Koenig, V. Chechik, *Langmuir* **2006**, *22*, 5168.
- [114] L. Sun, R. M. Crooks, V. Chechik, *Chem. Commun.* **2001**, 359.
- [115] C. Boyer, M. R. Whittaker, C. Nouvel, T. P. Davis, *Macromolecules* **2010**, 1792.
- [116] A. M. Alkilany, P. K. Nagaria, M. D. Wyatt, C. J. Murphy, *Langmuir* **2010**, *26*, 9328.
- [117] D. A. Fleming, M. E. Williams, *Langmuir* **2004**, *20*, 3021.
- [118] F. Liu, S. Agarwal, *Macromol. Chem. Phys.* **2015**, *216*, 460.
- [119] H. Pletsch, L. Peng, F. Mitschang, A. Schaper, M. Hellwig, D. Nette, A. Seubert, A. Greiner, S. Agarwal, *Small* **2014**, *10*, 201.
- [120] S. Ehlert, S. M. Taheri, D. Pirner, M. Drechsler, H. W. Schmidt, S. Förster, *ACS Nano* **2014**, *8*, 6114.
- [121] J. Bai, Y. Li, S. Yang, J. Du, S. Wang, J. Zheng, Y. Wang, Q. Yang, X. Chen, X. Jing, *Solid*

- State Commun.* **2007**, 141, 292.
- [122] S. Malynych, I. Luzinov, G. Chumanov, *J. Phys. Chem. B* **2002**, 106, 1280.
- [123] R. Seoudi, A. A. Fouda, D. A. Elmenshawy, *Phys. B Condens. Matter* **2010**, 405, 906.
- [124] G. Zotti, B. Vercelli, A. Berlin, *Chem. Mater.* **2008**, 20, 6509.
- [125] J. Liu, T. Tanaka, K. Sivula, a. P. Alivisatos, J. M. J. Fréchet, *J. Am. Chem. Soc.* **2004**, 126, 6550.
- [126] J. J. Chiu, B. J. Kim, E. J. Kramer, D. J. Pine, *J. Am. Chem. Soc.* **2005**, 127, 5036.
- [127] J. Q. Lu, S. S. Yi, *Langmuir* **2006**, 22, 3951.
- [128] K. Matyjaszewski, *Macromolecules* **2012**, 45, 4015.
- [129] K. Gries, K. Bubel, M. Wohlfahrt, S. Agarwal, U. Koert, A. Greiner, *Macromol. Chem. Phys.* **2011**, 212, 2551.
- [130] M.-Q. Zhu, L.-Q. Wang, G. J. Exarhos, A. D. Q. Li, *J. Am. Chem. Soc.* **2004**, 126, 2656.
- [131] W. Shen, Q. Qiu, Y. Wang, M. Miao, B. Li, T. Zhang, A. Cao, Z. An, *Macromol. rapid commun.* **2010**, 31, 1444.
- [132] A. Glaria, M. Beija, R. Bordes, M. Destarac, J.-D. Marty, *Chem. Mater.* **2013**, 25, 1868.
- [133] R. M. Crooks, M. Q. Zhao, L. Sun, V. Chechik, L. K. Yeung, *Acc. Chem. Res.* **2001**, 34, 181.
- [134] S. Chakraborty, S. W. Bishnoi, V. H. Pérez-Luna, *J. Phys. Chem. C* **2010**, 114, 5947.
- [135] C. Krüger, S. Agarwal, A. Greiner, *J. Am. Chem. Soc.* **2008**, 130, 2710.
- [136] X. Liu, J. G. Worden, Q. Dai, J. Zou, J. Wang, Q. Huo, *Small* **2006**, 2, 1126.
- [137] Q. Huo, J. G. Worden, *J. Nanoparticle Res.* **2007**, 9, 1013.
- [138] X. Zhang, L. Liu, J. Tian, J. Zhang, H. Zhao, *Chem. Commun.* **2008**, 6549.
- [139] M. F. V. Sashuk, R. Hołyst, T. Wojciechowski, *J. Colloid Interface Sci.* **2012**, 375, 180.
- [140] B. Wang, B. Li, B. Zhao, C. Y. Li, *J. Am. Chem. Soc.* **2008**, 130, 11594.
- [141] J. H. Yoon, J. Lim, S. Yoon, *ACS Nano* **2012**, 6, 7199.
- [142] F. della Sala, E. R. Kay, *Angew. Chem.* **2015**, 127, 4261; *Angew. Chem. Int. Ed.* **2015**, 54, 4187.
- [143] J. P. Hermes, F. Sander, U. Fluch, T. Peterle, D. Thompson, R. Urbani, T. Pfohl, M. Mayor,

- J. Am. Chem. Soc.* **2012**, *134*, 14674.
- [144] T. Peterle, P. Ringler, M. Mayor, *Adv. Funct. Mater.* **2009**, *19*, 3497.
- [145] S. Bokern, K. Gries, H.-H. Görtz, V. Warzelhan, S. Agarwal, A. Greiner, *Adv. Funct. Mater.* **2011**, *21*, 3753.
- [146] K. Gries, M. El Helou, G. Witte, S. Agarwal, A. Greiner, *Polymer* **2012**, *53*, 1632.
- [147] L. Bai, X. Ma, J. Liu, X. Sun, D. Zhao, D. G. Evans, *J. Am. Chem. Soc.* **2010**, *132*, 2333.
- [148] R. a. Sperling, T. Pellegrino, J. K. Li, W. H. Chang, W. J. Parak, *Adv. Funct. Mater.* **2006**, *16*, 943.
- [149] Y. Zheng, T. Thai, P. Reineck, L. Qiu, Y. Guo, U. Bach, *Adv. Funct. Mater.* **2013**, *23*, 1519.
- [150] S. Bidault, F. J. G. De Abajo, A. Polman, *J. Am. Chem. Soc.* **2008**, *130*, 2750.
- [151] J.-Y. Chang, H. Wu, H. Chen, Y.-C. Ling, W. Tan, *Chem. Commun.* **2005**, 1092.
- [152] C. Sönnichsen, B. M. Reinhard, J. Liphardt, A. P. Alivisatos, *Nat. Biotechnol.* **2005**, *23*, 741.
- [153] X. Wang, G. Li, T. Chen, M. Yang, Z. Zhang, T. Wu, H. Chen, *Nano Lett.* **2008**, *8*, 2643.
- [154] Y. Kang, K. J. Erickson, T. A. Taton, *J. Am. Chem. Soc.* **2005**, *127*, 13800.
- [155] Z. Nie, D. Fava, E. Kumacheva, S. Zou, G. C. Walker, M. Rubinstein, *Nat. Mater.* **2007**, *6*, 609.
- [156] J. M. Romo-Herrera, R. a Alvarez-Puebla, L. M. Liz-Marzán, *Nanoscale* **2011**, *3*, 1304.
- [157] L. Xu, H. Kuang, C. Xu, W. Ma, L. Wang, N. a Kotov, *J. Am. Chem. Soc.* **2012**, *134*, 1699.
- [158] L. H. Tan, H. Xing, H. Chen, Y. Lu, *J. Am. Chem. Soc.* **2013**, *135*, 17675.
- [159] J. H. Yoon, Y. Zhou, M. G. Blaber, G. C. Schatz, S. Yoon, *J. Phys. Chem. Lett.* **2013**, *4*, 1371.
- [160] N. Gandra, A. Abbas, L. Tian, S. Singamaneni, *Nano Lett.* **2012**, *12*, 2645.
- [161] Z. Zhang, S. Zhang, M. Lin, *Analyst* **2014**, *139*, 2207.
- [162] X. Liu, Q. Dai, L. Austin, J. Coutts, G. Knowles, J. Zou, H. Chen, Q. Huo, *J. Am. Chem. Soc.* **2008**, *130*, 2780.
- [163] S. Pierrat, I. Zins, A. Breivogel, C. Sönnichsen, *Nano Lett.* **2007**, *7*, 259.
- [164] R. L. Truby, S. Y. Emelianov, K. A. Homan, *Langmuir* **2013**, *29*, 2465.

2. Overview of the Thesis

The overall concept of the following chapters is to develop versatile methods for the preparation of the complex polymer architectures based on nanoparticle templates. The basic approach was to cross-link the polymer building blocks on the surface of nanoparticles. The resulting globular cross-linked polymer cage (Chapter 3 and 4) was applied in the precise chemistry for the control of the size and functionality of the metal nanoparticles. Furthermore, the foundation for the future prospect to prepare more complex polymer architecture, such as the cylindrical polymer brush, has been established as explicated in Chapter 5.



The concept of each paper is briefly introduced in the following. The polymer cage, presented in Chapter 3 and 4, demonstrated the application of the cross-linked multi-dentate polymer in the precise chemistry regarding the control over stoichiometric functionality and size of the metal nanoparticles. The Polymer cage is namely a cross-linked network of thiol-moieties with defined size and capacity, but tethered with single exterior carboxyl-functionality. Due to its unique structure, the polymer cage was utilized as the “fishing net” in Chapter 3 to separate the pre-synthesized AuNPs within a certain size range from an aqueous dispersion containing polydisperse AuNPs. Moreover, the polymer cage acted as a universal template (Chapter 4) for the precise bottom-up synthesis of metal nanoparticles. The resulted nanoparticles not only grew under perfect control of the polymer cage but also was grafted with mono-functionality in a feasible way.

As the initial step to explore the possibility of building a cross-linked cylindrical polymer brush, Chapter 5 introduced a telechelic poly(*N*-isopropylacrylamide) (PNiPAM) as the building block for the polymer brush. For the cylindrical structure, AuNRs were used as the templates. The aim of this chapter was to demonstrate the homogeneous distribution of the PNiPAM grafted on the AuNRs. For this purpose, AuNPs were involved to indicate the location of PNiPAM. PNiPAM was firstly grafted on the AuNRs through its thiol-end, whereas the other amine-end together with the amide components attracted the AuNPs around AuNRs forming the satellite-like structure. The distribution of PNiPAM was therefore visualized by the assembly of AuNPs around AuNRs. The spatial distance between AuNPs and AuNRs and the resulting optical property could be tuned by the temperature.

Later, a concluding overview presented in Section 2.1–2.3 and in Section 2.4 the individual contribution to joint publications was given.

2.1 Polymer/Nanoparticle Hybrid Material for Precise Dimensions by Size Exclusive Fishing of Metal Nanoparticles

Z. Fan, M. Köhn Serrano, A. Schaper, S. Agarwal, A. Greiner, *Adv. Mat.* **2015**, 27, 3888-3893.

In Chapter 3, a polymer cage system was designed for separating the metal nanoparticles according to their sizes. The polymer cage, a cross-linked polymer network, exhibited defined size and structure and contained numerous thiol groups. The size separation of the metal

2. Overview of the Thesis

nanoparticle also called the “fishing” process was demonstrated by the biphasic ligand exchange reaction with Ct@AuNPs in different sizes. The polymer cage showed excellent control over the size of nanoparticles compared to the linear non-crosslinking polymer system.

The size and shape separation of metal nanoparticles often requires advanced separation techniques, e.g. ultrafiltration via viscosity or density gradient, electrophoresis, size exclusive chromatography. Instead of the separation techniques, the polymer cage can separate the desired nanoparticles regarding its size and immobilize them in the desired polymer matrix in one step.

The synthesis of polymer cage (**Figure 2.1 A**) based on the “grafting-around” approach, which describes the surface radical polymerization of vinyl-ligands on AuNP surface initiated by an external functionalized azo-initiator. This method yields nanoparticles coated with a cross-linked polymer shell (the polymer cage) with mono-functionality introduced by the initiator. After the mono-functionality (in this work: carboxylic acid) was converted into vinyl, the AuNPs were used as an artificial monomer for copolymerization with methyl methacrylate (MMA). After etching the gold core with sodium cyanate (NaCN), the polymer cage with tailored PMMA chain was obtained. According to the Raman spectroscopy and long-time stability of the cage stabilized AuNPs in the presence of the excess of dodecanethiol (DDT), the polymer cage was proven to be cross-linked by the disulfide bonds as well as the backbone crosslinking. After staining with osmium tetroxide (OsO₄), an empty globular structure of the polymer cage was observed in TEM micrographs (**Figure 2.1 B**).

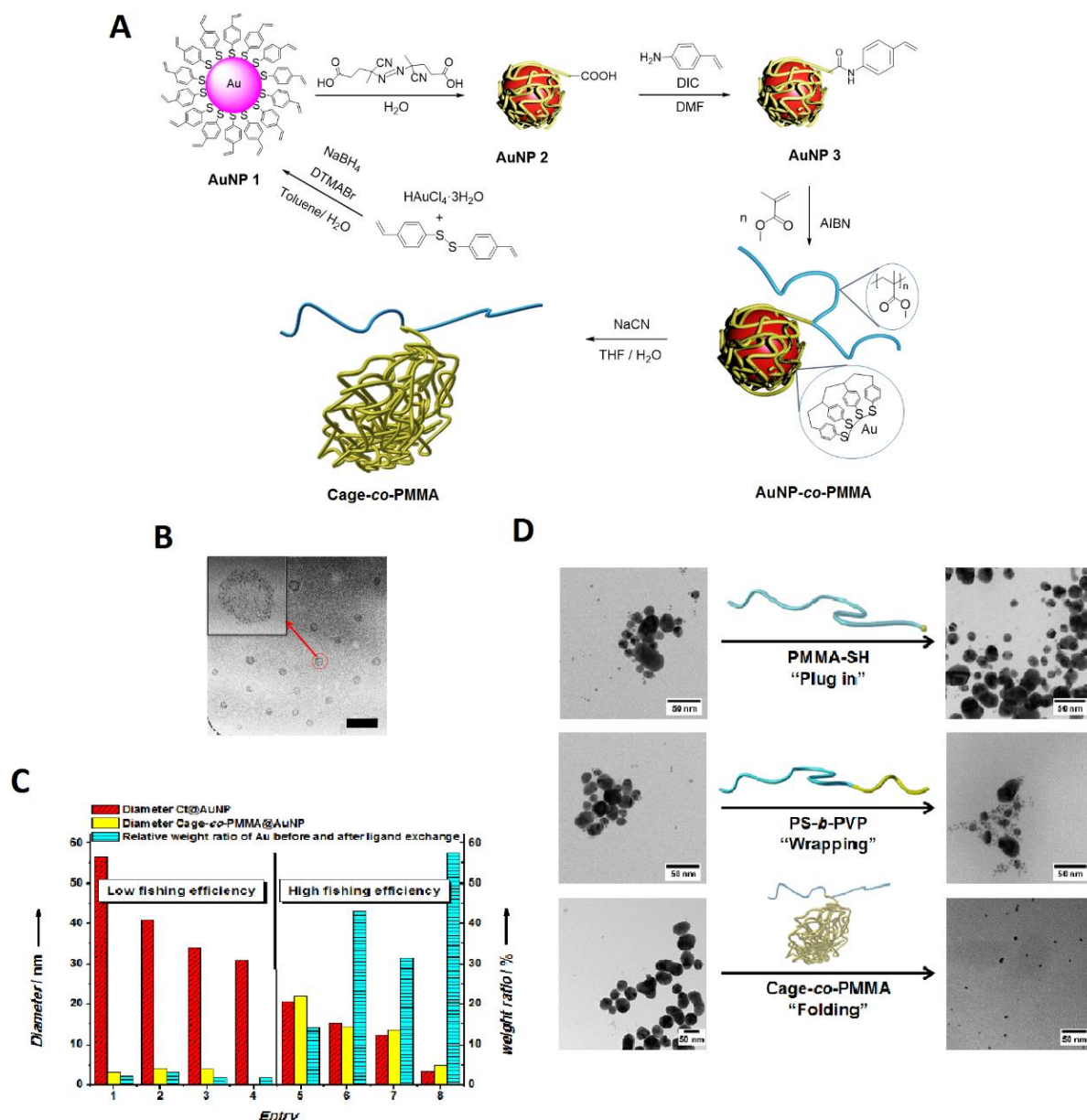


Figure 2.1. (A) Schematic illustration of the synthesis of Cage-co-PMMA based on the grafting-around approach. (B) TEM micrograph of the polymer cage stained with OsO_4 (Scale bar: 200 nm). (C) Qualitative and quantitative evaluation of the fishing process. The mean diameter of Ct@AuNP before fishing method (red column) was compared to that of AuNP in Cage-co-PMMA (yellow column) corresponding to the left y-axis. The relative weight ratio of Au atoms before and after the fishing process (blue column) was determined by ICP-OES (corresponding to the right y-axis).

For the fishing process, Ct@AuNPs of different sizes were used as fish in the aqueous phase, while the polymer cages were dissolved in the chloroform phase. Upon adding the phase transfer catalyst TOAB, the phase transfer of AuNPs occurred as the thiol groups are the stronger ligand for AuNPs compared to the citrates. The polymer cage was capable of extracting AuNPs under 15 nm in diameter with high efficiency and exclude nanoparticle above 30 nm. The smaller the AuNP is, the more efficient is the fishing process, which was

qualitatively characterized by UV-vis spectroscopy and TEM and quantitatively by ICP-OES (**Figure 2.1 C**).

The size selectivity of the polymer cage was verified compared to the other two polymer systems: the thiol-terminated linear PMMA (PMMA-SH) and diblock copolymer poly(styrene-*block*-4-vinylpyridine) (PS-*b*-PVP). The polyvinylpyridine (PVP) block acted as the non-crosslinked polymeric ligand wrapping around AuNPs. These two polymer systems for comparison had the ability to extract AuNPs up to 40 nm in diameter. To test the size selectivity of these three polymer systems, a mixed dispersion of Ct@AuNPs with mean diameters of 30 nm, 15 nm and 3 nm was used as "fish" for the ligand exchange reaction. In the organic phase containing PMMA-SH and PS-*b*-PVP AuNPs within all the three size ranges were found again as observed in TEM micrographs. In contrast, AuNPs over 30 nm were excluded from the polymer cage, which narrowed the size distribution of the fished AuNPs. Representative TEM images of the three polymer systems before and after the fishing process are shown in **Figure 2.1 D**. The difference in the size selectivity is attributed to the behavior of the polymers at the interface during the ligand exchange reaction. The end-functionalized linear polymer (PMMA-SH) undergoes a "plug in" mechanism, as the thiol-end of each polymer chain is directly immobilized onto AuNP surface without any influence on the conformation of PMMA chain. In the case of the diblock copolymer, each PVP block can wrap around the nanoparticle surface independently. The polymer cage, considered as a "mesh bag" consisted of cross-linked polymer chains, undergoes the "fold" process as approaching the nanoparticles during the ligand exchange reaction.

A cross-linked polymer cage with distinct size was prepared based on the concept of "grafting-around" approach, which was used as "fishing-net" for size selective separation of metal nanoparticles. The polymer cage exhibits higher size selectivity than other linear, non-crosslinked polymer systems. The concept of the polymer cage can be further applied to the synthesis of novel materials with desired size, shape, functionality and arrangement.

2.2 Polymer Cage as Universal Tools for the Precise Bottom-up Synthesis of Metal Nanoparticles

Z. Fan, X. Chen, M. Köhn Serrano, H. Schmalz, S. Rosenfeldt, S. Förster, S. Agarwal, A. Greiner, *Angew. Chem.* **2015**, *127*, 14747-1475; *Angew. Chem. Int. Ed.* **2015**, *54*, 14539-14544.

In Chapter 4, a facile bottom-up synthesis of metal nanoparticles with precisely controlled size and functionality was developed using the polymer cage as the template. The polymer cage consisting of the cross-linked macromolecules with pendant thiol groups was prepared by etching the gold core from the copolymer that was made by the "grafting-around" approach (see Chapter 2.1). The polymer cage exhibited a certain capacity and, therefore, was used as a template to control perfectly the growth of metal nanoparticles in the sub-5 nm range. Moreover, various mono-functionalized precious metal nanoparticles, such as silver-, palladium-, and platinum-nanoparticles were prepared in the polymer cage using the precise bottom-up synthesis.

The template-mediated synthesis generates nanomaterials with defined size and results in high reproducibility. For the precise preparation of metal nanoparticles, organic cages and dendrimers with defined structure and anchor groups are the most attractive templates. However, the size of nanoparticles prepared in such templates was limited to 3 nm due to the restriction of the template size. Hence, broadening the size range of applicable nanoparticles for the precise bottom-up synthesis remains a challenge.

The polymer cage was utilized as a universal template for the in-situ synthesis of mono-functionalized metal nanoparticles in the sub-5 nm size range. As earlier mentioned in Section 2.1, the polymer cage tailored with PMMA chain was synthesized via the "grafting-around" approach. Metal nanoparticles were prepared in the polymer cage by reducing the corresponding metal salts using sodium borohydride (NaBH_4) in the presence of the polymer cage, namely the in-situ reduction route. The concept of the precise bottom-up synthesis is presented in **Figure 2.2 A**.

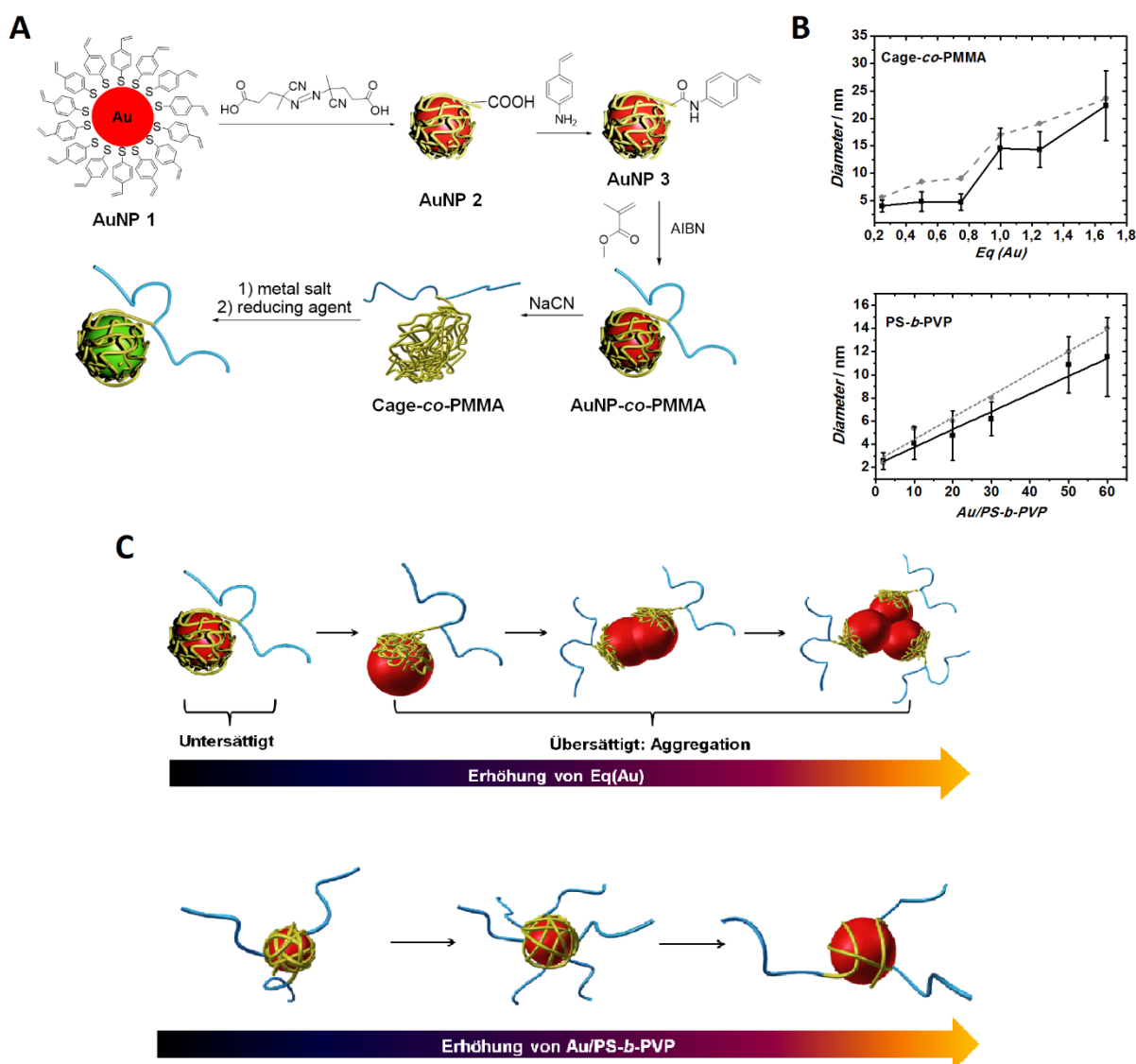


Figure 2.2. (A) Schematic illustration of the preparation of Cage-co-PMMA and subsequent bottom-up synthesis of metal nanoparticles. (B) Plot of AuNP size evolution in Cage-co-PMMA (top) and PS-b-PVP (bottom). Data points derived from TEM are presented as solid black trace while the gray dash trace represents the SAXS results. (C) Schematic illustration of size evolution of AuNPs in Cage-co-PMMA (top) and in PS-b-PVP (bottom). © 2015 Z. Fan et al.

To explore the underlying mechanism of nanoparticle evolution inside the polymer cage, the molar ratio of gold (HAuCl_4) versus cage in the feed varied. Based on the combined results derived from TEM, UV-vis spectroscopy, and SAXS (**Figure 2.2 B**), monodisperse spherical AuNPs in the sub-5 nm range were obtained, when the gold feed did not exceed the capacity of the polymer cage. As soon as the polymer cages were saturated or even in deficiency, AuNPs agglomerated immediately and thus the polymer cage lost its control over the AuNP growth. The size evolution of AuNPs in the diblock copolymer matrix (PS-*b*-PVP) differs significantly from that in the polymer cage. The size and size distribution of the PS-*b*-PVP

coated AuNPs increased continuously with the gold in the feed. No sudden agglomeration of AuNPs was observed.

The nanoparticle evolution is significantly dependent on the structure of the polymer matrices, as depicted in **Figure 2.2 C**. Due to the cross-linking, the polymer cage is less flexible than the linear block copolymer. As the gold amount exceeds the total capacity of the polymer cage, the polymer cage is only able to cover a limited surface area of AuNPs. Therefore, AuNPs tend to agglomerate at the bare area without the protection of the polymer cage and formed the irregular-shaped agglomerates afterwards. In the case of the linear block copolymer, the PVP block wrapped homogeneously around the AuNPs, which allowed the AuNPs grew without defined size control over a wide Au/PS-*b*-PVP range.

Since the sulfur compound is the known ligand for various precious metal nanoparticles, the polymer cage was successfully applied as the template for synthesis of Ag-, Pd-, and PtNPs. The as-prepared nanoparticles exhibited narrow size distribution. Furthermore, anisotropic Pd- and PtNPs were formed in the polymer cage, whose formation was attributed to the flexibility of the polymer cage.

In conclusion, the polymer cage was presented as a novel template for the bottom-up synthesis of mono-functionalized metal nanoparticles. For the future work, the polymer cage can be modified with variable sizes and functionalities, which is suitable for various nanoparticles. The concept of the precise bottom-up synthesis enables the design and fabrication of novel metal nanomaterials in a feasible way.

2.3 Assembly of Gold Nanoparticles on Gold Nanorods using Functionalized Poly(*N*-isopropylacrylamide) as Polymeric “Glue”

Z. Fan, M. Tebbe, A. Fery, S. Agarwal, A. Greiner, *Particle & Particle System Characterization* **2016**, submitted

In Chapter 5, a bi-end-functionalized linear polymer α -amino- ω -thiol-poly(*N*-isopropylacrylamide) (PNiPAM) was used to assemble AuNPs around AuNRs forming a satellite-like assembly (AuNP@AuNR) with controllable spatial distance. PNiPAM also known as the lower critical solution temperature (LCST)-type polymer, was involved as the polymer “glue” that was responsible for the interparticle linking of the gold building blocks. The

2. Overview of the Thesis

AuNP@AuNR assembly and its thermal behavior were characterized by TEM, DLS and UV-vis spectroscopy.

The bi-end-functional PNiPAM was synthesized by reversible addition-fragmentation chain transfer (RAFT) polymerization that was subsequently followed by hydrazinolysis (**Figure 2.3 A**). The RAFT-polymerization of *N*-isopropylacrylamide was carried out using the chain transfer agent phthalimidomethyl trithiocarbonate, yielding PNiPAM end-capped with phthalimide and trithiocarbonate groups. The end-groups were reduced to amine and thiol using the nucleophilic hydrazine, respectively. After the hydrazinolysis, PNiPAM exhibited a cloud point at 32 °C.

The gold building blocks used in this work was cetyltrimethylammonium bromide (CTAB)-stabilized AuNRs (CTAB@AuNR, length 88 ± 16 nm, width 26 ± 7 nm, aspect ratio 3.4) and citrate-stabilized AuNPs (Ct@AuNP) with a mean diameter of 12 ± 3 nm. The preparation of the assembly of these gold building blocks is illustrated in **Figure 2.3 B**. PNiPAM was firstly immobilized onto the AuNR surface through replacing the CTAB ligands by the thiol ends of PNiPAM. After this ligand exchange reaction, PNiPAM shell was observed to coat around the AuNRs. The hydrodynamic radius of PNiPAM grafted AuNRs (PNiPAM@AuNR) was decreased above the cloud point of PNiPAM as a result of the collapsed PNiPAM shell. The next step was to assemble the AuNPs around AuNRs through the ligand exchange of citrate ligands with nitrogen compound of PNiPAM. The two-step ligand exchange reactions generated satellite-like AuNP@AuNR assemblies in high yield, as the AuNPs were homogeneously distributed around the AuNRs as derived from the TEM images. Meanwhile, the AuNP@AuNR assembly presented unique optical property. When compared to the UV-vis spectrum of PNiPAM coated AuNRs, the low energy resonance of the AuNP@AuNR assembly was significantly red-shifted of about 85 nm and meanwhile an additional shoulder appeared at around 590 nm indicating the dipolar plasmonic coupling effect. **Figure 2.3 C** shows the representative UV-vis spectra and TEM micrographs of gold building blocks as well as the AuNP@AuNR assembly. Furthermore, the grafting density of AuNPs on AuNRs was tuned through adjusting the AuNP/AuNR ratio in the feed.

2. Overview of the Thesis

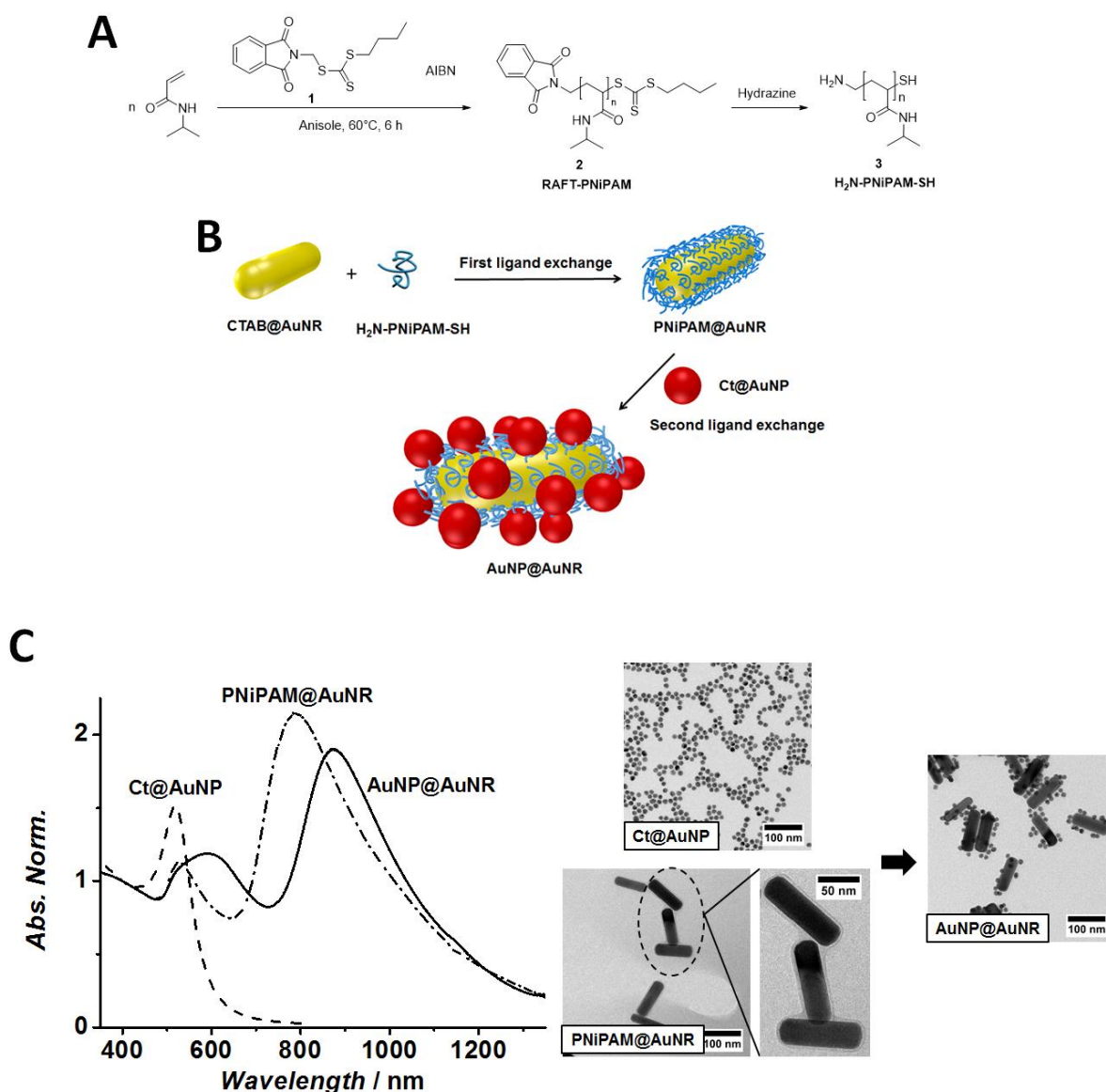


Figure 2.3. (A) Synthesis of α -amino- ω -thiol-poly(*N*-isopropylacrylamide) (PNiPAM). (B) Schematic illustration of preparation of the AuNP@AuNR assembly via a two-step ligand exchange reaction. (C) Left: UV-vis spectra of Ct@AuNP (dash trace), PNiPAM@AuNR (dash-dot trace) and AuNP@AuNR (solid trace). Right: Representative TEM micrographs of Ct@AuNP, PNiPAM@AuNR, and AuNP@AuNR.

The thermal behavior of the AuNP@AuNR assembly was characterized using cryo-TEM, UV-vis spectroscopy, and DLS. Cryo-TEM did not verify the change of the spatial gap between AuNPs and AuNRs, as the temperature was modulated above and under the cloud point of PNiPAM. Nevertheless, UV-vis spectroscopy and DLS has confirmed the thermal sensibility of the AuNP@AuNR assembly. The drawback of this type of assembly is that its thermal responsibility was lost after three consecutive heating-cooling circles, which could to be caused by the partially wrapping of the PNiPAM chain around AuNPs.

The functionalized PNIPAM was used as the polymer glue to assemble AuNPs around AuNRs in a spatial controllable distance. The plasmonic property of the assembly was tuned by the grafting density of the AuNPs on the AuNR surface. Moreover, due to the thermoresponsive polymeric interlayer, the optic property of the assembly changes with the temperature.

Contribution to joint publications

The publications presented in this thesis were achieved by collaborative projects performed by researchers from different backgrounds. The contribution of individual authors of the joint publications is given as follows.

Chapter 3

Polymer/Nanoparticle Hybrid Materials of Precise Dimensions by Size-Exclusive Fishing of Metal Nanoparticles

*Ziyin Fan, Melissa Köhn Serrano, Andreas Schaper, Seema Agarwal, and Andreas Greiner**

I synthesized and characterized the polymer cage, the thiol-terminated PMMA, and the citrate stabilized gold nanoparticles. I carried out all the ligand exchange reactions and wrote the manuscript. Melissa Köhn Serrano provided the diblock copolymer PS-*b*-PVP with characterizations, was involved in the scientific discussion and proofread the manuscript. Andreas Schaper carried out the TEM measurement of the polymer cage stained with OsO₄. Furthermore, ICP-OES was conducted by the external analysis center BayCEER. Seema Agarwal participated in the scientific discussion and proofread the manuscript. Andreas Greiner was involved as the supervisor of the project, in the scientific discussion and proof-reading of the manuscript.

Chapter 4

Polymer Cages as Universal Tools for the Precise Bottom-Up Synthesis of Metal Nanoparticles

*Ziyin Fan, Xuelian Chen, Melissa Köhn Serrano, Holger Schmalz, Sabine Rosenfeldt, Stephan Förster, Seema Agarwal, and Andreas Greiner**

I carried out the synthesis of the polymer cage and the bottom-up synthesis of nanoparticles in the polymer cage as well as in the PS-*b*-PVP matrix. I performed the TEM and UV-vis measurements and analysis and wrote part of the manuscript. Xuelian Chen carried out the SAXS measurements and data analysis. Furthermore, she wrote the part of the paper regarding the SAXS analysis. Holger Schmalz, Sabine Rosenfeldt, and Stephan Förster were involved in the scientific discussion and proofreading of the manuscript. Andreas Greiner supervised the project, participated in the scientific discussion and proofread the manuscript.

Chapter 5

Assembly of Gold Nanoparticles around Gold Nanorods using Functionalized Poly(*N*-isopropylacrylamide) as Polymeric “Glue”

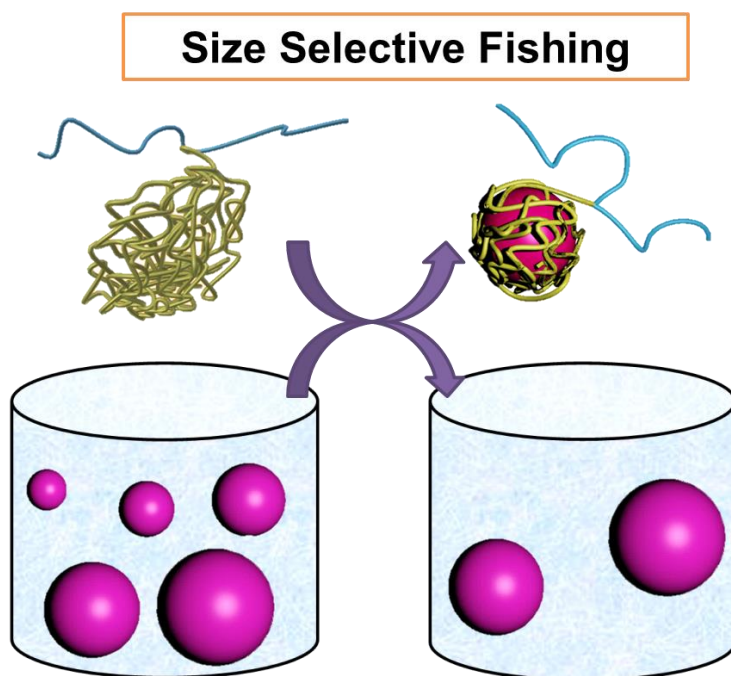
*Ziying Fan, Moritz Tebbe, Andreas Fery, and Andreas Greiner**

I synthesized the polymer, and the citrate stabilized AuNPs, while Moritz Tebbe provided the CTAB stabilized AuNRs. I performed the functionalization of the AuNRs and subsequent assembly of the gold building blocks. I carried out the characterizations, data analysis and wrote the manuscript. Moritz Tebbe was involved in data analysis, scientific discussion and proof-reading of the manuscript. Andreas Fery participated in the scientific discussion and proofread the manuscript. Andreas Greiner supervised the project, participated in the scientific discussion and proofread the manuscript.

Chapter 3

Polymer/Nanoparticle Hybrid Materials of Precise Dimensions by Size Exclusive Fishing of Metal Nanoparticles

*Ziyin Fan, Melissa Köhn Serrano, Seema Agarwal, and Andreas Greiner**



Polymer cages are designed for the formation of polymer/nanoparticle hybrid materials with precise dimensions by size selective separation of metal nanoparticles in a single step. They are synthesized by etching of gold nanoparticles from polymer templates prepared by “grafting around” method. The separation process is demonstrated as biphasic ligand exchange reaction that is completed within one minute with high separation efficiency and size selectivity.

The size and shape of metal nanoparticles are crucial for material properties in various applications e. g. in optics and catalysis.^[1–7] The direct synthesis of nanoparticles with precisely defined size and size distribution is still a challenge. Many efforts have been carried out to provide versatile separation techniques for size sorting of nanoparticles, such as membrane filtration,^[4,5] size exclusion chromatography,^[6,7] gel electrophoresis,^[8] asymmetric-flow field flow fraction,^[9,10] and ultracentrifugation using viscosity^[11] or density gradient.^[16] The use of novel polymer materials for size selective separation of metal nanoparticles is highlighted in the present work. In contrast to already known separation techniques for nanoparticles, our method separates directly the nanoparticles of desired size and thereby creates novel hybrid materials. A straight-forward “fishing” process is demonstrated for the separation of gold nanoparticles (AuNPs) as model with high size selectivity using polymer cages of predetermined size quasi as “mesh bag”. Previously, we have developed a novel concept for the preparation of core (AuNP)/shell (polymer) nanoparticles with predetermined functional groups by radical polymerization of thiol-functionalized vinyl monomers on the surface of AuNPs.^[13,14] This method is defined as “grafting around” of polymer on nanoparticle surfaces. As ligand, 4-vinylbenzenethiol was immobilized onto the AuNP surface using Brust-Schiffrin method^[15–17] using dodecyl trimethylammonium bromide (DTMABr) as phase transfer catalyst. Subsequent free radical polymerization using carboxylic-acid-functionalized azo-initiator enabled mono-functionalization of AuNP with carboxylic acid group within single step. The surface polymerization should be much faster than the decomposition of the initiator. Therefore, the overall concentration of the radical was low, which enabled the stoichiometric functionalization of AuNP. The monofunctionality of AuNP was demonstrated by C. Krüger et al. using coupling reactions.^[13] The “grafting around” method generates nanoparticles coated with single polymer chain with precisely controlled functionality. This provides in an easy way a new type of polymerizable vinyl monomers with AuNPs as substituents at the vinyl bond and their copolymers with other conventional vinyl monomers like methyl methacrylate (MMA) (**Figure 3.1**). The utility of such interesting copolymers with AuNPs as substituents along the polymer chain for the size-selective separation of metal particles is discussed in the present work. The AuNPs from the core of the substituents were etched for getting an empty polymer cage with coordinating thiol groups hanging on PMMA backbone (Cage-co-PMMA). The size-selective fishing of metal nanoparticles was carried out using these specially designed polymer cages for the separation of nanoparticles from a mixture of particles of different sizes. It

should be mentioned as well that refilling of previously etched polymer hollow capsules, prepared differently, were used for the encapsulation of uranyl acetate without any report on encapsulation efficiency.^[18]

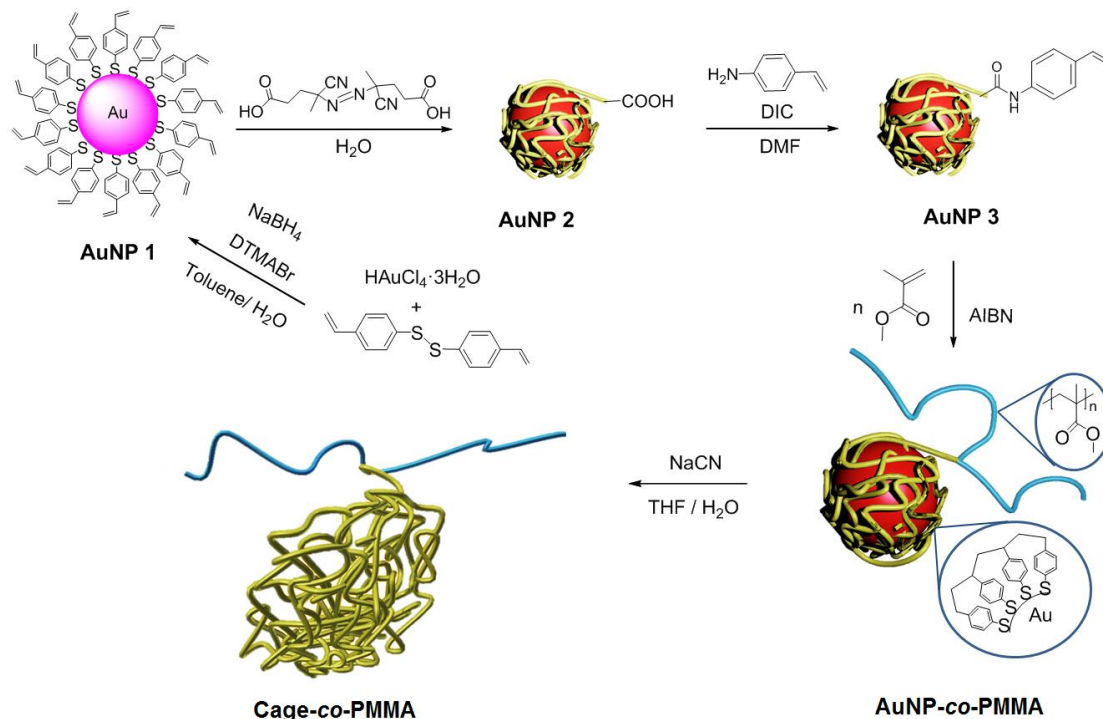


Figure 3.1. Schematic illustration of synthesis of polymer cage with attached PMMA chain (Cage-co-PMMA). AuNP covered with vinyl-monomer (AuNP **1**) was prepared using Brust-Schiffrin method. Then using the “grafting around” method, AuNP **2** with single carboxylic acid functionality was obtained, which reacted with 4-vinylaniline to generate the vinyl substituted AuNP **3** for copolymerization with MMA. PMMA (blue line) bound AuNP (red sphere) were used as templates for the formation of polymer cages (yellow surrounding mesh) by selective removal of AuNP core using NaCN as etching agent. The cage was presented as a cross-linked “mesh bag”-like polymer network. The size here does not correspond to the real values.

In the present work as a concrete example, the monovinyl-substituted AuNPs (AuNP **3**) were made by reaction of carboxylic acid group on single-polymer-chain-stabilized AuNP (AuNP **2**) surface with 4-vinylaniline using *N,N'*-diisopropylcarbodiimide (DIC) as coupling catalyst (Figure 3.1). The AuNP core had a diameter of 4.5 ± 2.3 nm, as measured by transmission electron microscopy (TEM) (Supporting Information). Further, the copolymers (AuNP-co-PMMA) of MMA with small amounts (2 wt%) of AuNP **3** were made by radical polymerization using azobisisobutyronitrile (AIBN) as initiator, according to our previously published procedure.^[19] The reason for copolymerization with MMA will be explained below. The details for preparation and characterization of the copolymer are presented in the Supporting Information.

The selective etching of the AuNPs from the core of the core-shell substituent of the copolymer by NaCN at room temperature led to the formation of empty polymer cages of poly(4-vinylbenzenethiol) covalently attached as side chains to the PMMA backbone (Figure 3.1, Cage-co-PMMA). The quantitative removal of AuNP for the formation of empty polymer cages was proven by UV-vis spectroscopy and elemental analysis (Supporting Information).

To deduce the morphology of the polymer cage, the AuNP template was etched after the “grafting around” process (AuNP **2**) leaving the pure polymer cage without attached PMMA chain. The TEM image in **Figure 3.2a** presents a globular shape of the empty polymer cage stained with osmium tetroxide (OsO_4) at its dry state. Moreover, the polymer cage exhibited high content of disulfide instead of thiolate, as measured by Raman spectroscopy. The disulfide bond was responsible for the cross-linking of the polymer cage (Figure 3.2b). The average diameter of the empty polymer cage was of 40 nm, which was larger than the size of the AuNP core. It is speculated that the disulfide cross-linking not only occurred within a single polymer cage but also with each other. Thus, the polymer cage in Figure 3.2a was revealed as a large cross-linked polymer network.

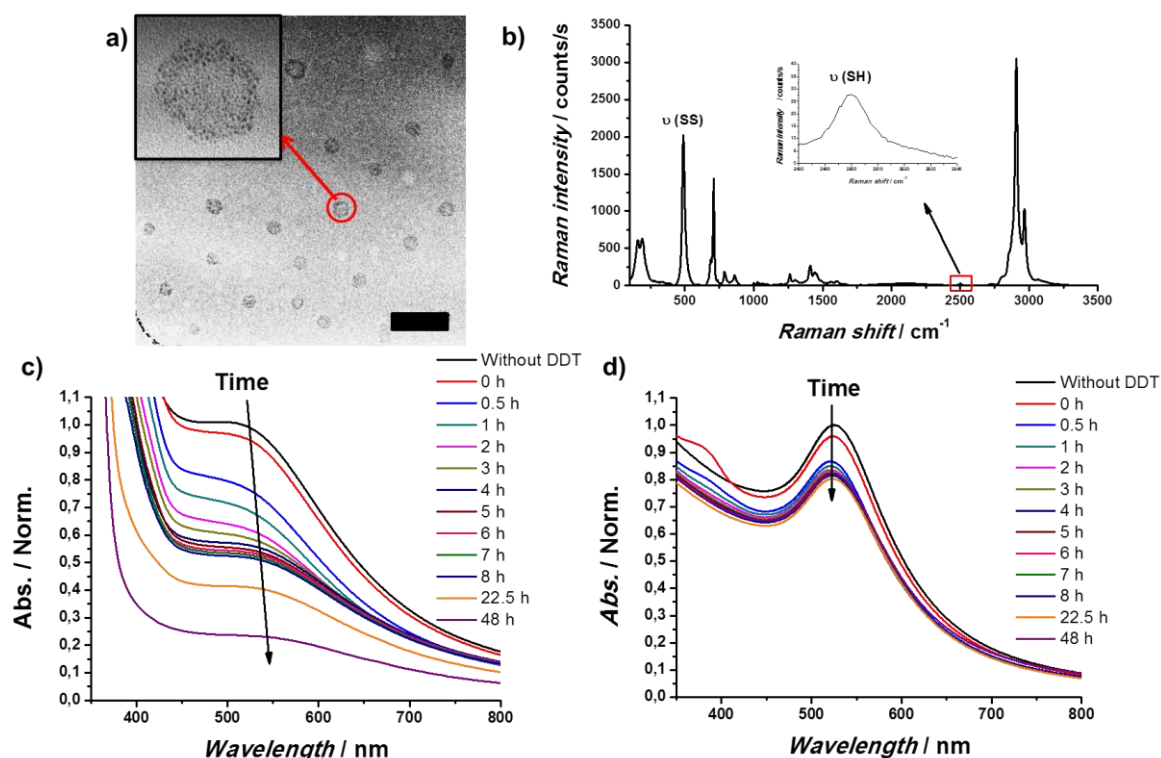


Figure 3.2. Characterization of the polymer cage. a) TEM image of the polymer cage stained with OsO_4 , scale bar is 200 nm. b) Raman spectrum of the polymer cage. The disulfide bond was found at a shift of 500 cm^{-1} with high intensity, while the thiol bond was nearly found at 2500 cm^{-1} . 2c) UV-vis spectra of AuNP **1** upon adding excess DDT in DMAc with time. d) UV-Vis spectra of AuNP **2** upon adding excess of DDT in DMAc with time.

To evaluate the shell cross-linking of the “grafting around” process, we investigated the stability of AuNPs before (AuNP **1**) and after (AuNP **2**) surface polymerization upon adding excess of dodecanethiol (DDT), according to the study of Schacher and co-workers.^[20] The thiolate ligand can be replaced by the competing ligand DDT in excess. DDT coated AuNPs are not stable in *N,N'*-dimethylacetamide (DMAc), which leads to the precipitation of AuNPs. Based on this principle, the UV-vis measurements were carried out for AuNP dispersions (AuNP **1** and **2**) in DMAc charged with excess of DDT and recorded every hour. The corresponding UV-vis spectra of AuNP **1** and **2** are shown in Figure 3.2c and d. The absorption maxima of AuNP **1** decreased continuously to 22 % of the initial value after 48 hours when a black brown precipitate was already observed at the bottom of the cuvette (for pictures see the Supporting Information). On the contrary, AuNP **2** after surface polymerization showed much higher stability in the presence of DDT in DMAc than AuNP **1**. The absorption maxima of AuNP **2** decreased only to 80 % of the initial value in the first hour and kept almost constant accompanying slightly decline after 48 hours. Comparable results were obtained by Schacher and co-workers to study the shell cross-linking efficiency of the thiolate-terminated block copolymer on AuNP surface. In our case, the difference of the stability between AuNP **1** and **2** provided convincing arguments not only for the successful polymerization of vinyl-ligand around AuNP but also for the shell cross-linking of the polymer chain during the “grafting around” process. The cross-linking of the macromolecule could be attributed to the chain transfer reaction or entanglement. As for AuNP **2**, DDT could attach to the vacant space in between the single cross-linked macromolecule around AuNP surface. This led to the change of the electronic structure and consequently the decline of the absorption maxima. In combination with the results from TEM and Raman analysis, we consider that the polymer cages consist of cross-linked macromolecules that result from disulfide bonds and backbone cross-linking. The polymer cage is similar to a “mesh bag” without a rigid structure.

Citrate stabilized gold nanoparticles (Ct@AuNP) of different sizes ranging from 57 nm to 3 nm prepared by using the Turkevich method^[21] were used as representative examples for the size selective separation of metal nanoparticles. The size selective nanoparticle separation process was carried out using ligand exchange reactions in a biphasic chloroform/water system (polymer cages in chloroform and Ct@AuNP in water) using the phase transfer catalyst (tetraoctyl ammonium bromide (TOAB)) at room temperature. As the polymer cage contained numerous thiolate and disulfide groups that have high affinity to AuNP surface, the citrate

ligand was replaced by thiol groups. The ligand exchange occurred at the interface, where AuNPs were partially covered by citrates and the polymer cages. Due to the lowered surface electrostatic repulsion, AuNPs tended to agglomerate in this stage at the interface.^[22] To prevent the agglomeration and increase the interface, TOAB was used as the phase transfer catalyst as is well-documented for the interfacial ligand exchange reactions involving silver nanoparticles.^[23] The ligand exchange reaction was followed by the transfer of the characteristic red-violet color of AuNPs from the aqueous phase to the organic phase. The organic phase was separated followed by precipitation in methanol and vacuum drying. The covalently bound PMMA chains served quasi as an “auxiliary grip for polymer cages” that increased the hydrophobicity and enabled the completion of the ligand exchange within one minute. As a side remark: PMMA chains were used here as a model polymer matrix and could be replaced by any other radical polymerizable hydrophobic monomer, which opens a wide field for fabrication of novel hybrid materials with nanoparticles of definite size.

The efficiency of the separation process was analyzed qualitatively by UV-vis spectroscopy and TEM and quantitatively by inductive coupled plasma-optical emission spectroscopy (ICP-OES). Experiments were carried out both with AuNPs of discrete size range with relatively narrow size distribution and also using a mixture of particles with different size and size distribution. The characterization of Ct@AuNP and AuNP after size separation (cage-co-PMMA@AuNP) using discrete sized Ct@AuNP is presented in **Table 3.1**.

Table 3.1. Analysis data of AuNP before and after size separation using discrete sized nanoparticles with narrow distribution.

Entry	Ct@AuNP			AuNP in polymer cages		
	Diameter ^{a)} [nm]	Absorption ^{b)} [nm]	Abs. ^{b)}	Diameter ^{a)} [nm]	Absorption ^{b)} [nm]	Abs. ^{b)}
1	56.5±10.2	532	0.463	3.1±0.7	545	0.005
2	41.0±7.3	536	0.988	4.1±2.1	568	0.011
3	34.2±5.6	532	0.943	3.9±1.1	567	0.005
4	30.9±5.6	530	0.952	--- ^{c)}	577	0.007
5	20.5±3.2	522	0.774	22.1±3.4	526	0.024
6	15.3±1.8	519	0.780	14.5±2.4	525	0.075
7	12.4±1.9	517	0.813	13.6±2.1	524	0.078
8	3.4±0.6	506	0.666	5.0±2.1	526	0.127

^{a)} The diameter of AuNPs was determined from TEM images. For each sample, more than 200 particles were measured. ^{b)} Absorption peak and absorbance (Abs.) were determined from UV-vis spectra. ^{c)} In this sample, only three particles were found in TEM images.

Using Ct@AuNP with a diameter over 30 nm (entries 1–4, Table 3.1), neither absorption of the organic phase typical for AuNPs nor AuNPs with corresponding size were observed in UV-vis spectra and in TEM images (**Figure 3.3b**), separately. ICP-OES measurements also showed negligible transfer, i.e. only 3.4% of gold in polymer cages in the organic phase. (Figure 3.3c) This indicated that the majority of AuNPs from the water phase could not undergo ligand exchange reaction since they did not fit into the polymer cages. As shown in Figure 3.3a, conspicuous increase of the absorption maxima of AuNP in polymer cages occurred by samples of Ct@AuNP smaller than 20 nm (entries 5–8, Table 3.1). Here, quantitative analysis of the AuNP in polymer cages by ICP-OES showed that 14.4% of gold was transferred from the aqueous phase to the chloroform phase. The polymer cages were most suitable for the ligand exchange reactions with AuNPs (Ct@AuNP) with diameter under 15 nm, since they fitted well into the polymer cages in the chloroform phase. This was verified by TEM analysis as AuNPs of the aqueous phase were identified after ligand exchange reaction in the chloroform phase. Correspondingly, ICP-OES analysis showed a large uptake of gold by the chloroform phase as high as 57.6%.

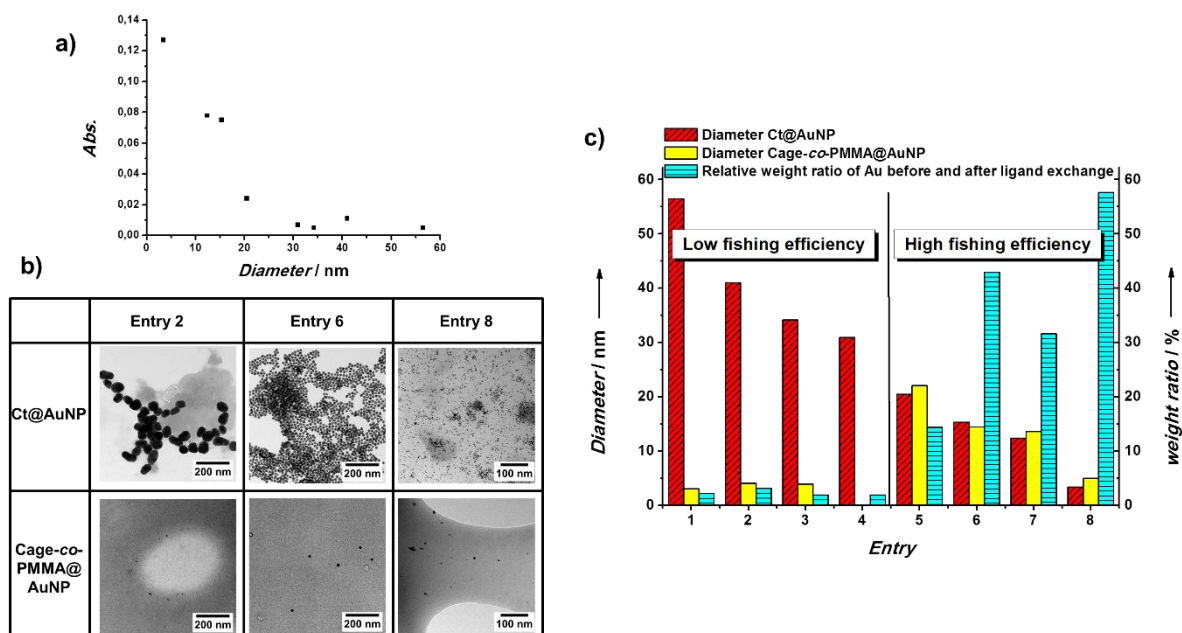


Figure 3.3. Characterization of the ligand exchange reaction of Ct@AuNP using Cage-co-PMMA. a) Plot of absorbance of AuNP in polymer cages after separation process in relationship with mean diameter of corresponding Ct@AuNPs before separation process. Polymer cages size selectively separated AuNPs of diameter under 30 nm. b) Representative TEM images of Ct@AuNP (top) and AuNP stabilized in the polymer cages (bottom) of entry 2, 6, and 8. c) Qualitative and quantitative evaluation of the separation of AuNP. Comparison of size of Ct@AuNP (left red textured column, corresponding to the left y-axis) and Cage-co-PMMA@AuNP (middle yellow column, corresponding to the left y-axis) derived from the TEM analysis and the relative weight ratio of gold atoms before and after the separation process as determined by ICP-OES (right blue textured column, corresponding to the right y-axis).

So far, only the separation of AuNPs by polymer cages was applied to AuNP dispersions with a discrete size range of AuNP and a relatively narrow size distribution. Further, the concept was verified for the size selective separation by taking a mixture of nanoparticles with different sizes: 31 nm, 15 nm and 3 nm in equal volume ratio. Comparing the TEM images before and after ligand exchange reaction, preferentially small AuNPs were found in the organic phase whereas the oversized gold nanoparticles (31 nm) were not found (**Figure 3.4**). The polymer cages clearly filtered off the bigger nanoparticles and thereby providing decreased size and size distribution of AuNPs after the separation process.

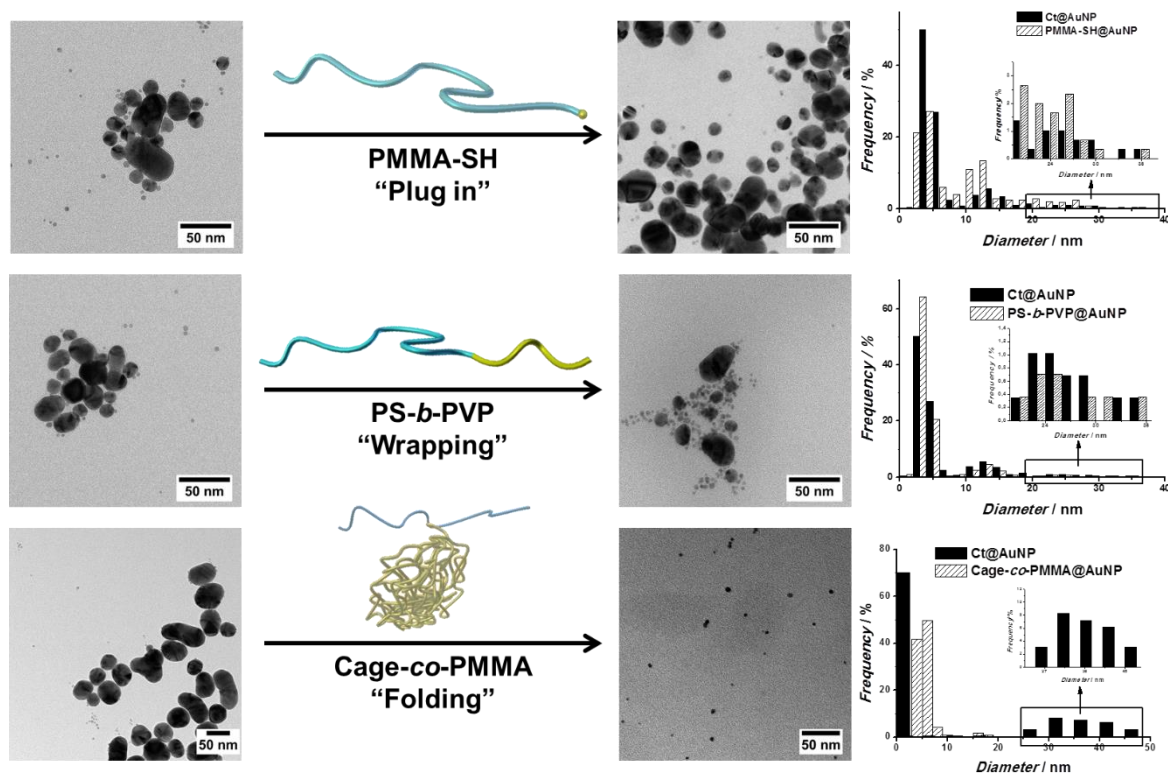


Figure 3.4. Comparison of size selectivity of PMMA-SH, PS-*b*-PVP and Cage-co-PMMA. Using Ct@AuNP mixture (30, 15, and 3 nm) as precursor (representative TEM images at the left-hand side), PMMA-SH and PS-*b*-PVP showed no size selectivity of AuNP after ligand exchange reaction. AuNPs of all three sizes were found in the organic phase. The size distribution (graphs at the right-hand side) of both samples had no change. As for Cage-co-PMMA, no large AuNPs (30 nm) were found in the TEM images and the size distribution was narrowed after ligand exchange reaction.

To verify the size selectivity of the polymer cage, we chose a linear polymer of thiol-terminated PMMA (PMMA-SH) and a block copolymer of polystyrene-*block*-poly(4-vinylpyridine) (PS-*b*-PVP) as comparison groups. PMMA-SH extracted AuNPs up to 30 nm quantitatively from aqueous phase to chloroform phase. Even larger AuNPs of about 40 nm were found in the organic phase when using Ct@AuNP with corresponding sizes in the aqueous phase. However, only a small portion of AuNPs was transferred to the organic phase, as a significant amount of AuNPs were aggregated at the interface (for TEM images and UV-vis spectra see the Supporting Information). Taking the mixture of Ct@AuNP of different sizes (30 nm, 14 nm and 4 nm) as precursors, all sizes of AuNP were found in the organic phase after ligand exchange. Hence, there was no change in size distribution after ligand exchange reaction using PMMA-SH.

In the case of PS-*b*-PVP, the pyridine moiety of the PVP block served as ligand for AuNPs. In contrast with the polymer cage, the PVP block is a non-cross-linked linear polymer that can

wrap the AuNPs. The PS block increased the hydrophobicity of the PS-*b*-PVP stabilized AuNP (PS-*b*-PVP@AuNP), which enabled the ligand exchange reaction in a biphasic system. The PS block consists of 77 units, while the repeat unit of PVP block is calculated with 34 units. The full characterization of PS-*b*-PVP is shown in the Supporting Information. The ligand exchange reactions using Ct@AuNP with discrete sizes were carried out under similar conditions. Quantitative phase transfer of AuNP up to 30 nm was also observed as in the case of PMMA-SH. Meanwhile, PS-*b*-PVP showed no size selectivity when using a mixture of Ct@AuNP in size as precursor (Figure 3.4). As a side mark, the polymer cage is not restricted to the thiolate ligand. Other ligands containing nitrogen like 4-vinylpyridine or sulfur can be fabricated into polymer cage for separation of AuNPs. The “fishing” concept is therefore universal for applications in different nanoparticle systems with suitable ligands.

Neither PMMA-SH nor PS-*b*-PVP had the ability to narrow the size distribution of AuNP by means of a biphasic ligand exchange. We attribute the difference of the size selectivity between these three types of polymers to how the polymer chain behaves at the interface during ligand exchange. PMMA-SH owns one thiol endgroup that can replace the citrate ligands. The rest PMMA chain has no direct interaction with AuNP. We define this behavior as “plug in” process. As for PS-*b*-PVP, each 4-vinylpyridine unit in a single chain can be attached to the AuNP surface by ligand exchange. As a consequence, the whole PVP chain is relatively fixed on the AuNP surface and interacts with AuNP surface in an equilibrium, which is called as “wrapping” process. The polymer cage is less flexible than PMMA-SH or PS-*b*-PVP due to disulfide and backbone cross-linking. Considering the polymer cage as a “mesh bag”, then the cage should be open and nonrigid in order to encapsulate AuNP. As shown in the TEM image (Figure 3.2a), the polymer cage forms spherical pad at its dry state with a mean radius of about 20 nm, the theoretical coating area is calculated of $800\pi \text{ nm}^2$ under the assumption that the pad consists of a double layer. This corresponds to the surface area of AuNP with a diameter of 20 nm. In other words, the polymer cage is only able to encapsulate AuNPs under 20 nm, which was proven by ligand exchange reaction using Ct@AuNPs with discrete sizes. If the polymer cage encounters a AuNP of 30 nm at interface, it could not expand or immobilize around the AuNP beyond its limit of coating area. This long-time insufficient coating hindered the transfer reaction of AuNP to the organic phase due to the lack of hydrophobicity. The large AuNPs were thus agglomerated because of the decrease of the electrostatic repulsion before

they could be immobilized into the organic phase. As a result we denote the ligand exchange using the polymer cage as “folding” process.

Copolymers of core (AuNP)/shell (polymer) monovinyl-functionalized nanoparticles and MMA as templates for polymer cages were synthesized using the “grafting around” method, where thiol-functionalized vinyl monomers were radically polymerized around the AuNP surface. Polymer cages with a distinct size were prepared by etching of AuNPs from the copolymer. The polymer cages were cross-linked as derived from TEM, Raman spectroscopy, and study of the long-time stability of the AuNP after “grafting around” process using UV-vis spectroscopy. The empty polymer cages were used for size-selective separation of AuNPs with an excellent size resolution by comparison with PMMA-SH and PS-*b*-PVP. The separation efficiency was verified qualitatively by UV-vis spectroscopy and TEM and quantitatively by ICP-OES. Despite numerous nice reports regarding nanoparticle syntheses with narrow size distribution,^[24] the size selective separation of nanoparticles is of great importance, which offers a broad choice for polymer/nanoparticle hybrid material synthesis with precisely designed dimensions. Although the polymer cage showed better size selectivity than linear (PMMA-SH) and block copolymer (PS-*b*-PVP), AuNPs under 15 nm cannot be separated efficiently. Future work is focused on altering of the size and exploring the 3D structure of the polymer cage to achieve higher selectivity and efficiency. Surely, the concept of size-selective separation of nanoparticles with polymer cages, in analogy to fishing, is not restricted to metal nanoparticles when other ligands in the polymer cages are provided. So far, the polymer cage has been successfully applied to the silver nanoparticle system (data not shown). The next is now to expand selective separation of nanoparticles with respect to shape and chemistry for making hybrid materials in a single step. Based on the separation concept, novel materials could be created e.g. by arrangement of different metal nanoparticles in the same polymer cages, which offers interesting perspective for new property profiles.

Acknowledgements

The authors are indebted to Fonds der Chemischen Industrie and SFB 840 for financial support.

References

- [1] P. K. Jain, K. S. Lee, I. H. El-Sayed, M. A. El-Sayed, *J. Phys. Chem. B* **2006**, *110*, 7238.
- [2] R. Kaminker, M. Lahav, L. Moitiei, M. Vartanian, R. Popovitz-Biro, M. A. Iron, M. E. van der Boom, *Angew. Chem.* **2010**, *122*, 1240; *Angew. Chem. Int. Ed.* **2010**, *49*, 3280.
- [3] C. R. Raj, T. Okajima, T. Ohsaka, *J. Electroanal. Chem.* **2003**, *543*, 127.
- [4] S. F. Sweeney, G. H. Woehrle, J. E. Hutchison, *J. Am. Chem. Soc.* **2006**, *128*, 3190.
- [5] E. Krieg, H. Weissman, E. Shirman, E. Shimoni, B. Rybtchinski, *Nat. Nanotechnol.* **2011**, *6*, 141.
- [6] G.-T. Wei, F.-K. Liu, C. R. C. Wang, *Anal. Chem.* **1999**, *71*, 2085.
- [7] F.-K. L. G.-T. Wei, *J. Chromatogr. A* **1999**, *836*, 253.
- [8] C. S. M. Hanauer, S. Pierrat, I. Zins, A. Lotz, *Nano. Lett.* **2007**, *7*, 2881.
- [9] F. R. L. Calzolari, D. Gilliland, C. P. García, *J. Chromatogr. A* **2011**, *1218*, 4234.
- [10] D.-H. Tsai, T. J. Cho, F. W. DelRio, J. Taurozzi, M. R. Zachariah, V. A. Hackley, *J. Am. Chem. Soc.* **2011**, *133*, 8884.
- [11] P. Qiu, C. Mao, *Adv. Mater.* **2011**, *23*, 4880.
- [12] L. Bai, X. Ma, J. Liu, X. Sun, D. Zhao, D. G. Evans, *J. Am. Chem. Soc.* **2010**, *132*, 2333.
- [13] C. Krüger, S. Agarwal, A. Greiner, *J. Am. Chem. Soc.* **2008**, *130*, 2710.
- [14] S. Bokern, K. Gries, H.-H. Görtz, V. Warzelhan, S. Agarwal, A. Greiner, *Adv. Funct. Mater.* **2011**, *21*, 3753.
- [15] M. Brust, M. Walker, D. Bethell, D. J. Schiffrin, R. Whyman, *J. Chem. Soc., Chem. Commun.* **1994**, 801.
- [16] L. M. Liz-Marzán, *Chem. Commun.* **2013**, *49*, 16.
- [17] P. J. G. Goulet, R. B. Lennox, *J. Am. Chem. Soc.* **2010**, *132*, 9582.
- [18] J. Fan, J. J. Bozzola, Y. Gao, *J. Colloid Interface Sci.* **2002**, *254*, 108.
- [19] K. Gries, M. El Helou, G. Witte, S. Agarwal, A. Greiner, *Polymer* **2012**, *53*, 1632.
- [20] C. Hörenz, T. Rudolph, M. J. Barthel, U. Günther, F. H. Schacher, *Polym. Chem.* **2015**, *6*, 5633.

- [21] P. C. S. J. Turkevich, J. Hiller, *Discuss. Faraday Soc.* **1951**, *11*, 55.
- [22] M. Karg, N. Schelero, C. Oppel, M. Gradzielski, T. Hellweg, R. von Klitzing, *Chemistry* **2011**, *17*, 4648.
- [23] H. Pletsch, L. Peng, F. Mitschang, A. Schaper, M. Hellwig, D. Nette, A. Seubert, A. Greiner, S. Agarwal, *Small* **2014**, *10*, 201.
- [24] K. Sohn, F. Kim, K. C. Pradel, J. Wu, Y. Peng, F. Zhou, J. Huang, *ACS Nano* **2009**, *3*, 2191.

Supporting Information

**Polymer / Nanoparticle Hybrid Materials of Precise Dimensions by Size
Exclusive Fishing of Metal Nanoparticles**

Keywords: polymer hybrids, gold nanoparticle, grafting around, ligand exchange

*Ziying Fan, Melissa Koehn, Seema Agarwal and Andreas Greiner**

Contents:

1. Chemicals
2. Instrumentation
3. Polymer Cage
4. Thiol-terminated Poly(methyl methacrylate) (PMMA-SH)
5. Polystyrene-block-poly-4-vinylpyridine (PS-*b*-PVP)
6. Citrate Stabilized Gold Nanoparticle (Ct@AuNP)
7. Ligand exchange of Ct@AuNP with polymer cages
8. Ligand exchange of Ct@AuNP with PMMA-SH
9. Ligand exchange of Ct@AuNP with PS-*b*-PVP

1. Chemicals

Chloroauric acid trihydrate ($\text{HAuCl}_4 \cdot 3\text{H}_2\text{O}$), trisodium citrate (Na_3Ct), sodium borohydride (NaBH_4), dodecanethiol (DDT), styrene, 4-vinylpyridine, 1,1'-diphenylethylene (DPE), and tetraoctylammonium bromide (TOAB) were purchased from Sigma-Aldrich. 4,4'-Azobis(4-cyanovaleric acid), dodecyl trimethylammonium bromide (DTMABr), 4-dimethylaminopyridine, *N,N'*-diisopropylcarbodiimide (DIC), azobisisobutyronitrile (AIBN), and 4-vinylaniline were purchased from Alfa Aesar. *sec*-Buthyllithium (*sec*-BuLi, 1,4 M) was purchased from Acros and used as received. Styrene, 4-vinylpyridine and 1,1'-diphenylethylene (DPE) were first dried over di-*n*-butylmagnesium, triethylaluminium, and calcium hydride and then condensed at reduced pressure under nitrogen. AIBN was recrystallized from Et_2O . Tetrahydrofuran (THF) was dried over Solvona® for two days and distilled under argon atmosphere. All the other solvents were purified by distillation at reduced pressure.

2. Instrumentation

The samples of citrate stabilized gold nanoparticle (Ct@AuNP) for **UV-vis spectroscopy** were measured in aqueous phase as prepared. The samples of AuNP in polymer cages were prepared in THF at a concentration of 4 g/L. The samples of AuNP stabilized with thiol terminated poly(methyl methacrylate) (PMMA-SH) and polystyrene-*block*-poly-4-vinylpyridine (PS-*b*-PVP) were measured in chloroform. The UV-Vis spectra were recorded using a two-beam-photometer JASCO with a quartz glass cuvette.

Transmission electron microscopy (TEM) samples were prepared by dripping the nanoparticle containing THF solution upon a carbon-covered copper grid (Carbon Support Films, 300 mesh, Quantifoil). The TEM images were performed using ZEISS EM922 Omega with an acceleration voltage of 200 kV.

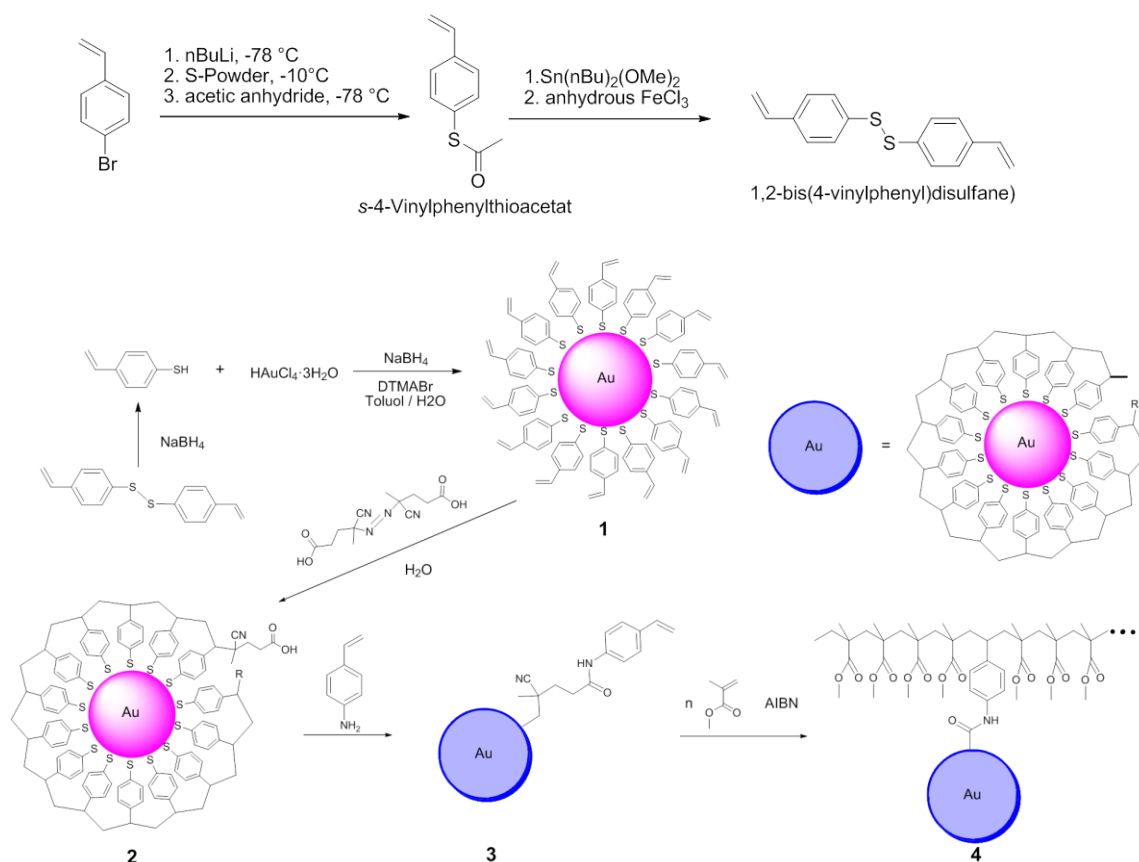
The samples of Ct@AuNP for **ICP-OES** were measured in aqueous phase as prepared. The samples of polymer cages stabilized AuNPs were first treated with aqua regia. The measurements were carried out using VARIAN VIASTA-PRO simultaneous ICP-OES in radial viewed plasma with purged polychromator configurations.

Elemental analysis was carried out by analytical service facility of department of chemistry in Phillips-University Marburg. Gold was determined by atomic absorption spectroscopy

NMR spectra were measured in CDCl_3 on a Bruker AMX300 spectrometer. Chemical shifts were referred to the solvent residue signal.

3. Polymer Cage

The polymer cage was prepared by the selective etching of the gold core from the AuNP template. The AuNP template was prepared by polymerization of 4-vinylbenzenethiol around AuNP surface. During the “grafting around” step, each AuNP was wrapped by a single macromolecule of poly(4-vinylbenzenethiol) carrying a carboxylate functionality introduced by the azo-initiator. As for the polymer cages with attached PMMA chain for ligand exchange, the carboxylate group on the AuNP template was further converted to vinyl group that enabled copolymerization with MMA. The generated copolymer is noted as AuNP-co-PMMA. The total synthesis of AuNP-co-PMMA is shown in Scheme S3.1.



Scheme S3.1. Synthesis of vinyl-carrying ligand for AuNP template and copolymer of AuNP template with MMA (AuNP-co-PMMA **4**).

3.1 Synthesis of *S*-4-Vinylphenyl thioacetate

n-BuLi (6.87 mL, 1.6 M in hexane, 11.0 mmol, 1.00 eq) was slowly added to a solution of *p*-bromostyrene (2.02 g, 11.0 mmol, 1.00 eq) in 50 mL THF/hexane (1:1) at -78 °C under argon atmosphere. The reaction mixture was stirred at -78 °C for 1.5 hours. Sulfur powder (352 mg, 11.0 mmol, 1.00 eq) was added in one portion. The reaction mixture was warmed to -10 °C and stirred for 30 min. After cooling to -78 °C, acetic anhydride (1.03 mL, 11.0 mmol, 1.00 eq) was added. After stirring at -78 °C for 2 hours, the reaction mixture was quenched with 25 mL water and left to warm to the room temperature, then extracted with Et₂O (30 mL). The combined organic phase was washed with 50 mL brine and dried over MgSO₄. The filtrate was concentrated in vacuum. The residue was purified by column chromatography (Et₂O : hexane = 1:10) and yielded 96 mg *s*-4-vinylphenylthioacetate (5.4 mmol, 49%) as colorless oil.

¹H NMR (300.1 MHz, CDCl₃, 25 °C) δ = 2.42 (s, 3H, CH₃), 5.32 (dd, ²*J*(C,H) = 0.7 Hz, ³*J*(C,H) = 10.9 Hz, 1H, CH=CH₂), 5.80 (dd, ²*J*(C,H) = 0.7 Hz, ³*J*(C,H) = 17.6 Hz, 1H, CH=CH₂), 6.72 (dd, ³*J*(C,H) = 17.6 Hz, ³*J*(C,H) = 10.9 Hz, 1H, CH=CH₂), 7.40 (m, 4H, ArH) ppm. ¹³C NMR (75 MHz, CDCl₃, 25 °C) δ = 193.9 (C=O), 138.7 (ArC), 135.9 (CH=CH₂), 134.5 (ArC), 127.0 (ArC), 126.8 (ArC), 115.3 (CH=CH₂), 30.1 (CH₃) ppm.

3.2 Synthesis of 1,2-bis(4-vinylphenoldisulfane)

Dibutyltindimethoxide (860 mg, 2.92 mmol, 0.65 eq) and *s*-4-vinylphenylthioacetate (800 mg, 4.48 mmol, 1.00 eq) were dissolved in 50 mL THF. After stirring at room temperature for 2 hours, anhydrous FeCl₃ (648 mg, 5.84 mmol, 1.30 eq) was added and the reaction mixture was stirred at room temperature overnight. The solution was poured into ice and extracted with Et₂O. The combined organic phase was washed with NaOH solution (15 mL, 10 M) and then with water until pH = 7. The solvent was concentrated in vacuum. Recrystallization from hexane/Et₂O delivered 212 mg (35%) of product as yellow solids.

¹H-NMR (300.1 MHz, CDCl₃) δ = 5.26 (dd, ²*J*(C,H) = 0.6 Hz, ³*J*(C,H) = 10.9 Hz, 2H, CH=CH₂), 5.73 (dd, ²*J*(C,H) = 0.6 Hz, ³*J*(C,H) = 17.6 Hz, 2H, CH=CH₂), 6.72 (dd, ³*J*(C,H) = 17.6 Hz, ³*J*(C,H) = 10.9 Hz, 2H, CH=CH₂), 7.39 (dd, ³*J*(C,H) = 8.4 Hz, ⁴*J*(C,H) = 33.4 Hz, 10H, ArH) ppm. ¹³C NMR (75 MHz, CDCl₃, 25 °C) δ = 136.7 (ArC), 136.3 (ArC), 135.9 (CH=CH₂), 128.0 (ArC), 127.0 (ArC), 114.3 (CH=CH₂) ppm.

3.3 Synthesis of 4-vinylbenzenethiol stabilized AuNP (1)

HAuCl₄·3H₂O (174 mg, 0.44 mmol, 1.00 eq) was dissolved in 50 mL of deionized water. DTMABr (604 mg, 1.95 mmol, 4.45 eq) was added in one portion. The orange reaction mixture was stirred at room temperature for 15 min. After adding 50 mL of toluene and 1,2-bis(4-vinylphenyl)disulfide (96 mg, 0.36 mmol, 0.80 eq) the mixture was stirred at room temperature for another 15 min. A fresh prepared aqueous solution of NaBH₄ (186 mg, 1.95 mmol, 9.98 eq, 50 mL) was added dropwise and the mixture was stirred at room temperature for 16 hours. The organic phase was separated and the dark purple aqueous phase was washed with 20 mL of toluene. The aqueous phase was directly used for the following step.

3.4 “Grafting around” of 4-vinylbenzenethiol on AuNP surface (2)

In a solution of NaOH (12 mg, 0.28 mmol, 2.00 eq) in 200 mL of deionized water 4,4'-azobis(4-cyanovaleric acid) (39.0 mg, 0.14 mmol, 1.00 eq) was added. This initiator solution was added to the aqueous dispersion of AuNP 1. The combined solution was degassed with Argon-inlet for 1 hour and polymerized at 40 °C for 3 days. The dark purple product was collected by centrifugation (8000 rpm, 30 min, room temperature) and washed three times with 30 mL of water. For further reaction, the product was not dried completely to prevent agglomeration.

3.5 Synthesis of vinyl-mono-functionalized AuNP (3)

N,N'-diisopropylcarbodiimide (200 µL, 1.284 mmol, 1.50 eq) was added to the dispersion of AuNP 2 in 5 mL of DMF. After stirring at room temperature for 1 hour, 4-vinylaniline (100 µL, 0.856 mmol, 1.00 eq) was added. After stirring 18 hours, the product was precipitated from 50 mL methanol, collected by centrifugation (8000 rpm, 30 min) and washed with methanol three times. The product was dried in vacuum at room temperature.

3.6 Copolymerization of AuNP with MMA (AuNP-co-PMMA 4)

Methyl methacrylate (833 mg, 8.32 mmol, 98 wt%) was added to the dispersion of AuNP 3 (17 mg, 2 wt%) in DMF. The concentration of MMA in DMF was set at 1 M. Then 105 µL of AIBN solution in DMF (0.032 g/mL) was added. The reaction mixture was degassed with Argon-inlet for 30 min and polymerized at 80 °C for 5 h. The product was precipitated from 300 mL

of methanol and collected by centrifugation (8000 rpm, 10 min, room temperature). After washing three times with methanol, the purple copolymer was dried in vacuum at 40 °C for 48 h. $M_n = 33000 \text{ g mol}^{-1}$, $M_w = 43500 \text{ g mol}^{-1}$, $PDI = 1.31$.

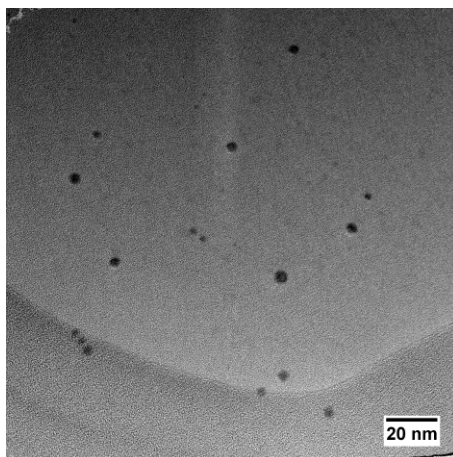


Figure S3.1. Representative TEM image of copolymer of AuNP with MMA as template for polymer cages.

3.7 Synthesis and characterization of polymer cages

To a solution of AuNP-co-PMMA (200 mg, 8.0 mg Au, 0.04 mmol Au, 1.0 eq) in THF an aqueous solution of NaCN (9.2 mg, 0.19 mmol, 4.6 eq) was added. The reaction mixture was stirred open to the air at room temperature for 24 hours. The characteristic color of AuNPs faded slowly indicating that the AuNPs were etched from the cages. The product was precipitated from 100 mL methanol and collected by centrifugation (8000 rpm, 10 min). After washing the white residue with methanol three times, the product was dried at 40 °C under 50 mbar.

Characterization:

Elemental analysis: C 59.55%, H 8.27%. No Au was detected.

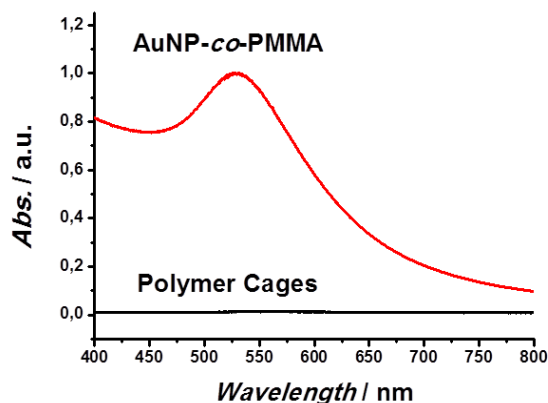


Figure S3.2 UV-Vis spectra of AuNP-co-PMMA as template for polymer cages before etching process (red trace) and polymer cages after etching process (black trace). The disappearance of absorption band of AuNPs indicated the successful removal of AuNPs.

3.8 Verification of the Cross-linking of the Polymer Cage

The cross-linking of the polymer cage was verified by UV-vis measurements of vinyl stabilized AuNP **1** and AuNP **2** after surface polymerization in the presence of excess of dodecanethiol (DDT) in DMAc. After 48 hours black precipitate was observed at the bottom of the cuvette of AuNP **1** dispersion, while the AuNP **2** dispersion was stable. (Figure S3.3)

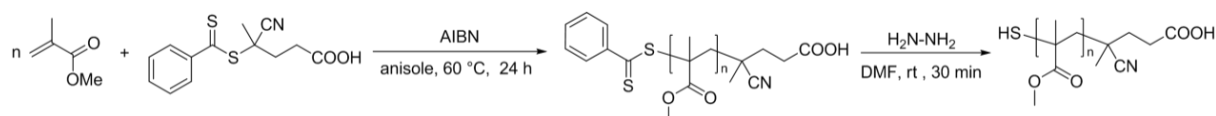


Figure S3.3. Photos of AuNP **1**(left) and **2** (right) dispersion in DMAc with excess of DDT after 48 hours.

4. Thiol-terminated Poly(methyl methacrylate) (PMMA-SH)

PMMA-SH was prepared by a two-step synthesis. In the first step, PMMA with trithiolcarbonate end was generated by RAFT polymerization. In the second step, the

trithiolcarbonate group was converted to thiol by aminolysis using hydrazine as nucleophile and antioxidant. (Scheme S3.2)



Scheme S3.2. Synthesis of PMMA-SH.

4.1 RAFT polymerization of PMMA (PMMA-RAFT)

MMA (2.102 g, 21.0 mmol, 500.0 eq), 4-cyano-4-(phenylcarbonothioylthio)pentanoic acid (11.7 mg, 0.042 mmol, 1.0 eq) and AIBN (3.9 mg, 0.024 mmol, 0.56 eq) were dissolved in 9.5 mL of anisole. The reaction mixture was degassed with argon inlet at 0 °C for 60 min. The polymerization was carried out at 60 °C for 24 hours. The polymer was diluted with THF and precipitated in MeOH. The procedure was repeated two times. The product was collected by centrifugation and then dried in vacuum at 45 °C overnight.

4.2 Hydrazinolysis (PMMA-SH)

PMMA-RAFT (787 mg, 0.032 mmol, 1.0 eq) was dissolved in 8 mL of DMF. The solution was degassed with argon inlet for 30 min. Hydrazine hydrate (8.0 mg, 0.158 mmol, 5.0 eq) was added at room temperature in one portion. The reaction mixture turned colorless in 10 min. After stirring at room temperature for 2 hours, the product was precipitated in excess of 1.2 M HCl aqueous solution. The collected product was dissolved in THF and precipitated in MeOH. The sample was washed with MeOH two times and dried in vacuum at 45 °C overnight.

4.3 Characterization

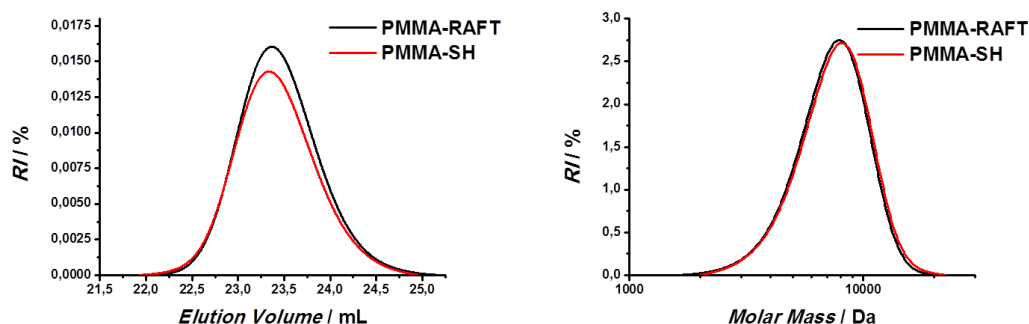


Figure S3.4. GPC chromatogram (left: elution volume, right: molecular weight) of PMMA-RAFT (black trace) and PMMA-SH (red trace).

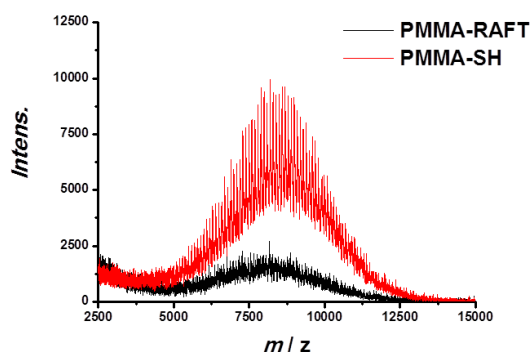


Figure S3.5. MALDI-TOF mass spectra of PMMA-RAFT (black trace) and PMMA-SH (red trace).

Table S4.1. Summary of characterization data of PMMA-RAFT and PMMA-SH.

Sample		Mn [Da]	Mw [Da]	PDI
PMMA-RAFT	GPC	6800	7680	1.13
	MALDI-TOF	8080	8460	1.05
PMMA-SH	GPC	6960	7880	1.13
	MALDI-TOF	8310	8560	1.03

5. Polystyrene-*block*-poly-4-vinylpyridine (PS-*b*-PVP)

PS-*b*-PVP was prepared by a sequential anionic living polymerization using *sec*-BuLi as initiator. The reaction was conducted in a 500 mL reactor at -78 °C. 1 mL of *sec*-BuLi was injected into 400 mL of abs. THF and the reaction solution turned yellow. The THF solution was warmed to room temperature before the reaction started. After adding 2.41 mL (3.6 mmol, 1.48 M, 1 eq.) of *sec*-BuLi, 29.6 g (284 mmol, 79 eq.) of styrene were transferred into the reactor over an ampule. The reaction solution turned orange due to the formation of styryl anion. After vigorous stirring for 10 min, a sample of polystyrene-precursor (PS-precursor) was taken for NMR and SEC analysis. Upon adding 0.63 mL (3.6 mmol, 1 eq.) of 1,1'-Diphenylethylene (DPE) for end capping of the styryl anion, the color of the solution turned deep red. After stirring for 30 min, 15.3 g (145 mmol, 40 eq.) of 4-vinylpyridine was added. In one hour, the reaction was terminated by degassed methanol. After warming up to room temperature, PS-*b*-PVP was

precipitated from pentane. The PS-precursor has 77 repeating units derived from the molecular weight measured by GPC in THF. The units of 4-vinylpyridine of 34 was calculated by NMR spectrum. The molecular weight of PS-*b*-PVP was calculated of 11600 g/mol. The polydispersity (PDI) of the block copolymer was characterized by GPC in DMF.

Characterization:

^1H -NMR (300 MHz, CDCl_3) δ = 8.62-7.98 (m, 2H, ArH of PVP), 7.24-5.81 (m, 17H ArH), 2.58-0.78 (CH_2CH), 0.80-0.45 (m, 6H of initiator) ppm.

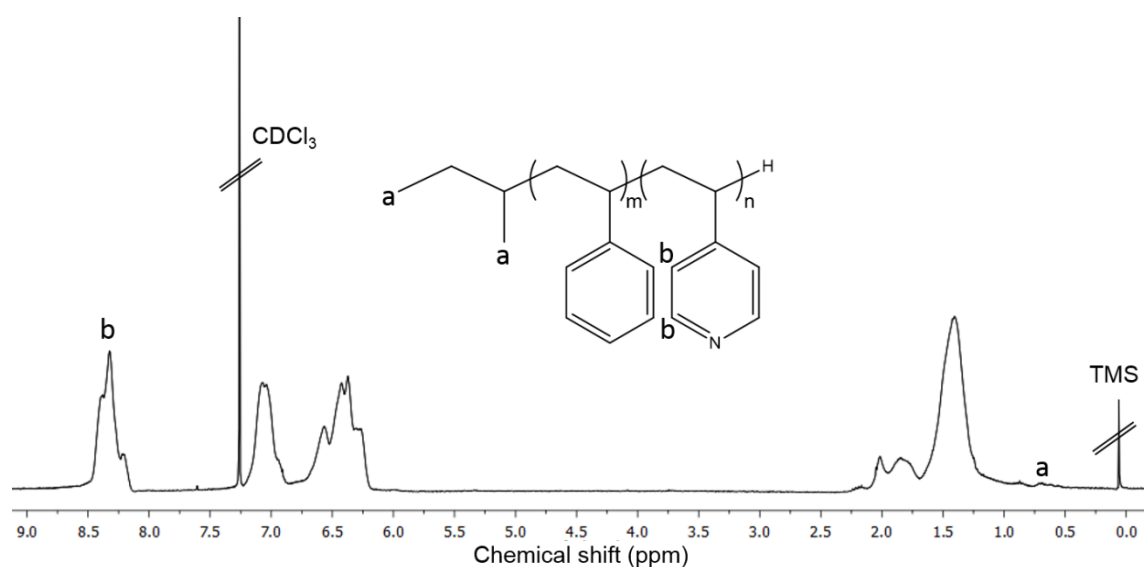


Figure S3.6. ^1H -NMR (300 MHz, CDCl_3) spectrum of PS-*b*-PVP.

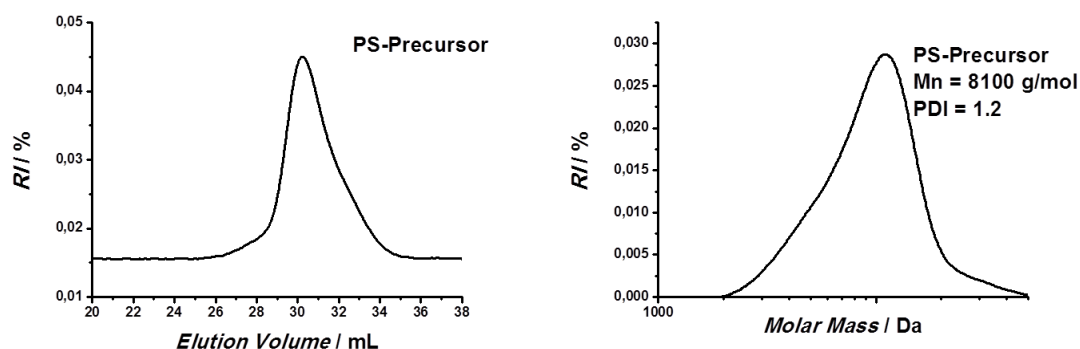


Figure S3.7. GPC chromatogram (left: elution volume, right: molecular weight) of PS-precursor in THF (PDI = 1.2, M_n = 8100 g/mol).

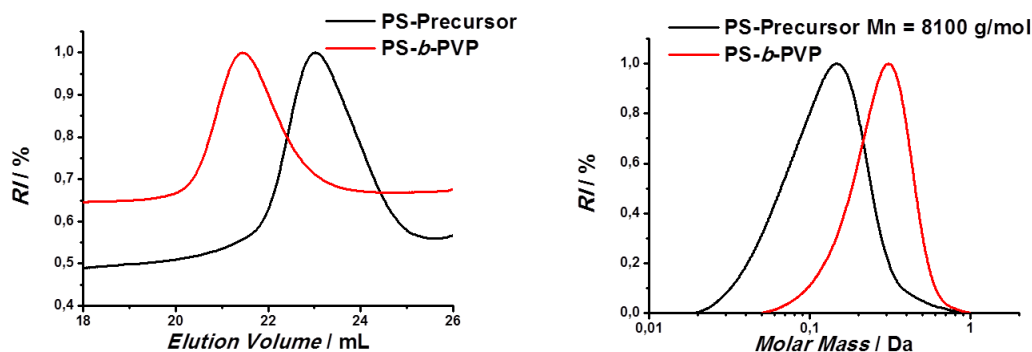


Figure S3.8. GPC chromatogram (left: elution volume, right: molecular weight) of PS-*b*-PVP in DMF (PDI = 1.2).

6. Citrate Stabilized Gold Nanoparticle (Ct@AuNP)

Ct@AuNPs of different sizes were prepared by two different protocols. Using Na_3Ct as reducing agent, AuNPs larger than 10 nm in diameter were obtained. The small Ct@AuNP with a mean diameter of about 3-4 nm was prepared by using NaBH_4 as reducing agent. The characterization of Ct@AuNP is shown in the part of ligand exchange.

6.1 Trisodium citrate as reducing agent

An aqueous solution of $\text{HAuCl}_4 \cdot 3\text{H}_2\text{O}$ (0.25 mM) was heated to boiling. Then an aqueous solution of trisodium citrate (5 wt%) was added in one portion. The solution turned from colorless to violet and in the end wine red. The solution was heated for another 5 min to ensure the reaction was completed. The reaction mixture was removed from heating and cooled to room temperature.

6.2 Sodium borohydride as reducing agent

An aqueous solution (40 mL) of 0.25 mM $\text{HAuCl}_4 \cdot 3\text{H}_2\text{O}$ and 0.25 mM trisodium citrate was prepared in a conical flask. Then, 1.2 mL aqueous solution of ice-cold, freshly prepared 0.1 M NaBH_4 was added. The solution turned red brown immediately. The AuNP dispersion was used within 2-5 h after preparation.

7. Ligand exchange of Ct@AuNP with polymer cages

In each vial, 41 mg of polymer cage with PMMA was dissolved in 2 mL CHCl_3 , followed by adding 2 mL of Ct@AuNP dispersion. After adding small portion of TOAB and vigorous shaking,

the characteristic red-violet color of AuNPs was transferred from aqueous phase to the organic phase indicating the successful phase transfer reaction. When the AuNPs aggregated at the interface, the ligand exchange failed. The organic phase was separated and precipitated from methanol. The resulting product was centrifuged at 6000 rpm for 10 min, washed with methanol three times and dried under vacuum at 45 °C. All the ligand exchange reactions were conducted at room temperature.

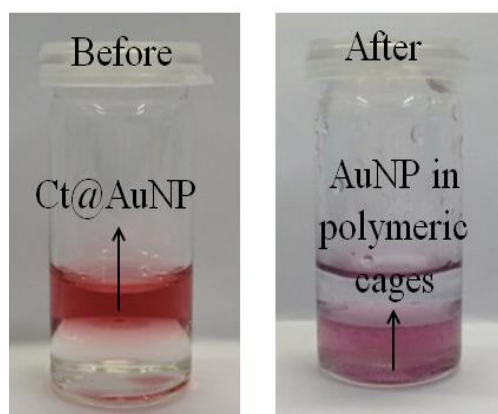
Characterization:

Figure S3.9. Photos of typical ligand exchange reaction (entry 9). Left: before ligand exchange, right: after ligand exchange.

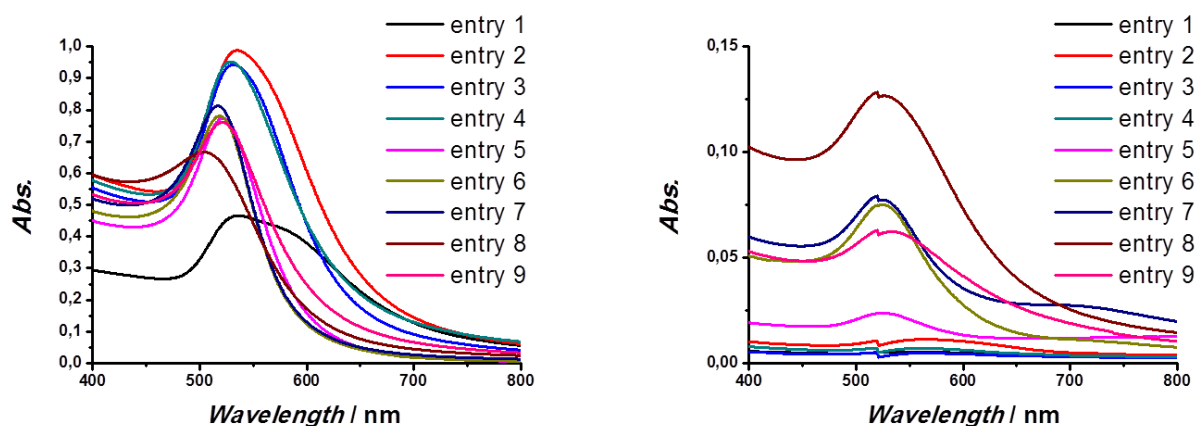


Figure S3.10. UV-vis spectra of Ct@AuNP (left) and polymer cage stabilized AuNP (polymer cage@AuNP) (right).

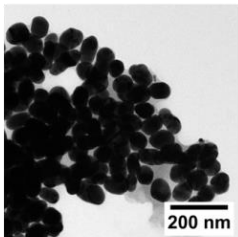
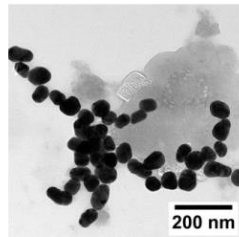
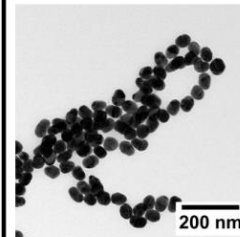
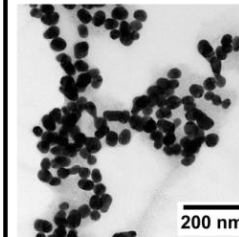
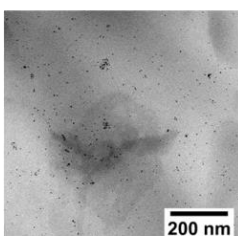
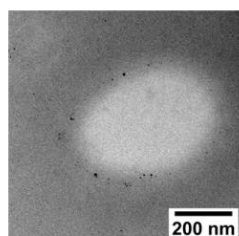
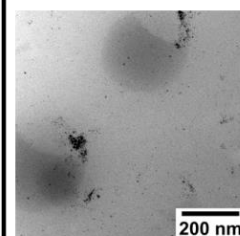
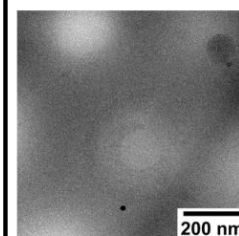
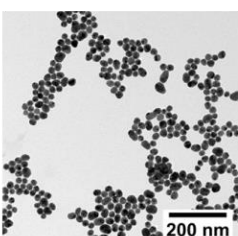
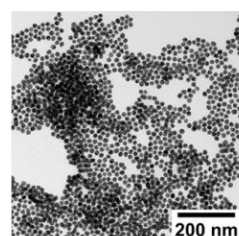
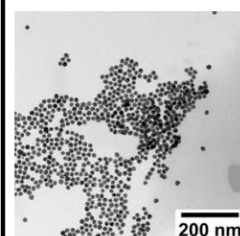
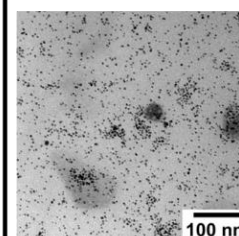
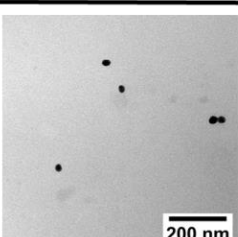
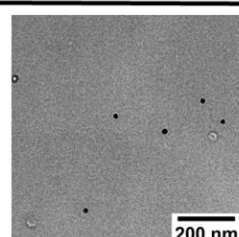
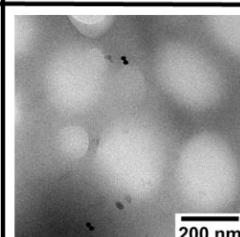
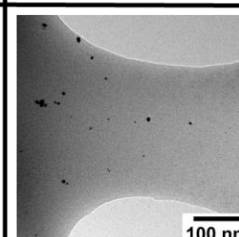
	Entry 1 56.5 ± 10.2 nm	Entry 2 41.0 ± 7.3 nm	Entry 3 34.2 ± 5.6 nm	Entry 4 30.9 ± 5.6 nm
Ct@AuNP				
Polymer Cage @AuNP				
	Entry 5 20.5 ± 3.2 nm	Entry 6 15.3 ± 1.8 nm	Entry 7 12.4 ± 1.9 nm	Entry 8 3.4 ± 0.6 nm
Ct@AuNP				
Polymer Cage @AuNP				

Figure S3.11. Representative TEM images of Ct@AuNPs and corresponding polymer cage@AuNP after ligand exchange. The mean diameters of Ct@AuNPs are given under **Entry Nr.**

Table S3.2 Au-content derived from ICP-OES measurements.

Entry	Ct@AuNP / mg/L	AuNP in polymer cages / mg/kg
1	37.7	40.9
2	43.3	66.5
3	42.2	<40
4	43.2	<40
5	35.7	252
6	38.9	819
7	44.4	688
8	48.0	1355
Mixture	43.4	568

8. Ligand exchange of Ct@AuNP with PMMA-SH

In each vial, 20 mg of PMMA-SH was dissolved in 10 mL CHCl₃. Ct@AuNP dispersion (10 mL) was carefully layered upon the CHCl₃ phase. No phase transfer reaction was observed until TOAB was added. After ligand exchange, the upper aqueous phase was discarded and the CHCl₃ was used for characterization directly. The samples of PMMA-SH stabilized AuNP are noted as PMMA-SH@AuNP.

Characterization:

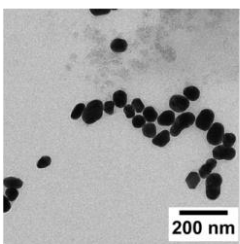
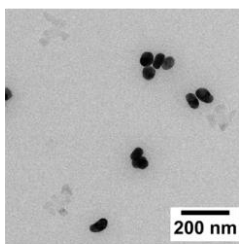
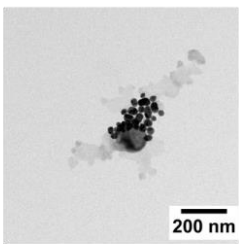
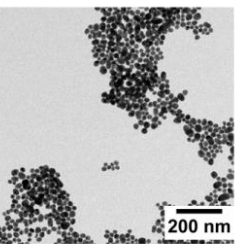
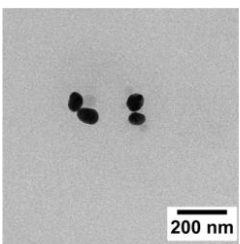
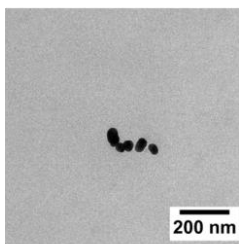
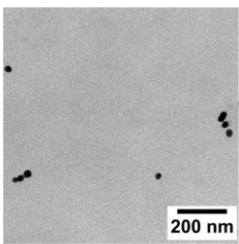
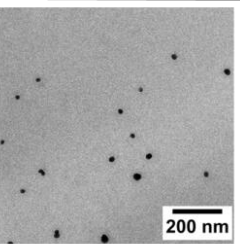
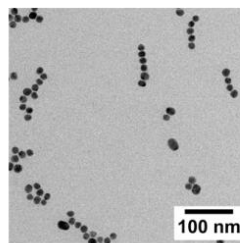
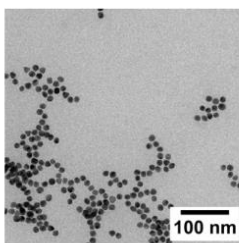
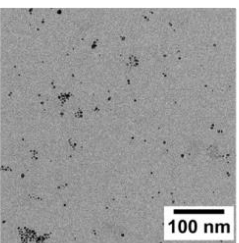
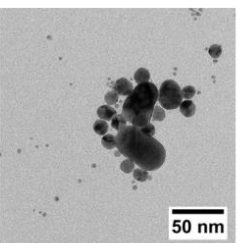
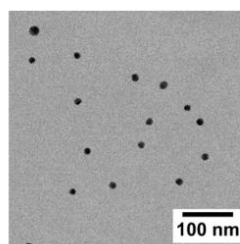
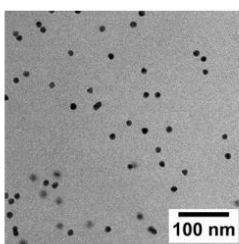
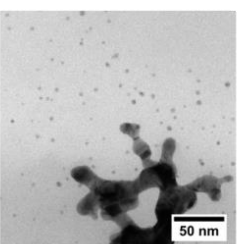
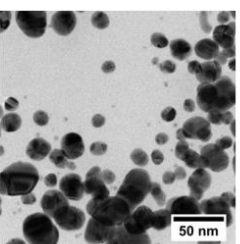
	Compare 1_1 53.4 ± 11.1 nm	Compare 1_2 38.8 ± 6.7 nm	Compare 1_3 29.5 ± 5.4 nm	Compare 1_4 20.1 ± 4.5 nm
Ct@AuNP				
PMMA-SH@AuNP				
	Compare 1_5 13.6 ± 1.9 nm	Compare 1_6 10.9 ± 1.3 nm	Compare 1_7 3.5 ± 0.8 nm	Compare 1_Mix 30 nm, 14 nm, 3 nm
Ct@AuNP				
PMMA-SH@AuNP				

Figure S3.12. Representative TEM images of Ct@AuNPs and corresponding PMMA-SH@AuNP after ligand exchange. The mean diameters of Ct@AuNPs are given under **Compare_1_Nr.**

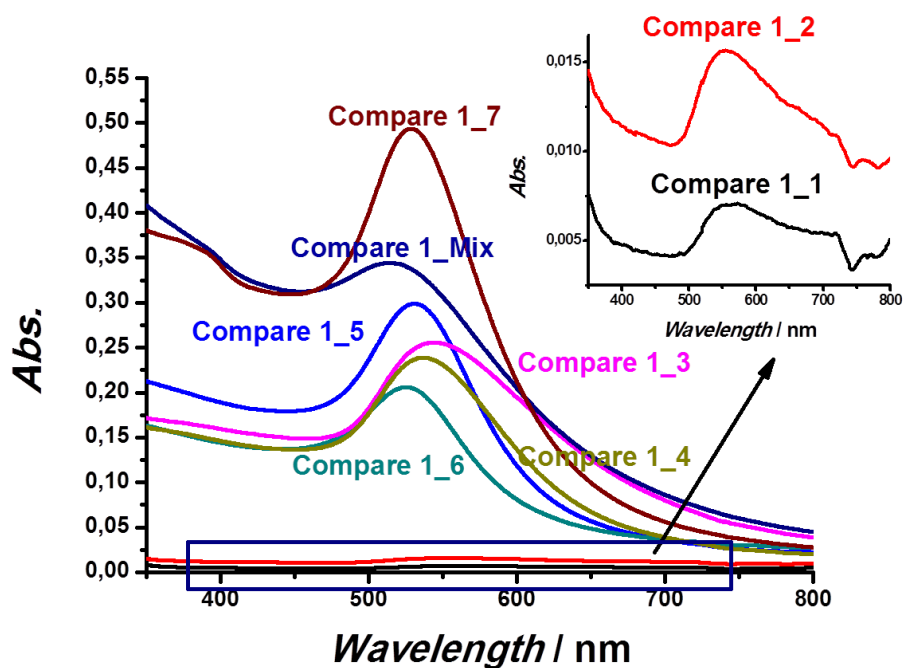


Figure S3.13. UV-vis spectra of PMMA-SH@AuNP.

9. Ligand exchange of Ct@AuNP with PS-*b*-PVP

In each vial, 10 mL of Ct@AuNP was mixed with 10 mL of PS-*b*-PVP solution in CHCl_3 (1 mg/mL) under vigorous shaking. The formed emulsion was slowly segregated under gentle shaking overnight. The organic phase was separated and the solvent was removed by reduced pressure. PS-*b*-PVP stabilized with AuNP was redispersed in 5 mL CHCl_3 .

Characterization:

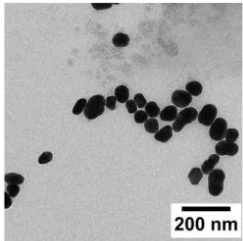
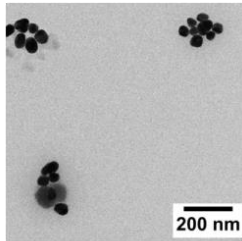
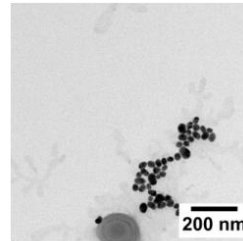
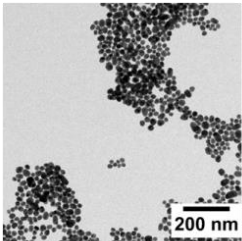
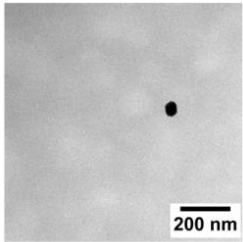
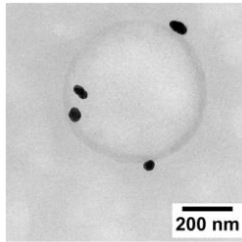
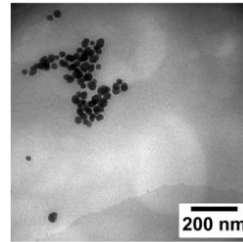
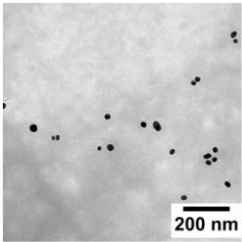
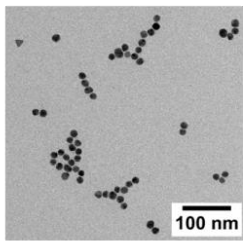
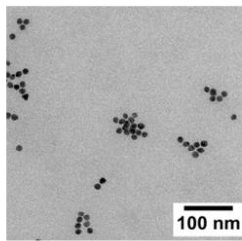
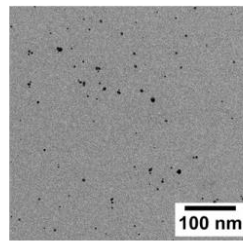
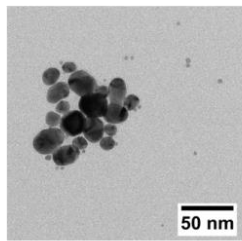
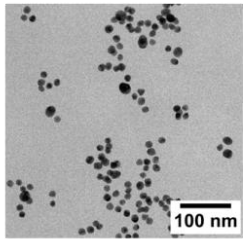
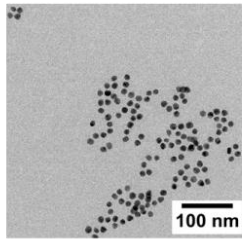
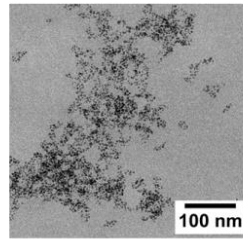
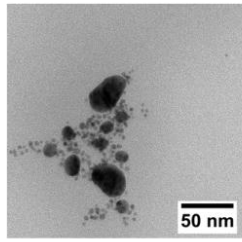
	Compare 2_1 53.4 ± 11.1 nm	Compare 2_2 38.8 ± 6.7 nm	Compare 2_3 29.5 ± 5.4 nm	Compare 2_4 20.1 ± 4.5 nm
Ct@AuNP				
PS- <i>b</i> -PVP@AuNP				
	Compare 1_5 13.6 ± 1.9 nm	Compare 1_6 10.9 ± 1.3 nm	Compare 1_7 3.5 ± 0.8 nm	Compare 1_Mix 30 nm, 14 nm, 3 nm
Ct@AuNP				
PS- <i>b</i> -PVP@AuNP				

Figure S3.14. Representative TEM images of Ct@AuNPs and corresponding PS-*b*-PVP@AuNP after ligand exchange. The mean diameters of Ct@AuNPs are given under **Compare_2_Nr.**

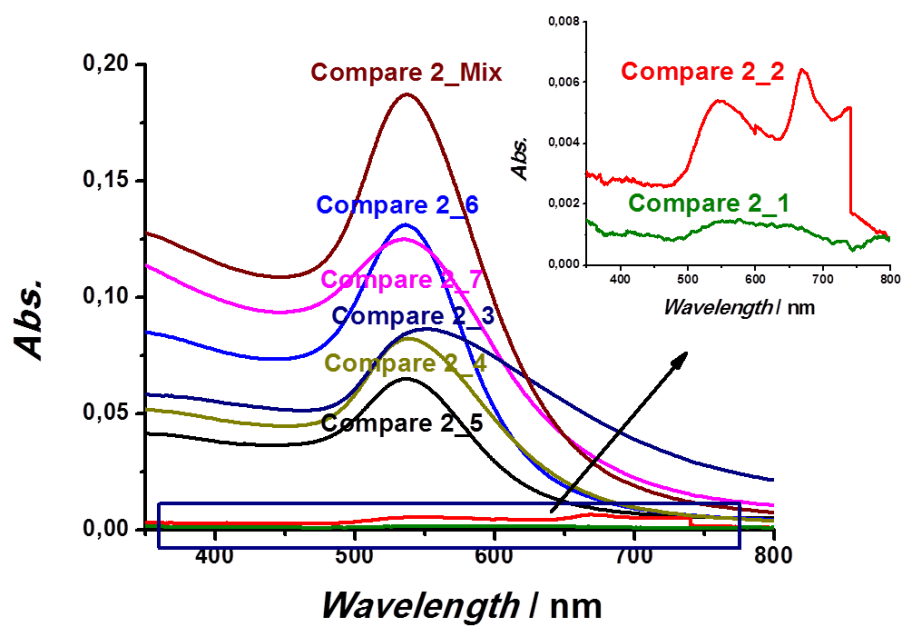
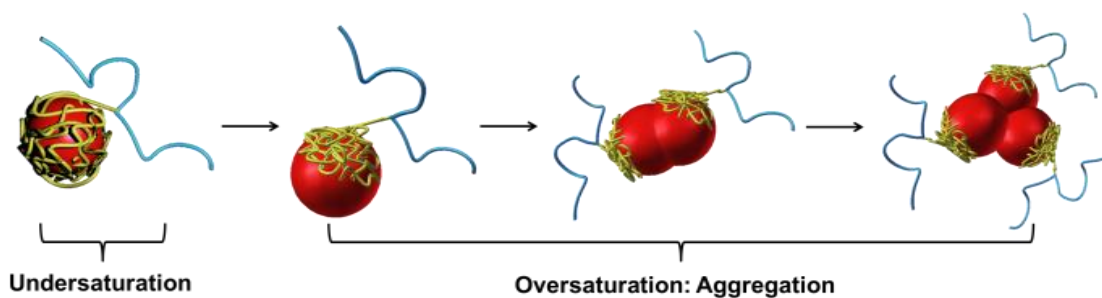


Figure S3.15. UV-vis spectra of PS-b-PVP@AuNP.

Chapter 4

Polymer Cages as Universal Tools for the Precise Bottom-up Synthesis of Metal Nanoparticles

*Ziying Fan, Xuelian Chen, Melissa Köhn Serrano, Holger Schmalz, Sabine Rosenfeldt, Stephan Förster, Seema Agarwal, and Andreas Greiner**



Polymer cages with sulfur moieties prepared by the “grafting-around” method were used as templates for the precise, size-controlled bottom-up synthesis of metal nanoparticles. In contrast to block copolymers as ligands for nanoparticles, the polymer cages exhibited the capacity for controlled nanoparticle encapsulation, which enabled their use as ideal templates for nanoparticles.

Abstract: A template synthesis allows the preparation of monodisperse nanoparticles with high reproducibility and independent from self-assembly requirements. Tailor-made polymer cages were used for the preparation of nanoparticles, which were made of cross-linked macromolecules with pendant thiol groups. Gold nanoparticles (AuNPs) were prepared in the polymer cages *in situ*, by using different amounts of cages versus gold. The polymer cages exhibited a certain capacity, below which AuNPs could be grown with excellent control over the size and shape control. Control experiments with a linear diblock copolymer showed a continuous increase in the AuNP size as the gold feed increased. This completely different behavior regarding the AuNP size evolution was attributed to the flexibility of the polymer chain depending on cross-linking. Moreover, the polymer cages were suitable for the encapsulation of AgNPs, PdNPs, and PtNPs by the *in situ* method.

Template-mediated synthesis enables the preparation of monodisperse nanomaterials with predetermined sizes and shapes. The resulting nanocomposites are of interest in the fields of sensorics,^[1,2] nanoelectronics,^[3,4] biotechnology,^[5] and heterogeneous catalysis.^[6,7] Different types of templates, such as hollow nanocapsules^[8-10] and nanocages,^[11,12] have been investigated to improve the compatibility and stability of nanocomposites, particularly for the synthesis of spherical metal nanoparticles. Polymer capsules have been prepared as templates by the layer-by-layer (LbL) deposition of polyelectrolytes onto sacrificial templates^[13,14] or by post cross-linking of grafted polymer brushes on the NP surfaces.^[15,16] The generated polymer networks usually exhibit dense polymer layers with good stability.^[17,18] The quantitative functionalization of these networks usually depends on the nature of the polymers.^[19] Cages with a well-defined structure, such as the organic molecular cage or especially the dendritic cage, are promising candidates for the precise stoichiometric functionalization of the templates, as they exhibit a monolayer with distinct anchor groups.^[20] For example, dumbbell-like assemblies of AuNPs were prepared by the homocoupling of monofunctionalized AuNPs as artificial molecules.^[21] However, the size of the NPs in such cages was limited to 1-2 nm, which demonstrates that increasing the size of the encapsulated NPs remains a challenge.

The advantage of templates with controlled functionality is the ability to precisely functionalize the encapsulated metal nanoparticles by simple bottom-up approaches, which enables the further manipulation of nanoparticle assemblies. For stoichiometric control over

the functionality of the nanoparticles, our group developed an efficient “grafting-around” approach, which involves a one-step synthesis that generates monofunctionalized nanoparticles wrapped with a cross-linked polymer chain.^[22] The monofunctionalized nanoparticles were further utilized as artificial molecules, which offers the potential for new versatile applications for the “grafting-around” concept.^[23,24] Recently, we have shown that polymer cages prepared by “grafting-around” can be used for the size-selective separation of colloidal AuNPs.^[25]

Based on the polymer cage concept, we developed a highly versatile tool for the precision bottom-up synthesis of metal NPs, which we report here with its possibilities and limitations. This concept was extended to AgNP, PdNP and PtNPs to demonstrate the versatility of the cages. The clear outcome of this study is that polymer cages are superior templates with respect to size control for metal nanoparticles than conventional diblock copolymers such as polystyrene-*block*-poly(4-vinylpyridine) (**PS-*b*-PVP**).

The concept for the precision bottom-up synthesis of metal nanoparticles by the use of polymer cages as templates is schematically depicted in **Figure 4.1**. First, AuNPs **1** coated with 4-vinylbenzenethiol were prepared. The following step is the “grafting-around” approach, where the polymerization of the vinyl-carrying ligands on AuNP **1** was initiated by 4,4'-azobis(4-cyanovaleric acid), which led to a polymer network with a single carboxylate functionality originating from the initiator (AuNP **2**). Subsequently, the carboxylate group on AuNP **2** reacted with 4-vinylaniline, which resulted in vinyl-functionalized AuNP **3**, which were copolymerized with MMA (**AuNP-co-PMMA**). The size [(4.5 ± 2.2) nm] of AuNPs remained the same during the whole procedure (characterization data are shown in the Supporting Information, Figure S4.1 and S4.2). The polymer cage (**Cage-co-PMMA**), namely, the cross-linked macromolecule shell around the AuNP surface, was prepared by etching of the AuNPs using sodium cyanide (NaCN; characterizations are given in Figures S4.3 and S4.4.) The polymer cages are cross-linked by chain transfer or entanglement during polymerization and by the formation of disulfide bonds from thiolates during oxidative etching. As the vinyl-polymerizable ligands were distributed on the AuNP surface, the resulting macromolecules were wrapped around the AuNPs and, thus, were more flexible than hollow capsules with much thicker shells.^[25]

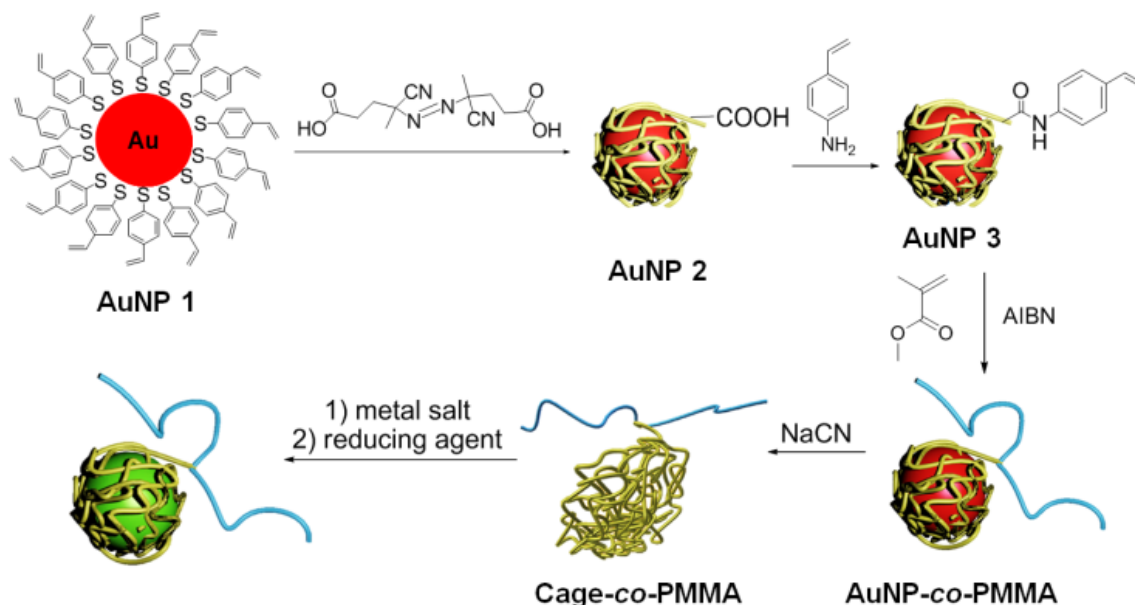


Figure 4.1. Synthesis of the polymer cage by the “grafting-around” approach and subsequent encapsulation of precious-metal nanoparticles by the *in situ* method. AIBN = azobis(isobutyronitrile)

The size of the AuNPs is tunable through alteration of the molar ratio between the Au and ligand.^[26] Thus, we anticipated a deviation from the known size evolution for encapsulated AuNPs prepared using Cage-co-PMMA templates. To test this, the Cage-co-PMMA templates were refilled with different Au feeds by *in situ* synthesis. For control experiments, we chose the linear diblock copolymer PS-*b*-PVP, whose pyridine moieties served as ligands for the AuNPs. We aimed to investigate how the flexibility/morphology of the polymer chain (here the polymer cage was cross-linked, whereas PS-*b*-PVP is non-cross-linked) influences the stability/size evolution of the encapsulated nanoparticles (characterizations of PS-*b*-PVP are given in Figures S4.5-S4.8). The Au concentration was maintained at 1 mM, whereas the polymer concentrations were adjusted to the desired Au/polymer molar ratios. Upon addition of the reducing agent, the Au^{III} ions were reduced to Au⁰, whereas the disulfide bonds were cleaved into thiolates. Therefore, the disulfide cross-linking did not play a role in the *in situ* synthesis. To focus on a comparison of the trend of the AuNP size evolution in different polymer matrices, the size evolution of AuNPs in Cage-co-PMMA was controlled by using the equivalent amount of Au in the feed as was originally used in the AuNP-co-PMMA synthesis (Eq(Au)). In the control experiments, the relationship between the AuNP size and the molar ratio between Au in the feed and PS-*b*-PVP (Au/PS-*b*-PVP) was investigated. The Au/ligand molar ratios are given in Table S4.1.

Figure 4.2a presents transmission electron microscopy (TEM) images and the representative small-angle X-ray scattering (SAXS) data of AuNPs synthesized in Cage-co-PMMA. As the Eq(Au) was increased from 0.25 eq. to 0.75 eq., only spherical AuNPs with a diameter of (4 ± 1.1) nm were observed by TEM analysis (the histograms are given in Figure S4.9). Very large particles are formed when Eq(Au) was increased from 1.00 eq. to 1.67 eq. and SAXS was performed to estimate the particle size (radius of gyration R_g) as well as obtain an indication of the nature of scattering inhomogeneities inside the sample. The investigated samples include nonsymmetrical particles or fractals. The data could not be described by the model of spheres. Nevertheless, the scattering intensity can be described by the Guinier-Porod approach. [Equation (1) and (2)]

$$I(q) \propto \frac{1}{q^s} \exp\left(\frac{R_g^2}{3-s}\right) \quad (1)$$

$$I(q) \propto \frac{1}{q^d} \quad (2)$$

The size (R_g) and dimensionality(s : $s = 0$ for spheres, $s = 1$ for rods and $s = 2$ for lamellae) of the object is included in the Guinier term. The Porod term is sensitive to inhomogeneities. For example, an exponent of $d = 4$ may arise from surface fractals or from the scattering of 3D objects such as spheres with a smooth surface, whereas an exponent of $d = 3$ can point to a collapsed polymer chain or to spheres with rough surface. The radius of gyration of the AuNPs increased from 2.8 nm to 11.8 nm as Eq(Au) was increased from 0.25 to 1.67. At the same time, the Porod exponent changed from $d = 3.1$ to $d = 3.8$. An Eq(Au) < 0.75 led to the low q range exhibiting an upturn in intensity. This trend vanishes as the Cage-co-PMMA content decreases. Such a progress can be caused by a non-negligible amount of objects with $R_g = 47$ nm (corresponding to a sphere with a radius of 60 nm). This phase was described as the “undersaturated” phase, where the AuNP size increased slightly (from 2.8 nm to 4.5 nm in R_g). Here, the presence of excessive Cage-co-PMMA allows control of the size and size distribution of the AuNPs. Upon a further increase of the Eq(Au) from 1.00 eq. to 1.67 eq., the AuNPs immediately formed large aggregates (11.8 nm), which was described as the “oversaturated” phase. The characterization (TEM and SAXS) of each sample was given in Figure S4.9. We attributed this sharp transition from a controlled growth to a sudden agglomeration as a result of the cage deficiency, which clearly demonstrated the role of Cage-

co-PMMA as a stabilizing template for the AuNPs. The UV-vis spectra of AuNPs in Cage-co-PMMA are shown in Figure S4.10, left.

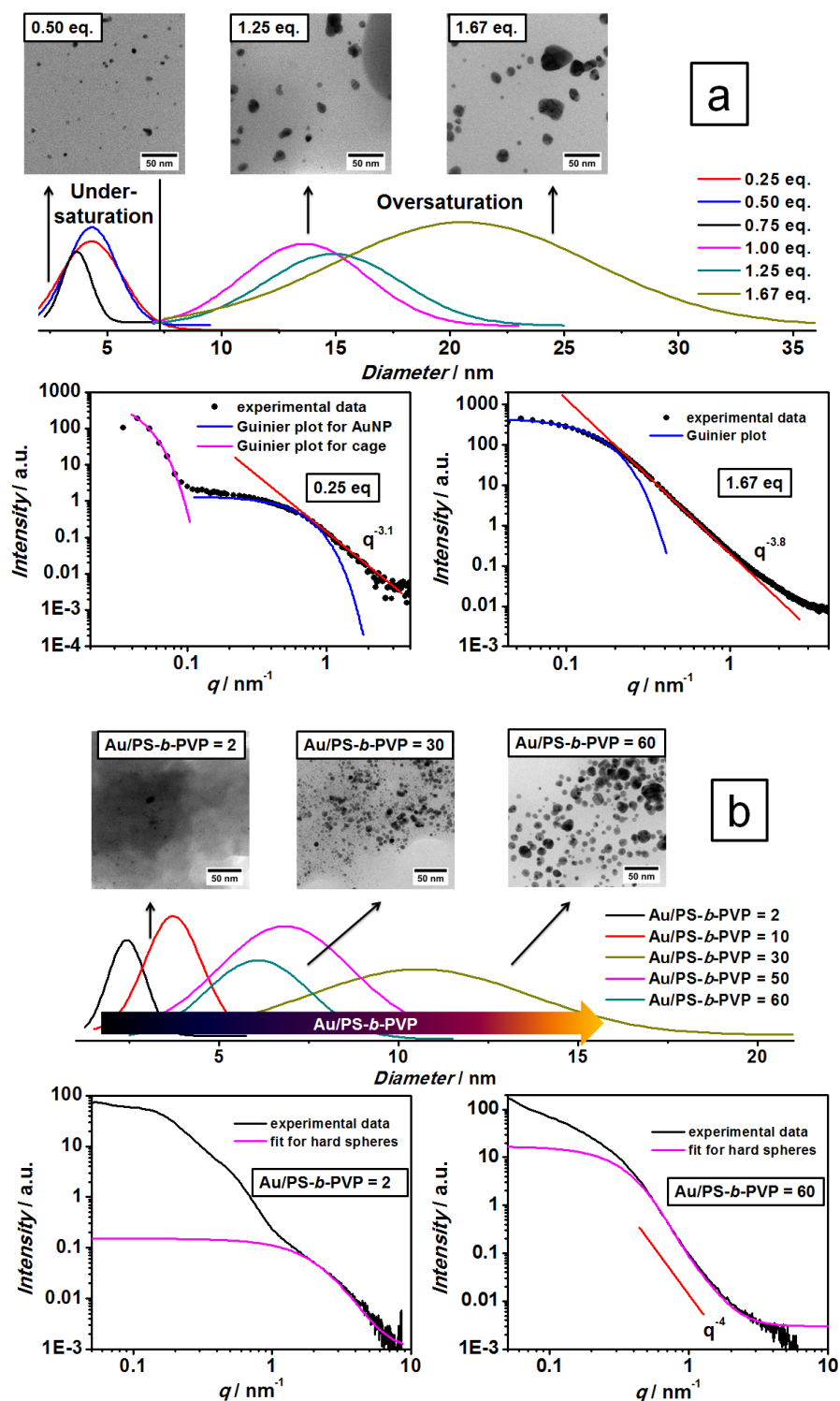


Figure 4.2. Comparison of the size evolution of AuNPs in a) Cage-co-PMMA and b) PS-*b*-PVP. Top: Gauss-Fit of the histograms of the AuNP size and size distribution with representative TEM images of various Au contents (equiv is denoted as the eq. for Cage-co-PMMA; Au/PS-*b*-PVP for the molar ratio between Au and PS-*b*-PVP). Representative SAXS data are shown below. Red trace: slope = $q^{-3.1}$ [(a), 0.25 equiv], $q^{-3.8}$ [(a), 1.67 equiv], q^{-4} (b); pink trace in (b): scattering of spheres having Schultz-Zimm distribution.

The behavior of PS-*b*-PVP in terms of the AuNP size evolution was significantly different from that when cages were used as templates (**Figure 4.2b**). A continuous growth of AuNPs from (2.6 ± 0.7) nm to (11.6 ± 3.4) nm was observed in TEM micrographs on increasing the Au/PS-*b*-PVP ratios. At higher Au/PS-*b*-PVP ratios, the fraction of small AuNPs decreased, whereas the amount of large AuNPs constantly increased. The increase in the AuNP size with increasing Au/PS-*b*-PVP ratio was also confirmed by the SAXS data, which yielded AuNP diameters ranging from 2.4 nm to 14 nm. (**Figure 4.3**, right) It is worth noting that for small q values the size is dominated by the PS-*b*-PVP and aggregates as evidenced by a sudden increase in $I(q)$, thus the SAXS curves are fitted at higher q values with spherical shape instead of Guinier approximation at low q range. TEM and SAXS analysis of each sample was given in Figure S4.11. Eventually, the AuNPs aggregated completely and precipitated (data not shown; the UV-vis spectra are shown in Figure S4.10, right.)

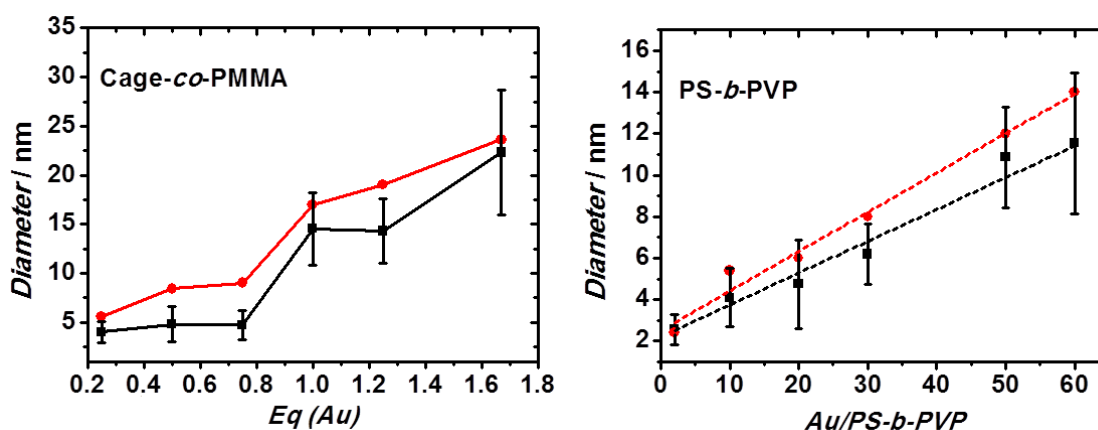


Figure 4.3. Plot of the AuNP size change derived by TEM (black) and SAXS (red) data as a function of Au equivalents (Eq(Au)) in the feed for Cage-co-PMMA (left) and the Au/PS-*b*-PVP molar ratio for PS-*b*-PVP (right).

The experimental observations are explained by the differences between the cage structure of Cage-co-PMMA and the linear chain structure of PS-*b*-PVP (**Figure 4.4**). At a high concentration of the cage in the “undersaturated” phase, the AuNPs were separately wrapped within a single Cage-co-PMMA. The diameter of the AuNPs, therefore, remained constant at approximately 5 nm with a narrow distribution (standard deviation less than 30%). When the Au content exceeded the capacity maximum of the cage, the cross-linked cages were not able to delocalize and, thus, not able to homogeneously around the AuNP surface because of the entropic effect. This insufficient distribution of ligands created large defect sites on the surface of the AuNP that significantly decreased the stability of the AuNPs. As a consequence, the

AuNPs aggregated at these bare areas to reduce the surface energy and formed irregular-shaped agglomerates in the “oversaturated” phase.^[26] In contrast, the PVP blocks of PS-*b*-PVP were rearranged on the AuNP surface until they were distributed homogeneously. Therefore, the AuNPs were stabilized over a large range of Au/PS-*b*-PVP ratios. However, the size distribution of the AuNPs was always broad due to Ostwald-ripening or coalescence during the later growth state.^[27]

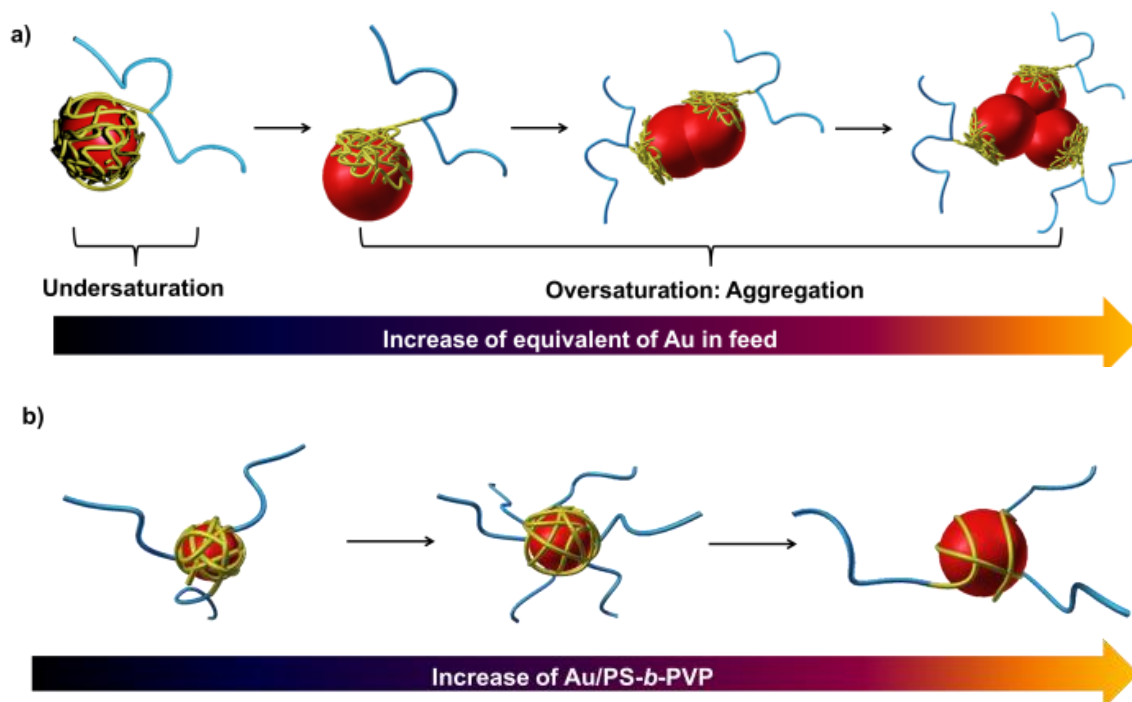


Figure 4.4. Size evolution of AuNPs in different templates. a): Isolated AuNPs with controlled size in the “undersaturated” phase were completely wrapped within single Cage-*co*-PMMA. As soon as the Au content exceeded the capacity of the Cage-*co*-PMMA, only a part of the AuNPs could be stabilized by the cages because of their cross-linked structure (“oversaturated” phase). Consequently, the AuNPs aggregated. b): In the case of PS-*b*-PVP, the surface coverage decreased as the Au/PS-*b*-PVP molar ratio increased. The polymer chains were always homogeneously distributed around the AuNP surface, thereby resulting in a continuous growth of spherical AuNPs.

The versatility of the grafting-around approach for precisely synthesized AuNPs templated by polymer cages was applied for other metals. Sulfur ligands in the polymer cages are well known to be stabilizers for various precious metal nanoparticles. Here, the syntheses of AgNPs, PdNPs, and PtNPs were investigated using Cage-*co*-PMMA as a template. All reactions were carried out in the “undersaturated” regime (0.8 equiv of the metal salt in the feed).

According to the TEM results (**Figure 4.5**), the AgNPs were spherical, with a mean diameter of (6.2 ± 2.4) nm. SAXS analysis indicated a larger average diameter (10.2 ± 2.2) nm. Aggregation was indicated by the up-turn in the low q -region.^[28] Rod-shaped PdNPs and PtNPs were

observed (additional TEM images, histograms and UV-vis spectra are given in Figure S4.12 and S4.13). Similar structures were also observed for PdNPs synthesized by the *in situ* method in the presence of polymer ligands.^[29] The formation of nanorods was attributed to the aggregation of primary spherical nanoparticles. Often, the nanoparticles were so labile that they formed large aggregates with a wormlike substructure. However, in our case, the formation of large aggregates was suppressed. The dispersions were stable, even after three months under ambient conditions. Rodlike structures were indicated by the scaling of $q^{-1.2}$. This low shape control of the polymer cage is speculatively explained by a certain flexibility of Cage-co-PMMA, which enabled the anisotropic growth of nanoparticles within the cage.

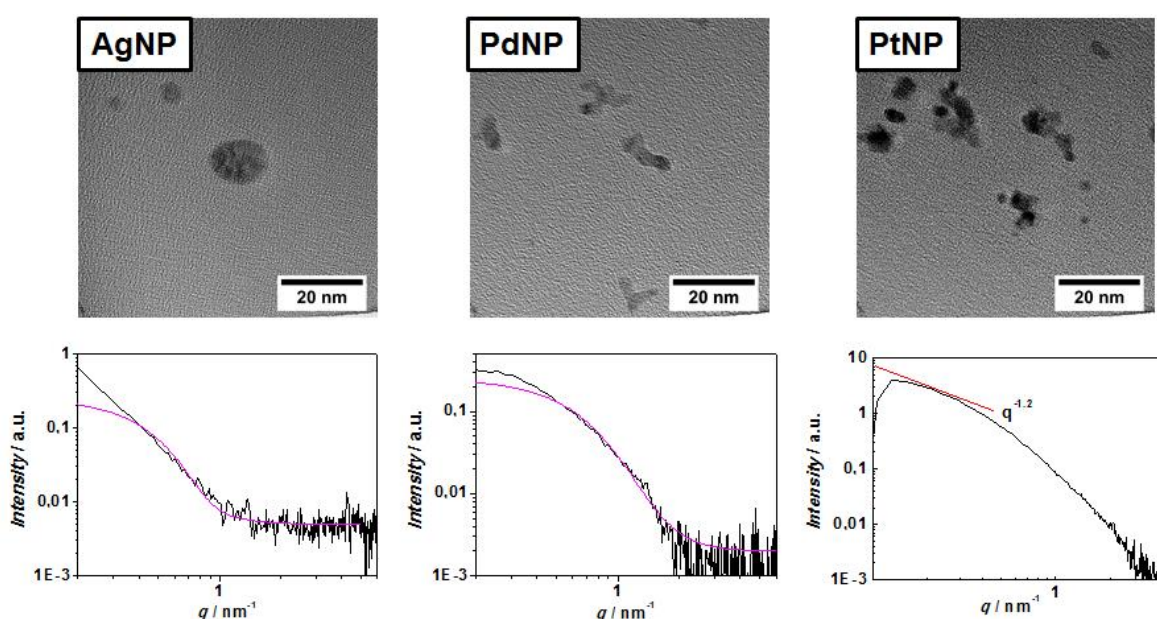


Figure 4.5. Representative TEM micrographs (top) and SAXS data (bottom; black trace: experimental data; pink trace for AgNPs and PdNPs: fit for hard spheres, Schultz-Zimm distribution; red trace for PtNP: scaling of $q^{-1.2}$) of metal nanoparticles in Cage-co-PMMA prepared by the *in situ* method.

In summary, mono-functionalized polymer cages with cross-linked polymer chains were used as efficient templates for the size-controlled bottom-up synthesis of metal nanoparticles. A series of *in situ* syntheses of AuNPs in Cage-co-PMMA using feeds with various Au concentrations demonstrated the relationship between the cage structure and the size evolution of the encapsulated NPs. The AuNPs underwent a sharp transition from a controlled and uniform size and shape to agglomeration when the maximum loading capacity of the cages was exceeded. Control experiments with a linear diblock copolymer (PS-*b*-PVP) under comparable conditions did not provide any size control for AuNPs. A plausible explanation for the inefficiency of PS-*b*-PVP is its chain flexibility. The size evolution of the AuNPs depends, to

a large extent, on the distribution of the polymer chains on the surface of the AuNP and on how the polymer chains adapt during nanoparticle growth, which is strongly linked to the chain flexibility. In turn, this unprecedented cage cross-linking was indirectly confirmed by this size evolution study, which revealed the polymerization mechanism on a nanoparticle surface in the sub-5-nm range. In upcoming studies we aim to prepare the polymer cages with controllable sizes, thus increasing the scope of size control of general nanoparticle syntheses. For example, through selecting the proper cage size and amount, AuNPs with 10 nm and 50 nm can be produced in one pot with desired populations. The grafted sulfur moieties make Cage-co-PMMA a universal template for the synthesis of various precious-metal nanoparticles. AgNPs, PdNPs and PtNPs were prepared accordingly with excellent size control. Here, the shape control of nanoparticles remains a challenge. The tailor-made nanocomposites based on polymer cagelike polymer templates are promising for the design of novel functional materials, where both the excellent size control and monofunctionality of Cage-co-PMMA are exploited.

Acknowledgements

We are indebted to the Fonds der Chemischen Industrie (Z. F.) and SFB 840 for financial support. We are also indebted to Elitenetzwerk Bayern for assistance with scientific writing.

References

- [1] M. Ding, D. C. Sorescu, G. P. Kotchey, A. Star, *J. Am. Chem. Soc.* **2012**, *134*, 3472.
- [2] L. Wang, H. Dou, Z. Lou, T. Zhang, *Nanoscale* **2013**, *5*, 2686.
- [3] S. Srivastava, J. L. Schaefer, Z. Yang, Z. Tu, L. A. Archer, *Adv. Mater.* **2014**, *26*, 201.
- [4] A. Rapakousiou, C. Deraedt, H. Gu, L. Salmon, C. Belin, J. Ruiz, D. Astruc, *J. Am. Chem. Soc.* **2014**, *136*, 13995.
- [5] O. Shimon, A. Postma, Y. Yan, A. M. Scott, J. K. Heath, E. C. Nice, A. N. Zelikin, F. Caruso, *ACS Nano* **2012**, *6*, 1463.
- [6] F. Mitschang, H. Schmalz, S. Agarwal, A. Greiner, *Angew. Chem.* **2014**, *126*, 5073; *Angew. Chem. Int. Ed.* **2014**, *53*, 4972.

- [7] H. Wu, Z. Liu, X. Wang, B. Zhao, J. Zhang, C. Li, *J. Colloid Interface Sci.* **2006**, *302*, 142.
- [8] S. M. Marinakos, J. P. Novak, L. C. Brousseau III, A. B. House, E. M. Edeki, J. C. Feldhaus, D. L. Feldheim, N. Carolina, *J. Am. Chem. Soc.* **1999**, *121*, 8518.
- [9] D. G. Shchukin, I. L. Radtchenko, G. B. Sukhorukov, *J. Phys. Chem. B* **2003**, *107*, 86.
- [10] T. Valdessolis, P. Vallevigon, M. Sevilla, A. B. Fuertes, *J. Catal.* **2007**, *251*, 239.
- [11] R. M. Crooks, M. Zhao, L. Sun, V. Chechik, L. K. Yeung, *Acc. Chem. Res.* **2001**, *34*, 181.
- [12] H. Lang, R. A. May, B. L. Iversen, B. D. Chandler, *J. Am. Chem. Soc.* **2003**, *125*, 14832.
- [13] M.-K. Park, S. Deng, R. C. Advincula, *Langmuir* **2005**, *21*, 5272.
- [14] X. Tao, J. Li, H. Möhwald, *Chem. Eur. J.* **2004**, *10*, 3397.
- [15] A. Samanta, M. Tesch, U. Keller, J. Klingauf, A. Studer, B. J. Ravoo, *J. Am. Chem. Soc.* **2015**, *137*, 1967.
- [16] Y. Kang, T. A. Taton, *Angew. Chem.* **2005**, *117*, 413; *Angew. Chem. Int. Ed.* **2005**, *44*, 409.
- [17] K. Ariga, Y. Lvov, T. Kunitake, *J. Am. Chem. Soc.* **1997**, *119*, 2224.
- [18] C. Boyer, M. R. Whittaker, C. Nouvel, T. P. Davis, *Macromolecules* **2010**, *43*, 1792.
- [19] D. Choi, B. Son, T. H. Park, J. Hong, *Nanoscale* **2015**, *7*, 6703.
- [20] H. Long, Y. Jin, A. Sanders, W. Park, W. Zhang, *J. Am. Chem. Soc.* **2014**, *136*, 1782.
- [21] J. P. Hermes, F. Sander, U. Fluch, T. Peterle, D. Thompson, R. Urbani, T. Pfohl, M. Mayor, *J. Am. Chem. Soc.* **2012**, *134*, 14674.
- [22] C. Krüger, S. Agarwal, A. Greiner, *J. Am. Chem. Soc.* **2008**, *130*, 2710.
- [23] S. Bokern, K. Gries, H.-H. Görtz, V. Warzelhan, S. Agarwal, A. Greiner, *Adv. Funct. Mater.* **2011**, *21*, 3753.
- [24] K. Gries, M. El Helou, G. Witte, S. Agarwal, A. Greiner, *Polymer* **2012**, *53*, 1632.
- [25] Z. Fan, M. Köhn Serrano, A. Schaper, S. Agarwal, A. Greiner, *Adv. Mater.* **2015**, *27*, 3888.
- [26] D. V. Leff, P. C. Ohara, J. R. Heath, W. M. Gelbart, *J. Phys. Chem.* **1995**, *99*, 7036.
- [27] J. Chai, X. Liao, L. R. Giam, C. A. Mirkin, *J. Am. Chem. Soc.* **2012**, *134*, 158.
- [28] N. Sakamoto, M. Harada, T. Hashimoto, *Macromolecules* **2006**, *39*, 1116.
- [29] S. Bokern, K. Volz, S. Agarwal, A. Greiner, *J. Nanoparticle Res.* **2012**, *14*, 1041.

Supporting Information

Polymer Cages as Universal Tools for the Precise Bottom-up Synthesis of Metal Nanoparticles

*Ziyin Fan, Xuelian Chen, Melissa Köhn Serrano, Holger Schmalz, Sabine Rosenfeldt, Stephan Förster, Seema Agarwal, and Andreas Greiner**

Contents

1. Materials
2. Instrumentation
3. Syntheses and Supplementary Analytical Data

1. Materials

Chloroauric acid trihydrate ($\text{HAuCl}_4 \cdot 3\text{H}_2\text{O}$), trisodium citrate (Na_3Ct), sodium borohydride (NaBH_4), styrene, 4-vinylpyridine, 1,1'-diphenylethylene (DPE), and tetraoctylammonium bromide (TOAB) were purchased from Sigma-Aldrich. 4,4'-Azobis(4-cyanovaleric acid), dodecyl trimethylammonium bromide (DTMABr), 4-dimethylaminopyridine, *N,N'*-diisopropylcarbodiimide (DIC), azobisisobutyronitrile (AIBN), and 4-vinylaniline were purchased from Alfa Aesar. *sec*-Butyllithium (*sec*-BuLi, 1.4 M in cyclohexane/hexane) was purchased from Acros and used as received. Styrene, 4-vinylpyridine and 1,1'-diphenylethylene (DPE) were first dried over di-*n*-butylmagnesium, triethylaluminium, and calcium hydride and then condensed at reduced pressure under nitrogen. AIBN was recrystallized from Et_2O . Tetrahydrofuran (THF) was dried over Solvona[®] for two days and distilled under argon atmosphere. All the other solvents were purified by distillation at reduced pressure.

2. Instrumentation

Transmission electron microscopy (TEM): TEM micrographs were obtained by a ZEISS EM922 Omega with an acceleration voltage of 200 kV. Samples were prepared by drop-coating the nanoparticle dispersion in THF (ca. 0.1 mM) onto a carbon-covered copper grid (Carbon Support Films, 300 mesh, Quantifoil). The micrographs were evaluated using *ImageJ* (National Institute of Health, USA, version 1.44c). For each sample at least 100 particles were measured.

UV-vis spectroscopy: The UV-vis spectra were recorded using a two-beam-photometer JASCO with a quartz glass cuvette. The samples were prepared in THF (ca. 0.1 mM) and measured at room temperature.

Small angle X-ray scattering (SAXS): The SAXS data were measured using a laboratory-based "Double Ganesha AIR" system (SAXSLAB, Denmark) with a micro-focused beam at $\lambda = 0.154$ nm as the X-Ray source, which consisted of a rotating anode (copper, MicroMax 007HF, Rigaku Corporation, Japan). A position sensitive detector (PILATUS 300 K, Dectris) was used for data recording. The samples were measured in 1 mm glass capillaries in THF (0.5 mM) (Hilgenberg, code 4007610, Germany) at different sample-to detector distances.

The scattering vectors q , the magnitude of the scattering wave vector, ranges from 0.05 to 10 nm⁻¹, which is defined as:

$$q = (4\pi / \lambda) \sin(\theta / 2)$$

Where ϑ is the scattering angle and λ represents the wavelength of X-ray. The averaged data of different detector distances were merged to single scattering curves covering the whole q -range. After the scattering contribution of the solvent and the capillary were subtracted, the data were analyzed and fitted using the established program SCATTER.

Evaluation of SAXS data: To extract morphological parameters, the derived experimental scattering curves were fitted with a model which describes the scattered intensity of hard spheres. The radius R , and polydispersity σ of the nanoparticles can be thus calculated as follows:

For spherical, noninteracting particles under dilute conditions, $F(q)$ is described as:

$$F(q, R) = \frac{3}{(qR)^3} (\sin(qR) - qR \cos(qR))$$

This form factor has a large impact on the size distribution function. In our case, the Shultz-Zimm distribution is used. The z-average of a function $f(q, R)$ is:

$$\langle f(q, R) \rangle_R = \int_0^\infty f(q, R) R^m h(R) dR$$

$$h(R) = \frac{(z+1)^{z+m+1} R^z}{\bar{R}^{z+m+1} \Gamma(z+m+1)} \exp \left[-(z+1) \frac{R}{\bar{R}} \right]$$

The distribution is normalized as $\int_0^\infty R^m h(R) dR = 1$

where $m = 6$ is the weighting factor for the radius R , the average \bar{R} , and the relative standard deviation σ_R . The relative standard deviation σ_R is: $\sigma_R = (z+1)^{-1/2}$

Thermogravimetric analysis (TGA): The mass losses of samples (ca. 10 mg) were characterized using a thermobalance TGA/SDTA 851° (Mettler Toledo) using 70 µm corundum crucibles. The samples were measured under nitrogen atmosphere from 20 °C to 800 °C at a heating rate of 10 K/min. The data were analyzed using the software Star® (Mettler Toledo, version 9.20).

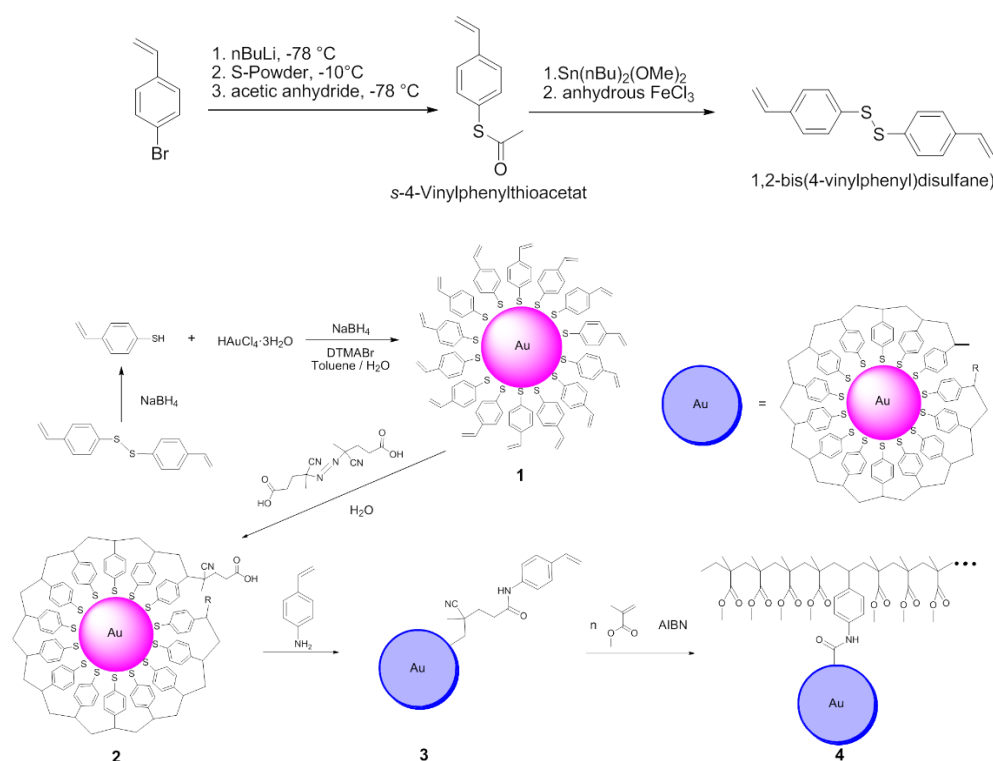
Gel permeation chromatography (GPC): DMF-GPC for characterization of samples containing AuNPs was carried out using a set-up consisting of a pump (Agilent Technologies 1260), an

autosampler (Agilent Technology 1200), a pre-column (8x50 mm, Gram 10 μm) and two columns (8x300 mm, Gram 10 μm , 100 \AA ; 8x300 mm, Gram 10 μm , 3000 \AA). The detector system is made up of one refractive index (RI) detector and a diode array detector (DAD). The samples were dissolved in DMF with 5 g/mL LiBr and measured at room temperature at a flow rate of 0.5 mL/min. THF-GPC for PS-*b*-PVP is equipped with one pre-column (8x50 mm, Gram 10 μm) and four columns (8x300 mm, Gram 10 μm , 100 \AA ; 8x300 mm, Gram 10 μm , 1000 \AA ; 8x300 mm, Gram 10 μm , 10^4 \AA ; 8x300 mm, Gram 10 μm , 10^5 \AA) and a RI detector. The samples were measured at 40 $^{\circ}\text{C}$ at a flow rate of 1 ml/min. The software for analysis was WinGPC Unity (Polymer Standards Service, Build 6807). The internal standard for both GPCs is toluene.

Nuclear magnetic resonance (NMR) spectroscopy: The NMR spectra were recorded by a Bruker Avance 300 UltraShieldTM spectrometer at room temperature using CDCl_3 as solvent. MestReNova (Mesterelab Research S.L., Version 6.0.2) was used for evaluation.

3. Syntheses and Supplementary Analytical Data

The synthesis of AuNP-co-PMMA **4** is presented in **Scheme S4.1**. The experimental details are given below.



Scheme S4.1. Synthesis of vinyl-carrying ligand for AuNP template synthesis and copolymerization of the AuNP template (**3**) with MMA (AuNP-co-PMMA **4**).

3.1 Synthesis of S-4-Vinylphenyl thioacetate

n-BuLi (6.87 mL, 1.6 M in hexane, 11.0 mmol, 1.00 eq) was slowly added to a solution of *p*-bromostyrene (2.02 g, 11.0 mmol, 1.00 eq) in 50 mL THF/hexane (1:1) at -78 °C under argon atmosphere. After stirring at -78 °C for 1.5 hours sulfur powder (352 mg, 11.0 mmol, 1.00 eq) was added. The reaction mixture was then warmed to -10 °C and stirred for 30 min until sulfur completely dissolved. Acetic anhydride (1.03 mL, 11.0 mmol, 1.00 eq) was added after cooling the reaction mixture again to -78 °C. After two hours the reaction mixture was quenched with 25 mL water and heated to room temperature. First, the reaction mixture was extracted with Et₂O (30 mL). Then, the combined organic phase was washed with 50 mL brine and dried over MgSO₄. The filtrate was concentrated in vacuum. The residue was purified by column chromatography (Et₂O:hexane = 1:10) and yielded 96 mg S-4-vinylphenylthioacetate (5.4 mmol, 49%) as colorless oil.

¹H NMR (300.1 MHz, CDCl₃, 25 °C) δ = 2.42 (s, 3H, CH₃), 5.32 (dd, ²*J*(C,H) = 0.7 Hz, ³*J*(C,H) = 10.9 Hz, 1H, CH=CH₂), 5.80 (dd, ²*J*(C,H) = 0.7 Hz, ³*J*(C,H) = 17.6 Hz, 1H, CH=CH₂), 6.72 (dd, ³*J*(C,H) = 17.6 Hz, ³*J*(C,H) = 10.9 Hz, 1H, CH=CH₂), 7.40 (m, 4H, ArH) ppm. ¹³C NMR (75 MHz, CDCl₃, 25 °C) δ = 193.9 (C=O), 138.7 (ArC), 135.9 (CH=CH₂), 134.5 (ArC), 127.0 (ArC), 126.8 (ArC), 115.3 (CH=CH₂), 30.1 (CH₃) ppm.

3.2 Synthesis of 1,2-bis(4-vinylphenoldisulfane)

Dibutyltindimethoxide (860 mg, 2.92 mmol, 0.65 eq) was mixed with S-4-vinylphenylthioacetate (800 mg, 4.48 mmol, 1.00 eq) in 50 mL THF and stirred for 2 hours. Anhydrous FeCl₃ (648 mg, 5.84 mmol, 1.30 eq) was added in one portion. The reaction mixture was stirred at room temperature overnight and subsequently poured into ice. The mixture was extracted with Et₂O. Then, the combined organic phase was washed with NaOH solution (15 mL, 10 M) and water until pH = 7. The solvent was removed in vacuum. Recrystallization from hexane/Et₂O delivered 212 mg (35%) of product as yellow solid.

¹H-NMR (300.1 MHz, CDCl₃) δ = 5.26 (dd, ²*J*(C,H) = 0.6 Hz, ³*J*(C,H) = 10.9 Hz, 2H, CH=CH₂), 5.73 (dd, ²*J*(C,H) = 0.6 Hz, ³*J*(C,H) = 17.6 Hz, 2H, CH=CH₂), 6.72 (dd, ³*J*(C,H) = 17.6 Hz, ³*J*(C,H) = 10.9 Hz, 2H, CH=CH₂), 7.39 (dd, ³*J*(C,H) = 8.4 Hz, ⁴*J*(C,H) = 33.4 Hz, 10H, ArH) ppm. ¹³C NMR (75 MHz, CDCl₃, 25 °C) δ = 136.7 (ArC), 136.3 (ArC), 135.9 (CH=CH₂), 128.0 (ArC), 127.0 (ArC), 114.3 (CH=CH₂) ppm.

3.3 Synthesis of 4-vinylbenzenethiol stabilized AuNP (1)

HAuCl₄·3H₂O (174 mg, 0.44 mmol, 1.00 eq) was dissolved in 50 mL of deionized water. After addition of DTMABr (604 mg, 1.95 mmol, 4.45 eq) the orange reaction mixture was stirred at room temperature for 15 min. 1,2-bis(4-vinylphenyl)disulfide (96 mg, 0.36 mmol, 0.80 eq) was dissolved in 50 mL of toluene and added to the reaction mixture, which was further stirred at room temperature for another 15 min. Subsequently, a freshly prepared aqueous solution of NaBH₄ (186 mg, 1.95 mmol, 9.98 eq, 50 mL) was added dropwise. Then, the mixture was stirred at room temperature for 16 hours. The organic phase was separated and the dark purple aqueous phase was washed with 20 mL of toluene. The aqueous phase was directly used for the following step.

3.4 “Grafting-around” of 4-vinylbenzenethiol on the AuNP surface (2)

4,4'-azobis(4-cyanovaleric acid) (39.0 mg, 0.14 mmol, 1.00 eq) was dissolved in a solution of NaOH (12 mg, 0.28 mmol, 2.00 eq in 200 mL of deionized water). This initiator solution was added to the aqueous dispersion of AuNP 1. The oxygen was removed by degassing with argon for 1 hour. The following polymerization was carried out at 40 °C for 3 days. The dark purple product was collected by centrifugation (8000 rpm, 30 min, room temperature) and washed three times with 30 mL of water. The product was not dried completely to prevent agglomeration.

Thermogravimetric analysis (TGA) indicated a Au content of 91 wt-% (Au/Cage = 9/1 (w/w)). The molar ratio between Au and S (Au/S) was calculated to be Au/S = 1/6.2 (n/n).

3.5 Synthesis of vinyl-mono-functionalized AuNP (3)

N,N'-diisopropylcarbodiimide (200 μL, 1.284 mmol, 1.50 eq) was added to the dispersion of AuNP 2 in 5 mL of DMF followed by stirring at room temperature for 1 hour. 4-Vinylaniline (100 μL, 0.856 mmol, 1.00 eq) was then added in one portion. After 18 hours the product was precipitated from 50 mL methanol, collected by centrifugation (8000 rpm, 30 min) and washed with methanol three times. The product was dried in vacuum at room temperature.

3.6 Copolymerization of AuNP (3) with MMA (AuNP-co-PMMA 4)

Methyl methacrylate (833 mg, 8.32 mmol, 98 wt%, 1M) was added to the dispersion of AuNP **3** (17 mg, 2 wt%) in DMF. A solution of AIBN in DMF (105 μ L, 0.032 g/mL) was injected. After removing oxygen by degassing with argon, the polymerization was carried out at 80 °C for 5 h. The product was precipitated from 300 mL of methanol and collected by centrifugation (8000 rpm, 10 min, room temperature). After washing three times with methanol, the purple copolymer was dried in vacuum at 40 °C for 48 h. $M_n = 33,000 \text{ g mol}^{-1}$, $PDI = 1.3$. The spherical AuNPs had a mean diameter of $4.5 \pm 2.2 \text{ nm}$. The Au content of **AuNP-co-PMMA** of 3.6 wt% was determined by TGA.

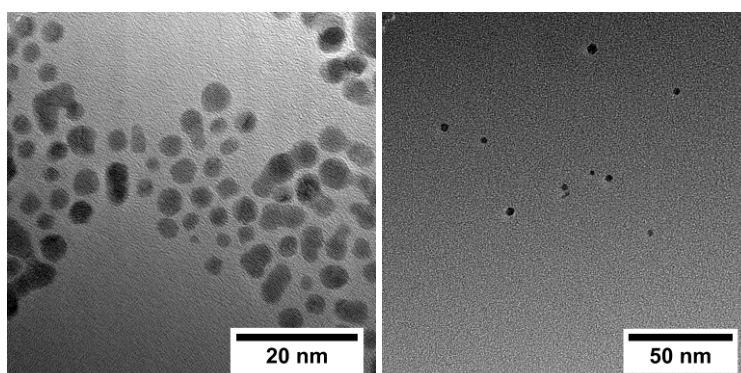


Figure S4.1. Representative TEM image of AuNP **1** (left) and AuNP-co-PMMA **4** (right).

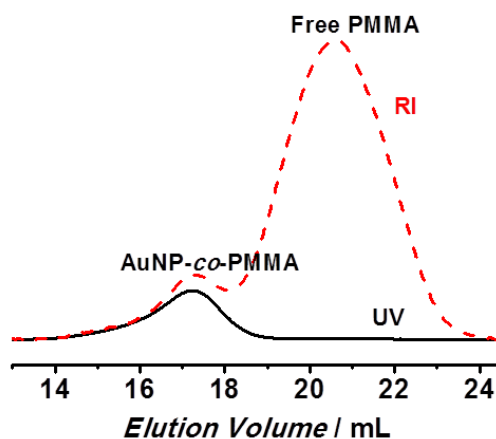


Figure S4.2. DMF-GPC chromatogram of AuNP-co-PMMA (red dashed trace: RI-detector, black solid trace: UV detector at $\lambda = 518 \text{ nm}$).

3.7 Synthesis and characterization of Cage-co-PMMA

An aqueous solution of NaCN (9.2 mg, 0.19 mmol, 4.6 eq) was added to the dispersion of AuNP-co-PMMA (200 mg, 8.0 mg Au, 0.04 mmol Au, 1.0 eq) in THF. The reaction mixture was

stirred open to the air at room temperature for 24 hours, until the solution turned colorless. The product was precipitated from 100 mL methanol and collected by centrifugation (8000 rpm, 10 min). After washing the white residue with methanol three times, the product was dried at 40 °C under 50 mbar. Isolated polymer cages without PMMA were observed as mono-disperse nanospheres in TEM micrographs after staining with osmium tetroxide (OsO_4). The corresponding Raman spectrum showed a significantly higher intensity of S-S- than S-H-vibration, indicating the formation of disulfide bonds during the oxidative etching process.

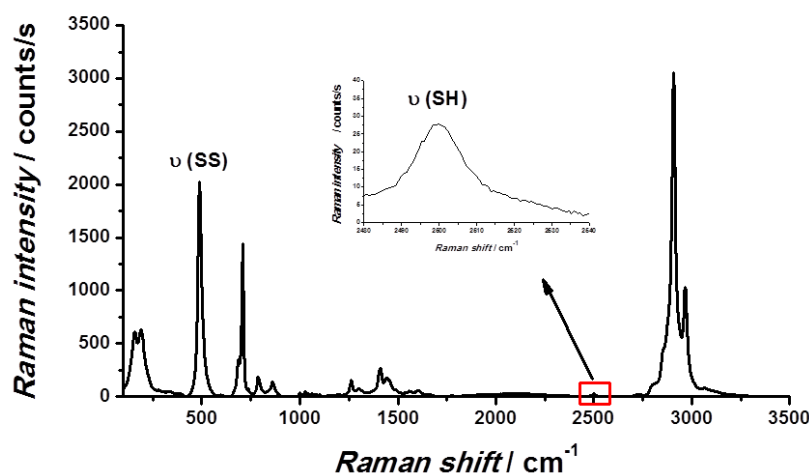


Figure S4.3. Raman spectrum of polymer cage without PMMA.

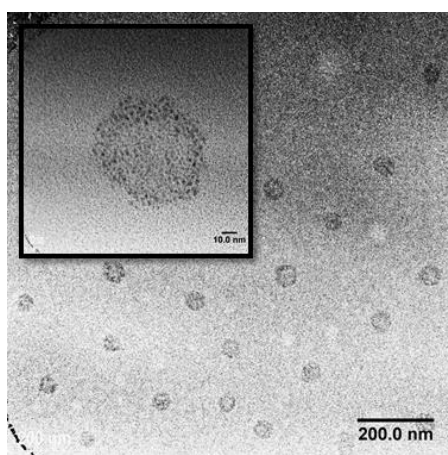


Figure S4.4. TEM image of polymer cage (OsO_4 staining).

3.8 Polystyrene-*block*-poly(4-vinylpyridine) (PS-*b*-PVP)

PS-*b*-PVP was prepared by sequential living anionic polymerization using *sec*-BuLi as initiator. The reaction was carried out in a thermostated laboratory autoclave (1 L, Büchi) at a

temperature of $-78\text{ }^{\circ}\text{C}$ using 400 mL of dried THF as solvent. After adding 2.41 mL (3.6 mmol, 1.48 M, 1 eq.) of *sec*-BuLi, 29.6 g (284 mmol, 79 eq.) of styrene were transferred into the reactor *via* an ampule. The reaction solution turned orange due to the formation of polystyryl anions. After stirring for 10 min, a sample of the polystyrene-precursor (PS-precursor) was taken for NMR and GPC analysis. Upon adding 0.63 mL (3.6 mmol, 1 eq.) of 1,1'-Diphenylethylene (DPE) for end capping of the living polystyryl anions, the color of the solution turned deep red. After stirring for another 30 min, 15.3 g (145 mmol, 40 eq.) of 4-vinylpyridine were added. After one hour, the reaction was terminated with degassed methanol. After warming up to room temperature, PS-*b*-PVP was precipitated from pentane. The composition and molecular weight of the PS-*b*-PVP was determined by ^1H -NMR using the M_n of the PS-precursor, determined by THF-GPC (PS calibration), for NMR signal calibration. Thus, the composition of the diblock copolymers was determined to PS₇₇-*b*-PVP₃₄ (numbers correspond to the number-averaged degree of polymerization of the respective block) with a M_n of 11,600 g mol⁻¹ and a polydispersity index $PDI = 1.2$ (determined by DMF-GPC).

Characterization:

^1H -NMR (300 MHz, CDCl_3) $\delta = 8.6\text{--}8.0$ (m, 2H, ArH of PVP), $7.2\text{--}6.2$ (m, 7H ArH), $2.3\text{--}0.8$ (CH_2CH), $0.8\text{--}0.4$ (m, 6H of initiator) ppm.

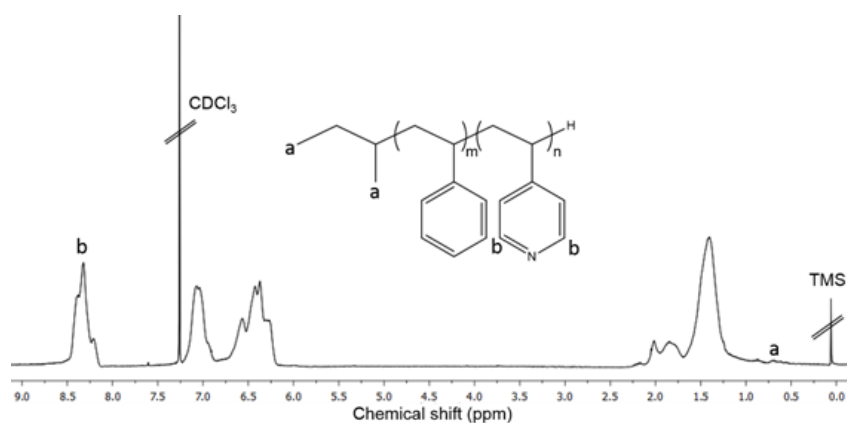


Figure S4.5. ^1H -NMR (300 MHz, CDCl_3) spectrum of PS-*b*-PVP.

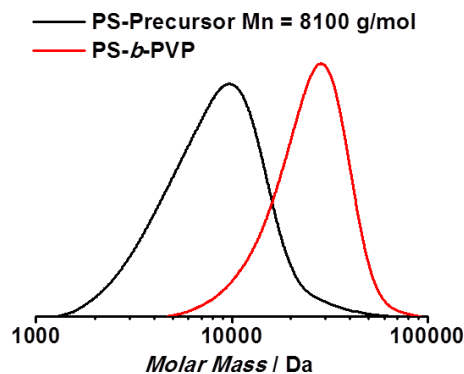


Figure S4.6. GPC chromatogram of PS- Precursor (black trace) and PS-*b*-PVP (red trace) in DMF ($PDI = 1.2$).

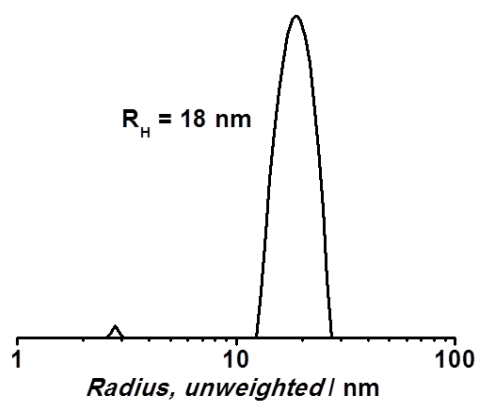


Figure S4.7. DLS measurement of PS-*b*-PVP in THF.

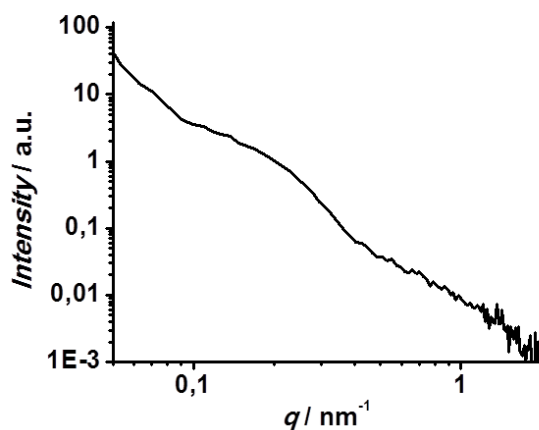


Figure S4.8. SAXS data of PS-*b*-PVP.

3.9 AuNPs in Cage-co-PMMA and PS-*b*-PVP prepared by in-situ method

In-situ Preparation of AuNPs in Cage-co-PMMA and in PS-*b*-PVP: Polymeric ligands (Cage-co-PMMA and PS-*b*-PVP) were dissolved in a stock solution of $\text{HAuCl}_4 \cdot 3\text{H}_2\text{O}$ (1 mM, 10 mL, 1.0 eq)

in THF. The reaction mixture was stirred at room temperature for 1 hour. Subsequently, a freshly prepared NaBH₄ solution (10.0 eq in MeOH) was slowly added to the reaction mixture. After 1 hour stirring at room temperature the product was precipitated from methanol and collected by centrifugation (8000 rpm, 10 min, 20 °C). After washing with water three times with methanol the nanoparticle/polymer composite was dried in vacuum at 40 °C for 24 hours.

***In-situ* Preparation of AgNP, PdNP and PtNPs in Cage-co-PMMA:** The stock solution of metal salts was added to the solution of Cage-co-PMMA in THF so that the concentration of metal salt was adjusted to 1 mM. The reaction mixture was stirred at room temperature for 1 h followed by the addition of Superhydride (0.2 mL, 1 M solution in THF). After 10 min the reaction mixture was precipitated from 100 mL methanol. The resulting product was collected by centrifugation (8000 rpm, 10 min, 20 °C) and washed three times with 30 mL methanol. The solids were dried at 40 °C under 50 mbar.

Table S4.1. Reaction parameters for the *in-situ* syntheses of AuNPs in Cage-co-PMMA and PS-*b*-PVP.

Cage-co-PMMA		PS- <i>b</i> -PVP	
Eq(Au)	n(Au)/n(S)	Au/PS- <i>b</i> -PVP	n(Au)/n(N)
0.25	1/25	2	1/17
0.50	1/12.5	10	1/3.4
0.75	1/8.3	20	1/1.7
1.00	1/6.2	30	1/1.1
1.25	1/5.0	50	1/0.7
1.67	1/3.7	60	1/0.6

3.10 Characterization of AuNP in Cage-co-PMMA and PS-*b*-PVP

UV-Vis spectra, TEM micrographs, histograms of AuNP diameter from TEM analysis and SAXS data of each sample are presented as follows.

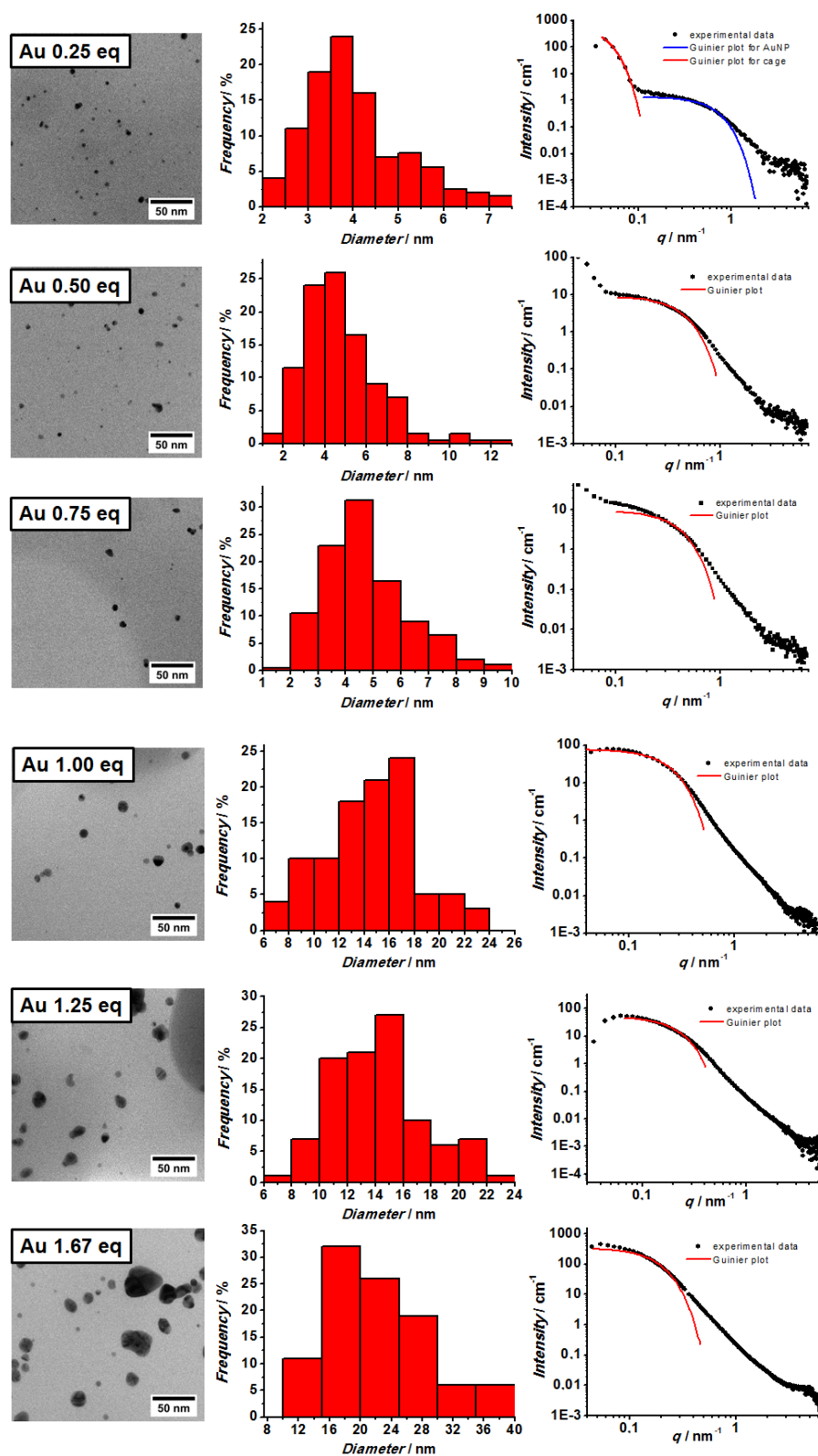


Figure S4.9. Size evolution of AuNPs in Cage-co-PMMA.

All the UV-Vis spectra for AuNPs were normalized at 400 nm.

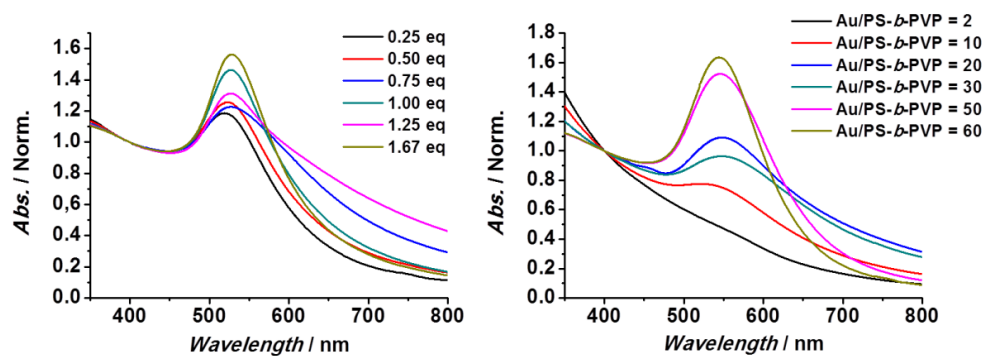


Figure S4.10. UV-Vis Spectra of AuNPs stabilized by Cage-*co*-PMMA (left) and PS-*b*-PVP (right) prepared by the *in-situ* method.

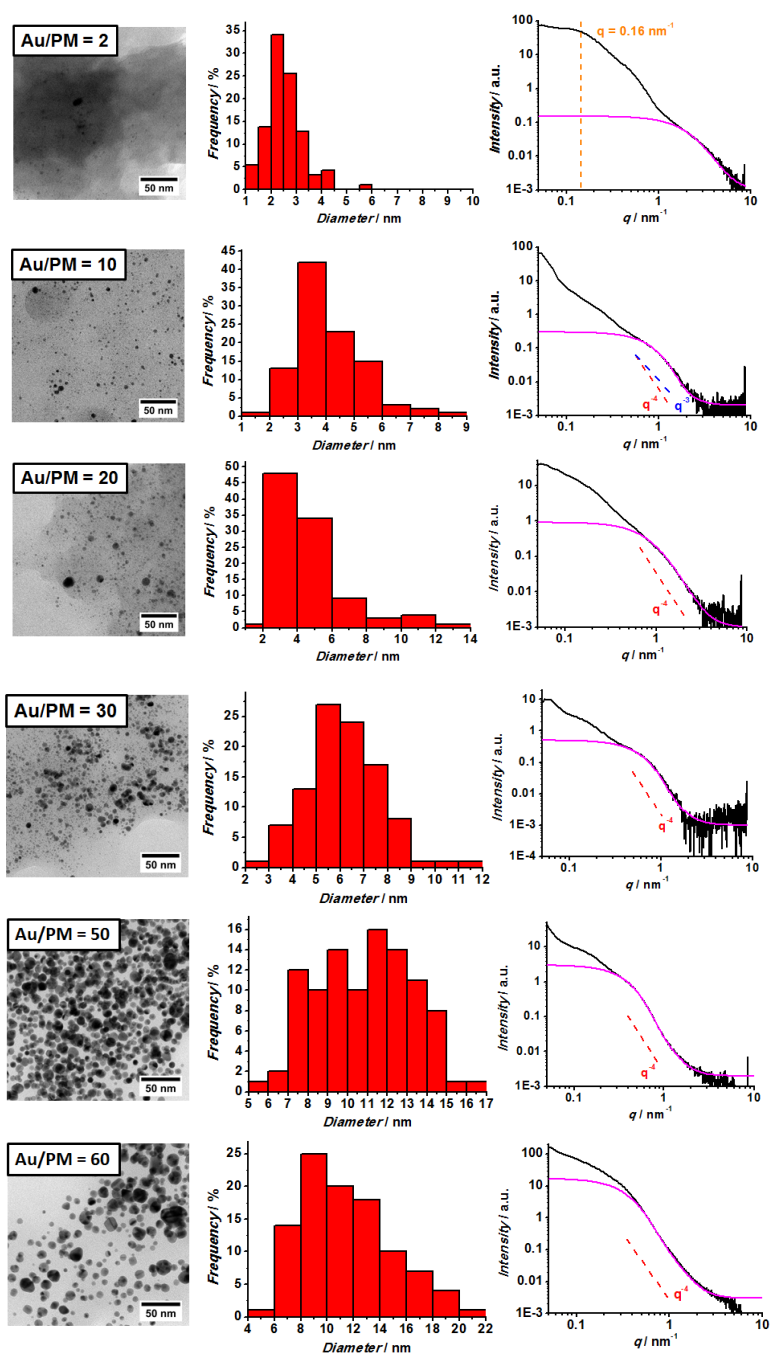


Figure S4.11. Size evolution of AuNPs in PS-*b*-PVP.

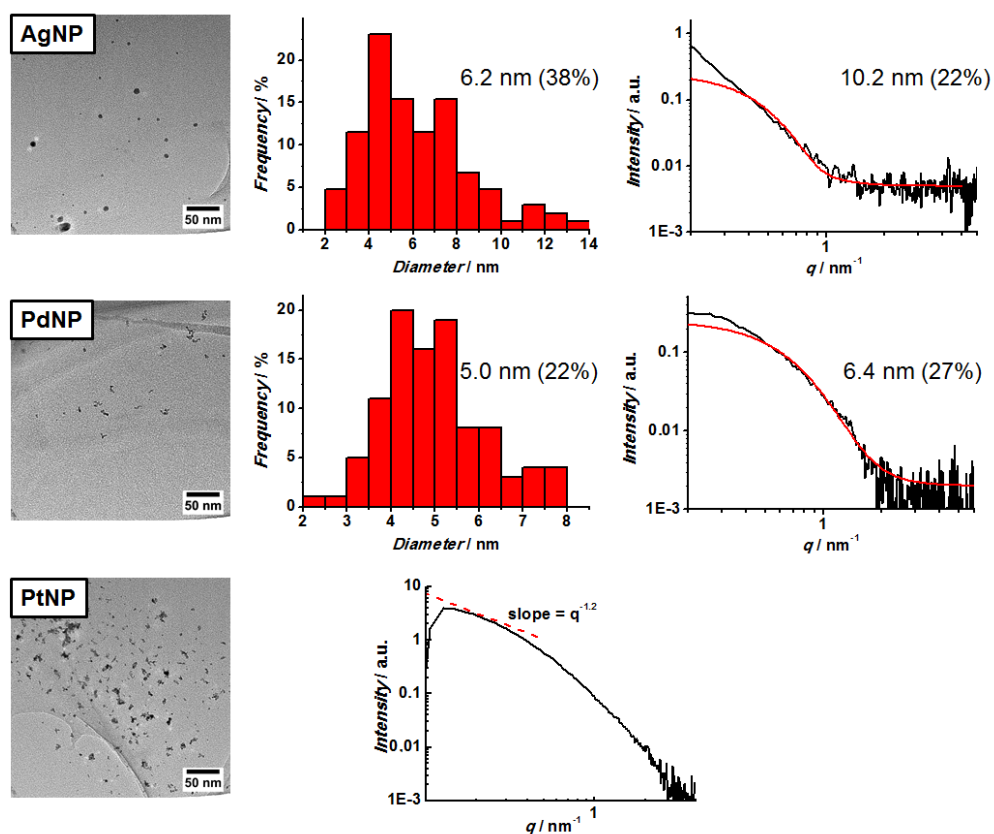


Figure S4.12. TEM analysis and SAXS data of AgNP, PdNP, and PtNP prepared in Cage-co-PMMA using *in-situ* method.

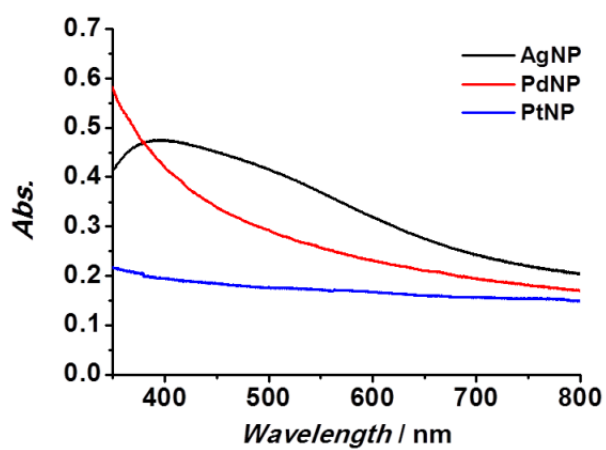
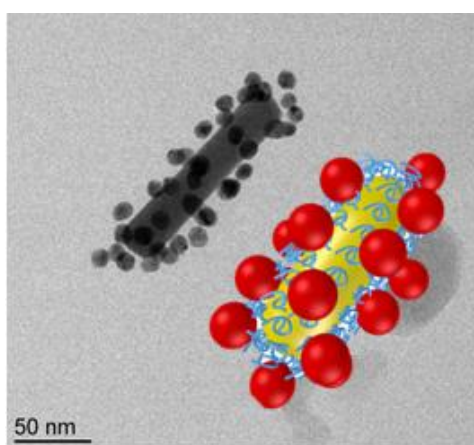


Figure S4.13. UV-Vis spectra of refilled Ag-, Pd-, and PtNPs in Cage-co-PMMA.

Chapter 5

Assembly of Gold Nanoparticles on Gold Nanorods using Functionalized Poly(*N*-isopropylacrylamide) as Polymeric “Glue”

*Ziyin Fan, Moritz Tebbe, Andreas Fery, Seema Agarwal, and Andreas Greiner**



Self-assembly of gold nanoparticles around gold nanorods is prepared by using functionalized poly(*N*-isopropylacrylamide) as polymer “glue”. The resulting nanomaterial shows certain thermoresponsive behavior. The grafting density of gold nanoparticles on the surface of gold nanorods is fine-tuned by adjusting the molar ratio between gold nanoparticles and nanorods in feed.

Abstract: A telechelic thermoresponsive polymer, α -amino- ω -thiol-poly(N-isopropylacrylamide) (H₂N-PNIPAM-SH), is used as the polymeric glue to assemble gold nanoparticles (AuNPs) around gold nanorods (AuNRs) into a satellite structure. Prepared by reversible addition-fragmentation chain transfer (RAFT) polymerization followed by hydrazinolysis, H₂N-PNIPAM-SH is able to interlink the two types of the gold building blocks with the thiol-end grafting on AuNRs and the amine-end coordinating on the AuNP surface. The density of the grafted AuNPs on AuNRs can be tuned by adjusting the molar ratio between AuNPs and AuNRs in the feed. The resulted satellite-like assembly exhibits unique optical property that was responsive to temperature change.

The heterogeneous array of nanoclusters is defined as the assembly of different types of nanomaterials regarding their size, shape, composition, and arrangement.^[1] For instance, the assembly of DNA-functionalized spherical gold nanoparticles (AuNPs) with gold nanorods (AuNRs) was applied for *in-situ* Raman spectroscopy^[2] or exploration of the mechanism of chirality based on its multiplex circular dichroism (CD) bands.^[3] The interparticle separation of the core-satellite gold nanoparticles was modulated by a reconfigurable DNA link between the gold core and satellites.^[4] These nanoparticle assemblies exhibit coupled localized surface plasmon resonances resulting from the near-field interactions of individual plasmonic nanoparticles.^[5,6] Based on the unique coupled plasmonic property, nanoparticle assemblies are designed for numerous applications in the field of biomedicine^[7], e.g. as plasmonic rulers^[8], for surface enhanced Raman spectroscopy (SERS) based on encoded NPs^[9] or clusters^[10]. This type of nanomaterial was mainly prepared through bioconjugation using e.g. DNA complementary linkers^[11–13] or biotin-streptavidin systems.^[14] Therefore, it is widely applied in bio-sensing.^[15–17] Many examples of organosulfur compounds as linkers were also well demonstrated for assembling heterogeneous nanoparticles with a controllable spatial gap down to the subnanometer range.^[18–20] In contrast, limited examples of heterogeneous nanomaterial assemblies were reported which were prepared using synthetic polymers as linker.^[21] Here, we present a versatile approach to assemble AuNPs around AuNRs forming assembled structures. We use bi-end-functionalized PNIPAM as “glue”, which provides high yields of organized nanoclusters. The thiol-end of PNIPAM was introduced as the anchor group strongly attached to the AuNR surface, while the amine-end as well as the amide component

was responsible for self-assembly of AuNPs like satellites around AuNRs. The as-prepared hierarchical nanomaterial and its thermal responsive behavior resulting from the PNIPAM “glue” was characterized by transmission electron microscopy (TEM), UV-Vis spectroscopy, and dynamic light scattering (DLS).

The assembly of AuNPs around AuNRs (AuNP@AuNR) was achieved utilizing a two-step ligand exchange approach as illustrated in **Figure 5.1a**. During the first ligand exchange, linear α -amino- ω -thiol-poly(*N*-isopropylacrylamide) (H_2N -PNIPAM-SH) displaced the native cetyl trimethylammonium bromide (CTAB) ligand on AuNR (CTAB@AuNR) surface, as thiol / disulfide groups exhibit stronger affinity towards the gold surface compared to CTAB. In the following step, the as-prepared PNIPAM grafted AuNRs (PNIPAM@AuNR) attracted the citrate-stabilized AuNPs (Ct@AuNPs) through the nitrogen compounds located within the polymer chain and at the end of PNIPAM.

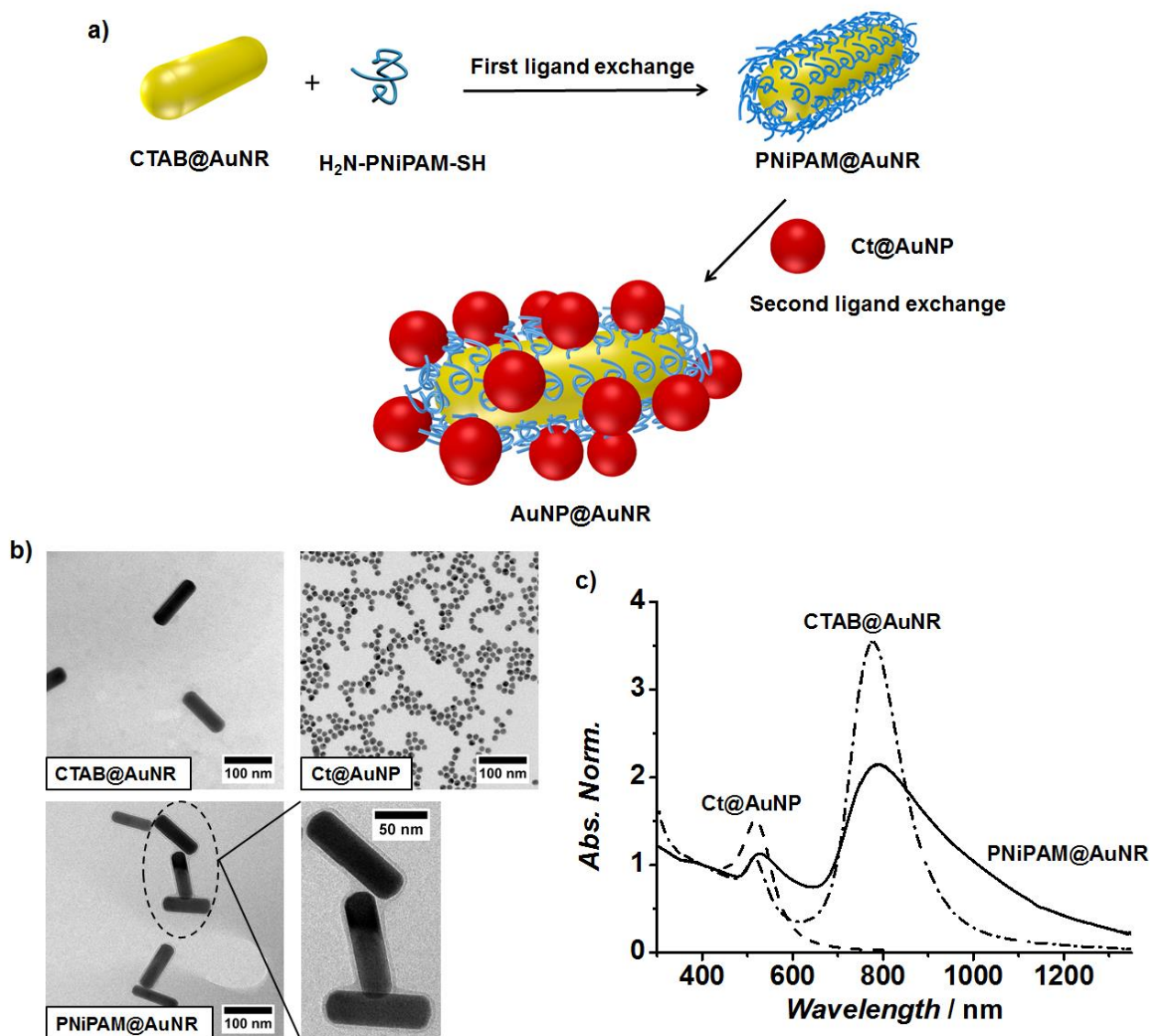


Figure 5.1. a) Schematic preparation of AuNP@AuNR assembly through functionalized PNIPAM via the two-step ligand exchange reaction. b) Representative TEM micrographs of CTAB@AuNR, Ct@AuNP, and PNIPAM@AuNR. c) UV-vis spectra of Ct@AuNP (dash trace), CTAB@AuNR (dash dot trace), and PNIPAM@AuNR (solid trace).

The polymer “glue” – the bi-end-functionalized PNIPAM – was prepared by reversible addition-fragmentation chain transfer (RAFT) polymerization with subsequent hydrazinolysis (Figure S5.1). The RAFT-polymerization of *N*-isopropylacrylamide (RAFT-PNIPAM) was carried out using phthalimidomethyl trithiocarbonate as chain transfer agent (CTA), from which RAFT-PNIPAM with trithiocarbonate on one chain end and phthalimide on the other end was generated. To demonstrate the concept of the polymeric “glue” for the nanomaterial assembly, RAFT-PNIPAM with the molecular weight of 23 400 g·mol⁻¹ (M_n : number average molecular weight, polydispersity $PDI = 1.04$, determined by matrix-assisted laser desorption ionization – time of flight mass spectrometry (MALDI-TOF MS)) was used. Hydrazine was

utilized as nucleophile and the trithiocarbonate and phthalimide ends were converted to thiol and amine, respectively. The successful deprotection of chain ends was clearly verified by NMR as the shift of the aromatic protons and aliphatic protons of trithiocarbonate disappeared after hydrazinolysis. Here, mono-dentate thiol was applied instead of bi-dentate trithiocarbonate as anchor group in order to achieve high packaging densities of grafted PNiPAM on AuNRs.^[22] Meanwhile, the amine-end was deliberately chosen to avoid unnecessary change of the properties of PNiPAM due to disulfide cross-linking and backbiting of the thiol-end in the case of bi-thiol-endfunctionalized PNiPAM. Gel permeation chromatography (GPC) analysis revealed a bimodal molecular weight distribution of H₂N-PNiPAM-SH. The additional peak was located at the double molecular weight of the original peak. This indicated the formation of disulfide bonds.^[23] Both thiol and disulfide moieties can undergo efficient ligand exchange reactions with CTAB@AuNR. The cloud point of H₂N-PNiPAM-SH (32 °C) was determined to be slightly higher compared to RAFT-PNiPAM (30 °C) due to its hydrophilic chain ends.^[24] Characterizations of RAFT-PNiPAM and H₂N-PNiPAM-SH (NMR, GPC, MALDI and phase transition behavior) are given in Figure S5.2, Supporting Information).

Highly monodisperse CTAB@AuNR were synthesized following a modified seed-mediated method published by Vigdermann et al.^[25] using hydroquinone as reducing and silver nitrate as growth agent compared to ascorbic acid which is applied in conventional CTAB@AuNR synthesis.^[26] Consequently, the reaction kinetics are reduced and in combination with a large excess of hydroquinone. The well-controlled synthesis provides high aspect ratio AuNRs (~8), high gold conversion rates (~100%), and most importantly, low amounts of unfavorable byproducts like spheres and cubes (<1%). Thus, the CTAB@AuNR particles could be functionalized in a subsequent step with polymer without further purification steps. The obtained CTAB@AuNR exhibited a mean length of 88 ± 16 nm and width of 26 ± 7 nm derived from TEM analysis (Figure 5.1b) and the aspect ratio was calculated to be 3.4. According to the UV-Vis spectrum (Figure 5.1c), the transverse and longitudinal surface plasmon resonance (TSPR and LSPR) peaks of CTAB@AuNR were located at 514 nm and 777 nm, respectively. Ct@AuNP with a mean diameter of 12 ± 3 nm and SPR mode at 517 nm were prepared by the well-established Turkevich method.^[27] The details of the preparation of CTAB@AuNR and Ct@AuNP are given in the Supporting Information.

After the obtained AuNRs had been grafted with H₂N-PNiPAM-SH, the UV-vis spectrum of AuNRs experienced a red-shift by about 10 nm as a result of the changing refractive index in close proximity of the AuNRs surface due to the applied polymer shell. It is observed in the UV-vis spectra of PNiPAM@AuNR that the LSPR band with a shift around 790 nm was broadened and the ratio of the absorbance of LSPR to TSPR was increased. This was resulted from the fusion of the PNiPAM-shell on AuNRs during purification, which led to the formation of the interconnected AuNRs in different geometries (side-by-side, end-to-end, and end-to-side). Furthermore, the PNiPAM shell around AuNRs could be clearly identified in the TEM micrographs (Figure 5.1b). The thermoresponsive behavior of PNiPAM@AuNR was characterized by DLS. Above the cloud point, the hydrodynamic radius of PNiPAM@AuNRs was significantly decreased as the polymer shell surface shrank. (DLS analysis^[28] of PNiPAM@AuNR is given in Figure S5.3.)

The self-assembly of AuNPs around AuNRs took place upon adding Ct@AuNP to the dispersion of PNiPAM@AuNR in 2-(*N*-morpholino)ethanesulfonic acid (MES) buffer solution (10 mM). The as-prepared hierarchical AuNP@AuNR assemblies were purified by centrifugation to remove the unbounded AuNPs. The satellite-like nanostructure of the assembly was confirmed by TEM as shown in **Figure 5.2a**. The grafted AuNPs were homogeneously distributed around the AuNRs, at their sides as well as at their ends. The optical properties of AuNP@AuNR assemblies were characterized by UV-vis spectroscopy as shown in Figure 3.2b including the data obtained for Ct@AuNP and PNiPAM@AuNR for comparison. After the grafting of the AuNPs, the low-energy resonance was significantly red-shifted by about 85 nm to 875 nm, compared to the LSPR of PNiPAM@AuNR located at 790 nm. The high-energy resonance of the coupled plasmonic assemblies appeared with an additional broad shoulder at around 590 nm featuring the quadrupolar resonance.^[6,29]

The grafting density of AuNPs on AuNR surface could be easily tuned by adjusting the ratio of AuNP to that of AuNR (AuNP/AuNR) in feed. As observed in the TEM micrographs (Figure 5.2e), the number of grafted AuNPs per AuNR was increased from 6 ± 2 to 18 ± 3 as a consequence of the increased gold atom ratio of AuNP/AuNR from 0.2 to 0.8 (Figure 5.2d). Moreover, the shoulder of the high-energy resonance in the UV-vis spectrum developed with the AuNP/AuNR ratio and eventually transformed into a single peak centered at 592 nm. (Figure 5.2c) as a

result of strong interparticle plasmonic coupling.^[5] Additional examples of AuNP@AuNR assemblies are given in Figure S5.4, Supporting Information.

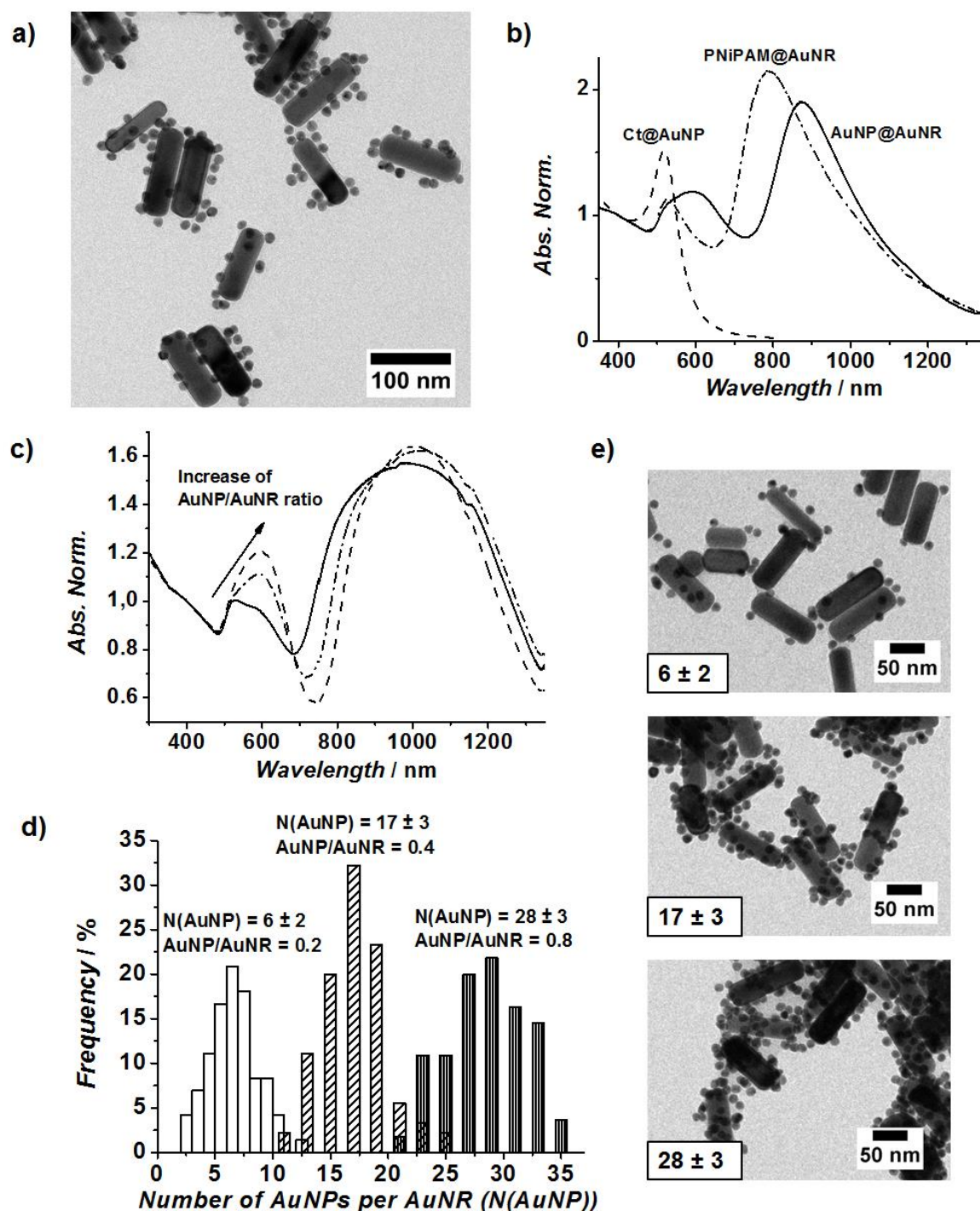


Figure 5.2. Characterizations of AuNP@AuNR assembly. a): Representative TEM images of AuNP@AuNR assembly. b): Comparison of UV-vis spectra of Ct@AuNP (dash trace), PNiPAM@AuNR (dash dot trace), and AuNP@AuNR assembly (solid trace). c): UV-vis spectra of AuNP@AuNR assemblies with different AuNP/AuNR ratio in feed. All UV-vis spectra were normalized at 400 nm. d): Frequency counts of the number of AuNPs ($N(\text{AuNP})$) on each AuNR depending on the AuNP/AuNR ratio. e): Representative TEM images showing the grafting density of AuNPs increased with the AuNP/AuNR ratio.

The prepared AuNP@AuNR assemblies exhibited a thermoresponsive behavior derived from the DLS and UV-vis measurements as expected for a PNIPAM anchor polymer. Above the cloud point, the collapse of the PNIPAM chain resulted in a decrease of the hydrodynamic radius of AuNP@AuNR (Figure S5.3). However, the cryo-TEM measurements detected no significant change of the distance between AuNPs and AuNR in single AuNP@AuNR assembly at 6 °C and 45 °C. (**Figure 5.3a**) This is due to the limited resolution of this technique and challenges for the evaluation process caused by the two-dimensional (2D) projection of the assembled structures in TEM micrographs. TEM tomography would circumvent these problems but is beyond the scope of this work. The UV-vis spectra of AuNP@AuNR assemblies were recorded at different temperatures confirming the thermoresponsible behavior of AuNP@AuNR assemblies (Figure 5.3b). After the dispersion was heated to 45 °C, the high and low energy resonance peaks of AuNP@AuNR assembly were both red-shifted by about 10 nm, which indicated the increased coupling efficiency due to a decrease in inter-particle distance between AuNPs and AuNRs. During several consecutive heating-cooling cycles, the AuNP@AuNR assembly displayed moderate thermal reversibility as characterized by DLS and UV-Vis spectra (Figure S5.3 and S5.5). One plausible explanation could be taken into account. PNIPAM chains were partially wrapped around the AuNPs and therefore the chains lose their mobility which results in a change of the thermal reversibility of PNIPAM. Furthermore, AuNPs on AuNRs were not organized in a perfectly identical manner, which could undermine the significant optical change in response to the temperature.

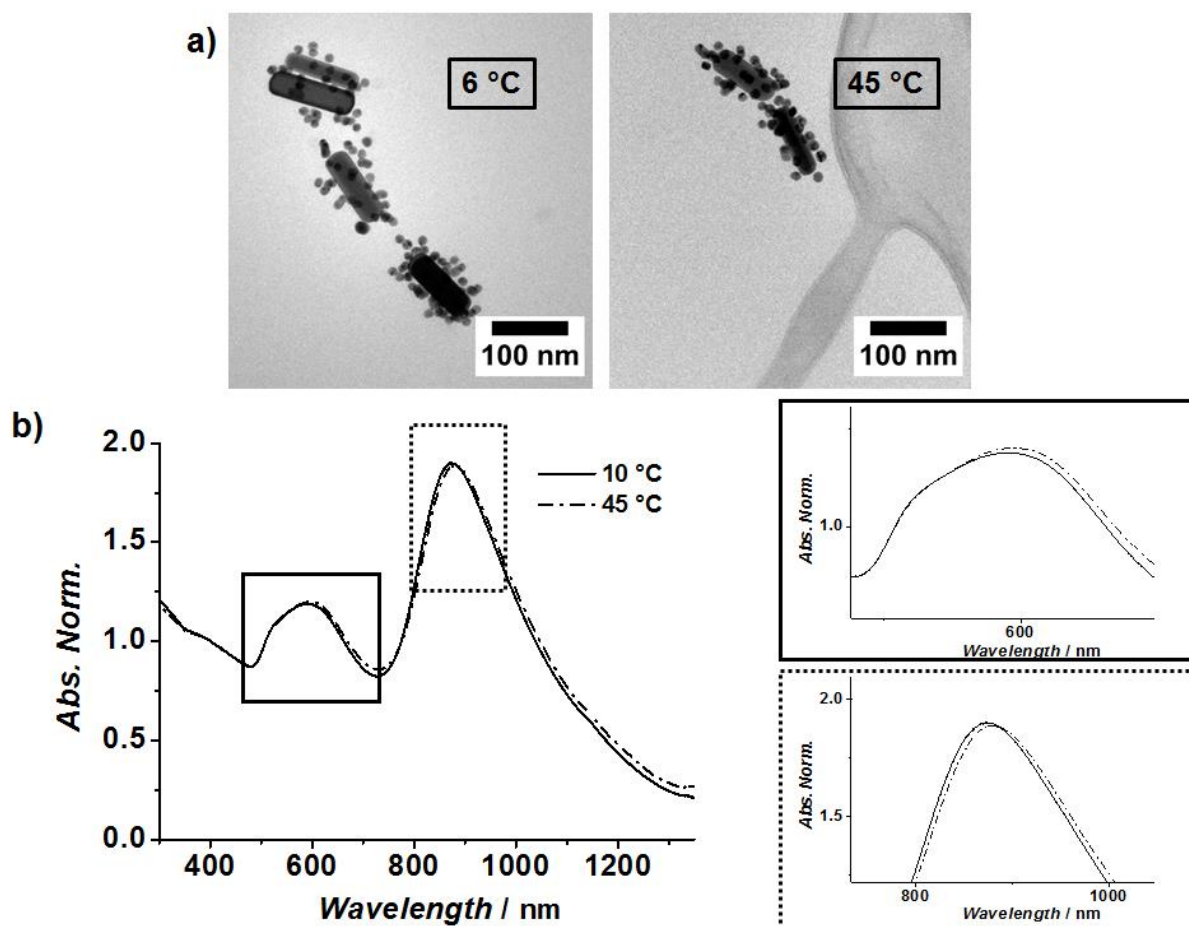


Figure 5.3. Characterization of the thermoresponsibility of AuNP@AuNR assembly. a): Representative cryo-TEM micrographs, left: measured at 6 °C, right: measured at 45 °C. b): UV-Vis spectra of AuNP-AuNR assembly measured at 10 °C (solid trace) and 45 °C (dash dot trace). The magnifications of the low (marked in the dash square box) and high energy resonance (marked in the solid square box) are given on the right side.

In this work, assemblies of AuNPs around AuNRs were successfully prepared *via* a two-step ligand exchange approach using bi-end-functionalized PNIPAM (H₂N-PNIPAM-SH) as an interlayer between gold building blocks. The functionalized PNIPAM was synthesized through RAFT polymerization followed by hydrazinolysis for the modification of the end groups, which exhibited the cloud point at 32 °C in the aqueous solution. CTAB-stabilized AuNR (CTAB@AuNR) was coated by PNIPAM shell through ligand exchange with the thiol end. The polymer shell around AuNR was directly observed in a TEM micrograph and the thermoresponsibility of PNIPAM@AuNR was verified by DLS analysis. Subsequently, AuNPs with a mean diameter of 13 nm were assembled around AuNRs by exchanging the citrate ligand with the nitrogen moieties of the PNIPAM-glue. The grafting density of AuNPs on AuNR surface and its resulting plasmonic property was tuned by changing the molar ratio of AuNP/AuNR in the feed. The obtained hierarchical plasmonic nanomaterial exhibits unique optical property due to the interparticle coupling effect. The thermal responsive behavior of

the satellite-like assembly of gold nanoclusters resulted from the PNIPAM interlayer. When the temperature was increased above the cloud point, the collapsed PNIPAM interlayer triggered the decrease of the spatial gap between AuNPs and AuNRs and thus the red-shift of the measured UV-Vis spectrum. In the future work, the concept of the polymer glue will be optimized to prepare regiospecific assemblies and the study of the SERS characteristic of such nanomaterials with core-satellite structure in correlation of temperature change will be carried out. Based on the unique properties, this nanomaterial assembly has a promising future in the field of biomedicine and biosensing.

Acknowledgements

The work is financially supported by SFB 840 and by the European Research Council under grant ERC-2012-StG 306686 (METAMECH: Template-assisted assembly of METAmaterials using MECHANical instabilities). Ziyin Fan and Moritz Tebbe were supported by the Elite Network Bavaria in the frame of the Elite Study Program “Macromolecular Science” and funded via a grant for Ph.D. candidates according to the Bavarian Elite Promotion Act (BayEFG). The authors thank Dr. Markus Drechsler (University of Bayreuth) for the cryo-TEM measurement.

References

- [1] J. M. Romo-Herrera, R. Alvarez-Puebla, L. M. Liz-Marzán, *Nanoscale* **2011**, 3, 1304.
- [2] L. Xu, H. Kuang, C. Xu, W. Ma, L. Wang, N. Kotov, *J. Am. Chem. Soc.* **2012**, 134, 1699.
- [3] C. Hao, L. Xu, W. Ma, L. Wang, H. Kuang, C. Xu, *Small* **2014**, 10, 1805.
- [4] D. S. Sebba, J. J. Mock, D. R. Smith, T. H. LaBean, A. A. Lazarides, *Nano Lett.* **2008**, 8, 1803.
- [5] S. K. Ghosh, T. Pal, *Chem. Rev.* **2007**, 107, 4797.
- [6] S. J. Barrow, X. Wei, J. S. Baldauf, A. M. Funston, P. Mulvaney, *Nat. Commun.* **2012**, 3, 1275.
- [7] J. N. Anker, W. P. Hall, O. Lyandres, N. C. Shah, J. Zhao, R. P. Van Duyne, *Nat. Mater.* **2008**, 7, 443.

- [8] C. Sönnichsen, B. M. Reinhard, J. Liphardt, A. P. Alivisatos, *Nat. Biotechnol.* **2005**, 23, 741.
- [9] M. Sanles-Sobrido, W. Exner, L. Rodríguez-Lorenzo, B. Rodríguez-González, M. A. Correa-Duarte, R. A. Alvarez-Puebla, L. M. Liz-Marzán, *J. Am. Chem. Soc.* **2014**, 2699.
- [10] N. Pazos-perez, C. S. Wagner, J. M. Romo-herrera, L. M. Liz-marzún, F. J. G. De Abajo, A. Wittemann, A. Fery, R. A. Alvarez-puebla, *Angew. Chem.* **2012**, 124, 12860; *Angew. Chem. Int. Ed.* **2012**, 51, 12688.
- [11] C. A. Mirkin, R. L. Letsinger, R. C. Mucic, J. J. Storhoff, *Nature* **1996**, 382, 607.
- [12] L. H. Tan, H. Xing, H. Chen, Y. Lu, *J. Am. Chem. Soc.* **2013**, 135, 17675.
- [13] Y. Zheng, T. Thai, P. Reineck, L. Qiu, Y. Guo, U. Bach, *Adv. Funct. Mater.* **2013**, 23, 1519.
- [14] S. Pierrat, I. Zins, A. Breivogel, C. Sönnichsen, *Nano Lett.* **2007**, 7, 259.
- [15] D. Radziuk, H. Moehwald, *Phys. Chem. Chem. Phys.* **2015**, 17, 21072.
- [16] L. Cui, J. Wu, J. Li, Y. Ge, H. Ju, *Biosens. Bioelectron.* **2014**, 55, 272.
- [17] X. Liu, Q. Dai, L. Austin, J. Coutts, G. Knowles, J. Zou, H. Chen, Q. Huo, *J. Am. Chem. Soc.* **2008**, 130, 2780.
- [18] J. H. Yoon, Y. Zhou, M. G. Blaber, G. C. Schatz, S. Yoon, *J. Phys. Chem. Lett.* **2013**, 4, 1371.
- [19] N. Gandra, A. Abbas, L. Tian, S. Singamaneni, *Nano Lett.* **2012**, 12, 2645.
- [20] J. H. Yoon, J. Lim, S. Yoon, *ACS Nano* **2012**, 6, 7199.
- [21] R. L. Truby, S. Y. Emelianov, K. a Homan, *Langmuir* **2013**, 29, 2465.
- [22] B. C. Mei, E. Oh, K. Susumu, D. Farrell, T. J. Mountziaris, H. Mattoussi, *Langmuir* **2009**, 25, 10604.
- [23] H. Pletsch, L. Peng, F. Mitschang, A. Schaper, M. Hellwig, D. Nette, A. Seubert, A. Greiner, S. Agarwal, *Small* **2014**, 10, 201.
- [24] Y. Xia, N. A. D. Burke, H. D. H. Stöver, *Macromolecules* **2006**, 39, 2275.
- [25] L. Vigdeman, E. R. Zubarev, *Chem. Mater.* **2013**, 25, 1450.
- [26] B. Nikoobakht, M. A. El-sayed, *Chem. Mater.* **2003**, 15, 1957.
- [27] J. Turkevich, P. C. Stevenson, J. Hiller, *Discuss. Faraday Soc.* **1951**, 11, 55.

- [28] H. Liu, N. Pierre-Pierre, Q. Huo, *Gold Bull.* **2012**, 45, 187.
- [29] J. Rodríguez-Fernández, J. Pérez-Juste, F. J. García De Abajo, L. M. Liz-Marzán, *Langmuir* **2006**, 22, 7007.
- [30] A. Postma, T. P. Davis, R. A. Evans, G. Li, G. Moad, M. S. O'Shea, *Macromolecules* **2006**, 39, 5293.

Supporting Information

Assembly of gold nanoparticles on gold nanorods using functionalized Poly(*N*-isopropylacrylamide) as Polymeric “Glue”

*Ziyin Fan, Moritz Tebbe, Andreas Fery, Seema Agarwal and Andreas Greiner**

Contents:

1. Chemicals
2. Instrumentation
3. α -Amino- ω -thiol-poly(*N*-isopropylacrylamide)
4. Citrate-stabilized gold nanoparticle (Ct@AuNP)
5. CTAB-stabilized gold nanorods (CTAB@AuNR)
6. Assembly of gold nanoparticles around gold nanorods (AuNP@AuNR)

1. Chemicals:

Tetrachloroauric acid trihydrate ($\text{HAuCl}_4 \cdot 3\text{H}_2\text{O}$), hydrazine-1-hydrate, and *N*-isopropylacrylamide were purchased from Alfa Aesar. Trisodium citrate dihydrate, *N*-(bromomethyl)phthalimide, 1-butanethiol, carbon disulfide, triethylamine, azobisisobutyronitril (AIBN), 2-(*N*-morpholino)ethanesulfonic acid (MES) sodium borohydride (NaBH_4 , $\geq 99.99\%$), gold(III) chloride trihydrate ($\text{HAuCl}_4 \cdot 3\text{H}_2\text{O}$, $\geq 99.9\%$), silver(I) nitrate (AgNO_3 , $\geq 99.9\%$), and hydroquinone (HQ, $\geq 99\%$) were purchased from Sigma Aldrich. Hexadecyltrimethylammonium bromide (CTAB, 99%, iodine content: 0.44 mg/kg (ICP-MS)) was purchased from Merck KGaA. *N*-isopropylacrylamide was recrystallized from hexane/diethyl ether ($v/v = 6/1$) and AIBN was recrystallized from diethyl ether before use. All other chemicals were used as received without further purification. The glassware used for the synthesis of nanoparticles and nanorods was cleaned with aqua regia. Chloroform was dried over calcium hydride and stored over a molecular sieve (0.4 nm). All other solvents were of PA grade and Milli-Q water (Millipore) with a final resistivity of 18.2 M Ω cm was used in all experiments.

2. Instrumentation:

Transmission electron microscopy (TEM): TEM measurements were performed on a ZEISS EM922 Omega with an acceleration voltage of 200 kV. Samples were prepared by drop-casting of the concentrated nanoparticle dispersion in water (ca. 0.1 mM) onto a carbon-covered copper grid (Carbon Support Films, 300 mesh, Quantifoil, first treated with Argon plasma). The micrographs were evaluated using *ImageJ* (National Institute of Health, USA, version 1.44c). For each sample at least 100 particles were measured. For calculation of the number of AuNPs around AuNR, at least 50 assemblies were counted.

Cryo transmission electron microscopy (Cryo-TEM): The sample for cryo-TEM was prepared by drop-casting of the concentrated nanoparticle dispersion in water on a lacey carbon-covered copper grid (Science Service, Munich). The liquid was removed from the grid via the shock vitrifying in liquid ethane in a temperature-controlled freezing unit (Zeiss Cryobox, Zeiss NTS GmbH, Oberkochen, Germany). The sample was transferred using a cryo-transfer holder at 90K. TEM micrographs were measured on a ZEISS EM922 Omega EF-TEM.

UV-Vis spectroscopy: The UV-Vis spectra were recorded using a two-beam-photometer JASCO with a quartz glass cuvette. The samples were prepared in water and measured at different temperatures.

Dynamic light scattering (DLS): DLS measurement was carried out using an ALV DLS/SLS-SP 5022F equipment at a scattering angle of 90°. The DLS equipment consists of an ALV-SP 125 laser goniometer, an ALV 5000/E correlator, and a He-Ne laser operating at a wavelength of 632.8 nm. The samples were prepared in filtered aqueous dispersion and measured at different temperatures. The collected data were analyzed by the software ALV/Static and Dynamic FIT and PLOT 4.23.

Matrix-assisted laser desorption ionization – time of flight mass spectroscopy (MALDI-TOF MS): MALDI-TOF MS was carried out on a Bruker Reflex III apparatus equipped with a N₂ laser emitting radiation with a wavelength of 337 nm in linear mode at an acceleration voltage of 20 kV. The samples were prepared by “dried-droplet” method: the matrix ditranol (20 mg/mL), analyte, and salt sodium trifluoroacetate (NaTFA) were dissolved in THF separately and subsequently mixed in a ratio of 20:5:1. 0.5 µL of the mixture was dropped on the target spot and dried under air.

Gel permeation chromatography (GPC): The applied DMF-GPC set-up consists of a pump (Agilent Technologies 1260), an autosampler (Agilent Technology 1200), a pre-column (8x50 mm, Gram 10 µm), and two columns (8x300 mm, Gram 10 µm, 100 Å; 8x300 mm, Gram 10 µm, 3000 Å). The combined detector system consists of a refractive index (RI) detector and a diode array detector (DAD). The samples were dissolved in DMF (2 g/l) with 5 g/L LiBr and measured at room temperature at a flow rate of 0.5 mL/min. The DMF-GPC was calibrated with linear poly(methyl methacrylate) (PMMA). The software WinGPC Unity (Polymer Standards Service, Build 6807) was used for analysis. The internal standard for DMF-GPC is toluene.

Nuclear magnetic resonance (NMR) spectroscopy: The NMR spectra were recorded utilizing a Bruker Avance 300 UltraShield™ spectrometer at room temperature using purified CDCl₃ as solvent. The software MestReNova (Mesterelab Research S.L., Version 6.0.2) was used for data evaluation.

3. α -Amino- ω -thiol-poly(N-isopropylacrylamide) (H_2N -PNiPAM-SH)

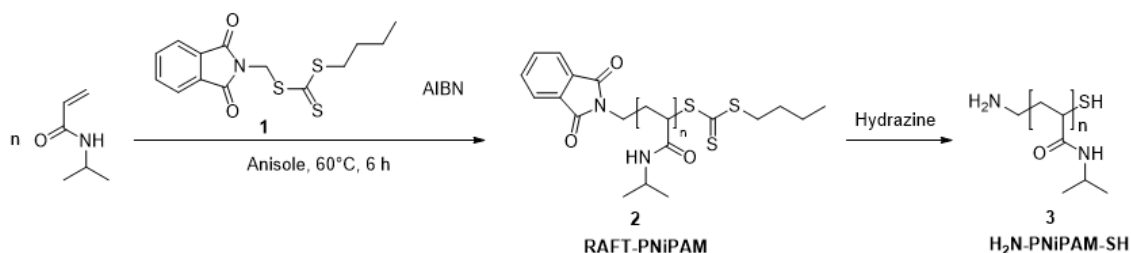


Figure S5.1. Schematic illustration of synthesis of H_2N -PNiPAM-SH.

Synthesis of CTA: Butyl Phthalimidomethyl Trithiocarbonate 1

The CTA was synthesized according to the published paper^[S1] by mixing butanethiol (0.939 g, 10.4 mmol, 1.00 eq) and carbon disulfide (1.586 g, 20.8 mmol, 2.00 eq) in 8 mL abs. chloroform under argon. Triethylamine (2.170 g, 21.5 mmol, 2.06 mmol) was added dropwise while stirring at room temperature. The color turned to yellow/orange. The mixture was kept stirring at room temperature for 3 h. (TLC: $R_f = 0.1$ in CH_2Cl_2) Then *N*-(bromomethyl)phthalimide (2.577 g, 10.4 mmol, 1.00 eq) was added. The reaction mixture became turbid and was stirred at room temperature for 16 h. (TLC: $R_f = 0.6$ in CH_2Cl_2) The mixture was diluted with CH_2Cl_2 and washed with 2×20 mL of each: deionized water, 2M $\text{H}_2\text{SO}_4(\text{aq})$, and saturated brine. The solvent was removed under reduced pressure. The crude (3.089 g, 91.1%) was purified by recrystallization in acetone.

$^1\text{H-NMR}$ (CDCl_3) δ = 0.95 (t, $^3J_{\text{HH}} = 7.3$ Hz, 3H, CH_3), 1.44 (dd, $^2J_{\text{HH}} = 15.0$ Hz, $^3J_{\text{HH}} = 7.3$ Hz, 2H, $\text{CH}_3\text{CH}_2\text{CH}_2\text{CH}_2$), 1.69 (dd, $^2J_{\text{HH}} = 15.0$ Hz, $^3J_{\text{HH}} = 7.3$ Hz, 2H, $\text{CH}_3\text{CH}_2\text{CH}_2\text{CH}_2$), 3.40 (t, $^3J_{\text{HH}} = 7.4$ Hz, 2H, $\text{CH}_3\text{CH}_2\text{CH}_2\text{CH}_2$), 5.68 (s, 2H, N- CH_2 -S), 7.77 (dd, $^3J_{\text{HH}} = 5.5$ Hz, $^4J_{\text{HH}} = 3.1$ Hz, 2H, ArH), 7.90 (dd, $^3J_{\text{HH}} = 5.5$ Hz, $^4J_{\text{HH}} = 3.1$ Hz, 2H, ArH) ppm.

$^{13}\text{C-NMR}$ (CDCl_3) δ = 13.7 (CH_3), 22.2 ($\text{CH}_3\text{CH}_2\text{CH}_2\text{CH}_2$), 31.9 ($\text{CH}_3\text{CH}_2\text{CH}_2\text{CH}_2$), 37.1 ($\text{CH}_3\text{CH}_2\text{CH}_2\text{CH}_2$), 42.1 (N- CH_2 -S), 123.9 (*o*-Ph CH), 132.0 (Ph C), 134.6 (*p*-Ph CH), 166.8 (C=O), 201.4 (CS_3) ppm.

Synthesis of poly(*N*-isopropylacrylamide) 2 by RAFT polymerization (RAFT-PNiPAM)

N-isopropylacrylamide (2082.2 mg, 18.4 mmol, 250.0 eq), butyl phthalimidomethyl trithiocarbonate (24.0 mg, 73.6 μ mol, 1.0 eq), and AIBN (1.2 mg, 7.4 μ mol, 0.1 eq) were dissolved in 5 mL anisole. The reaction mixture was degassed with an Argon inlet for 45 minutes. The polymerization was carried out at 60 °C for 6 h. The reaction was quenched by placing the flask in liquid nitrogen under open air. Samples were diluted with THF and precipitated in Et₂O two times. The polymer was collected by centrifugation and dried under vacuum at 45 °C for 18 hours yielding 1986,4 mg (95%) of poly(*N*-isopropylacrylamide) (RAFT-PNiPAM).

Synthesis of α -amino- ω -thiol-poly(*N*-isopropylacrylamide) 3 (H₂N-PNiPAM-SH)

RAFT-PNiPAM (802 mg, 1.0 eq) was dissolved in 8 mL DMF. The solution was degassed with an Argon inlet for one hour at room temperature. Hydrazin-1-hydrate (93 μ L) was added in one portion. The reaction mixture was stirred at room temperature for 18 h. Afterwards the reaction mixture was added dropwise to 100 mL of 1.2 M HCl. The solution was dialyzed against water with acetic acid at pH = 4. The as-prepared polymer was freeze-dried under vacuum yielding 773 mg (96.3%) of H₂N-PNiPAM-SH. The bimodal polydispersity of H₂N-PNiPAM-SH with an additional peak shifted at double molar mass compared to RAFT-PNiPAM indicated the formation of disulfide.

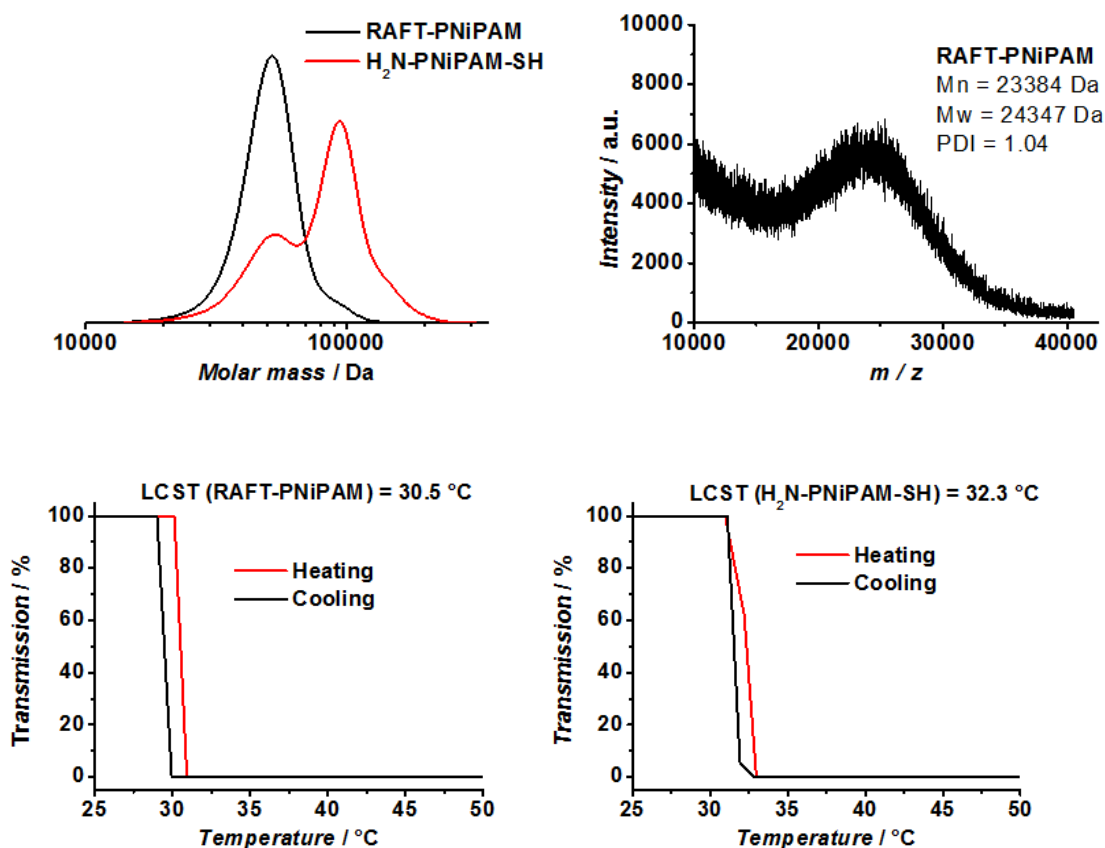


Figure S5.2. Characterizations of RAFT-PNIPAM and H₂N-PNIPAM-SH. Top left: GPC-traces of RAFT-PNIPAM (black trace) and H₂N-PNIPAM-SH (red trace). Top right: MALDI-TOF MS analysis of RAFT-PNIPAM. Bottom: Phase transition behavior of RAFT-PNIPAM (left) and H₂N-PNIPAM-SH (right) of a 0.1 wt% solution in water.

4. Citrate-stabilized gold nanoparticle (Ct@AuNP)

Synthesis of Ct@AuNP

An aqueous solution of HAuCl₄·3H₂O (0.5 mM) was heated to boiling while stirring at 500 rpm. Subsequently an aqueous solution of trisodium citrate dihydrate (5 wt%, 1.5 mL) was added in one portion. The reaction mixture was stirred while boiling at 500 rpm for 3 minutes followed by stirring at 200 rpm for 17 min. During this period the reaction mixture turned from colorless to violet and in the end wine red. The reaction mixture was cooled to room temperature while stirring at 200 rpm for 18 hours.

5. CTAB-stabilized gold nanorods (CTAB@AuNR)

The synthesis was performed following a modified procedure published by Vigdermann et al.^[52] Briefly, seeds were prepared by mixing 5 mL of two aqueous solutions. Solution 1 is a 0.2 M CTAB solution prepared by adding 0.364 g CTAB to 5 mL Milli-Q water. Solution 2 contained 0.5 mM gold precursor prepared by adding 25 μ L of a 0.1 M aqueous HAuCl₄ stock solution to 5 mL Milli-Q water. After mixing a color change from light to dark yellow indicates the formation of a gold-CTAB complex. Fast reduction was performed under vigorous stirring (1200 rpm) by adding 600 μ L of a freshly prepared 0.01 M NaBH₄ solution. The solution immediately changed its color to a light brown indicating seed formation and was let undisturbed for 30 minutes prior to use.

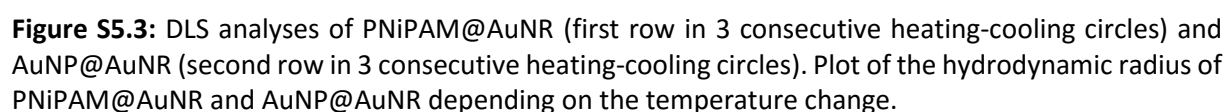
Synthesis of CTAB@AuNR was performed in a 250 mL growth solution containing 0.1 M CTAB (9.111 g). 1250 μ L of a 0.1 M aqueous HAuCl₄ stock solution was added (f.c.: 0.5 mM). Subsequently, 750 μ L of a 0.1 M silver nitrate stock solution was added (f.c.: 0.3 mM). Finally, 12.5 mL of a 0.1 M hydroquinone solution was added (f.c.: 5mM) and the solution turned clear within seconds upon shaking. The reaction was induced by injection of 4 mL of the as-prepared seed solution under vigorous stirring (1200 rpm). To prevent CTAB from crystallization and ensure constant reaction conditions the solution was stored at 32°C over night. After 5 hours a color change from clear to brownish indicated a successful AuNR growth. After synthesis the solution was concentrated to a final Au gold concentration of 2.45 mM by centrifugation at 5000 RCF.

6. Assembly of gold nanoparticles around gold nanorods (AuNP@AuNR)

Synthesis of H₂N-PNiPAM-SH coated gold nanorods (PNiPAM@AuNR)

CTAB@AuNR (3 mL, 2.45 mM [Au]) was concentrated to 100 μ L by another centrifugation step at 5000 RCF for 30 minutes at 28 °C and the concentration of CTAB was lowered to 1 mM. H₂N-PNiPAM-SH (125 mg) was dissolved in 30 mL MES buffer solution (10 mM) at 10 °C. CTAB@AuNR was added dropwise to the PNiPAM solution while stirring at 500 rpm. After stirring for 10 min, the reaction mixture was ultrasonicated for 20 minutes at 10 °C and stored at 4 °C for 18 hours. After concentrating the AuNRs by centrifugation at 4500 RCF, the product was purified by dialysis against Milli-Q water.

Characterization



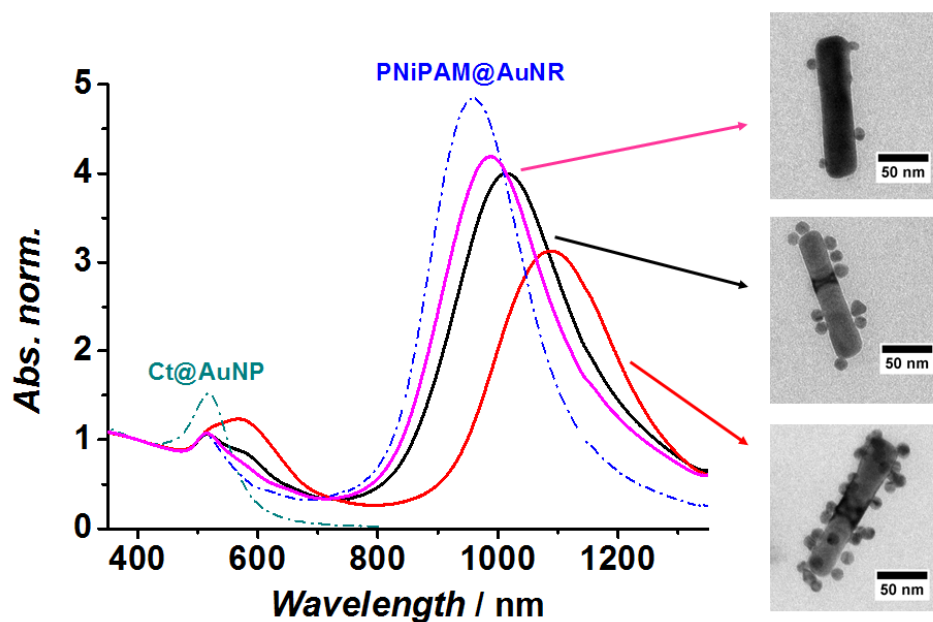


Figure S5.4. Additional examples of AuNP@AuNR assemblies with varied AuNP/AuNR ratios. Left: UV-Vis spectra of AuNP@AuNR assemblies (solid trace) and Ct@AuNP and PNiPAM@AuNR (dash dot trace) for comparison. Right: corresponding TEM micrographs of AuNP@AuNR assemblies. The diameter of AuNP was 13 ± 3 nm. The AuNP exhibited a length of 133 ± 20 nm and a width of 32 ± 7 nm.

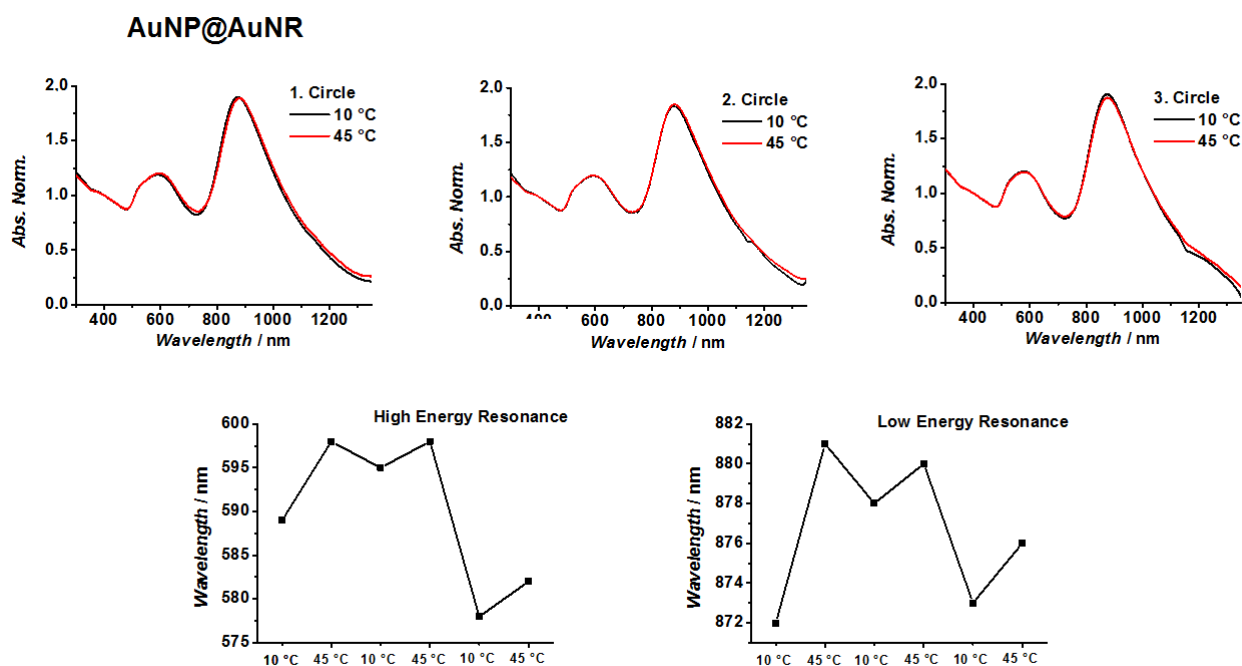


Figure S5.5. UV-vis spectra of AuNP@AuNR assembly measured in three consecutive heating-cooling cycles (top three). Plot of high (bottom left) and low (bottom right) energy resonance depending on the temperature change.

6. List of Abbreviations and Symbols

<i>A</i>₄₅₀	absorption at the wavelength of 450 nm
AFM	atomic force microscopy
AIBN	azobisisobutyronitrile
ATRP	atom-transfer radical-polymerization
AuNP	gold nanoparticle
AuNR	gold nanorod
((BiBOE) ₂ S ₂)	bis[2-(2-bromoisobutyryloxy)ethyl]disulfide]
Cage-co-PMMA	copolymer of the polymer cage with methyl methacrylate
CTA	chain transfer agent
CTAB	cetyltrimethylammonium bromide
CTAB@AuNR	CTAB stabilized gold nanorods
Ct@AuNP	citrate-stabilized gold nanoparticles
<i>d</i>	diameter in nm
DDT	dodecanethiol
DIC	<i>N,N'</i> -diisopropylcarbodiimide
DLS	dynamic light scattering
DMAc	<i>N,N'</i> -dimethylacetamide
DNA	deoxyribonucleic acid
DTMABr	dodecyl trimethylammonium bromide
ect.	and so on (Latin: <i>et cetara</i>)
e.g.	for example (Latin: <i>exempli gratia</i>)
EPR	Electron paramagnetic resonance
et al.	And others (Latin: <i>et alii</i>)

6. List of Abbreviations and Symbols

ICP-OES	inductively coupled plasma optical emission spectroscopy
IR	infrared
λ_{\max}	absorption maxima
LSPR	Longitudinal surface plasmon resonance
MenMA	L-mentholarcylate
M_n	number average molecular weight
MUMA	11-mercaptoundecyl methacrylate
M_w	weight average molecular weight
<i>N</i>	the number density of the particles
NaBH ₄	sodium borohydride
NaCN	sodium cyanate
NMR	nuclear magnetic resonance spectroscopy
OA	oleic acid
OsO ₄	osmium tetroxide
PDI	polydispersity
PEO	polyethylenoxide
PMenMA	Poly(L-mentyl methacrylate)
PMMA	polymethyl methacrylate
PMMA-SH	thiol-terminated linear polymethyl methacrylate
PNAGA	poly(<i>N</i> -acryloylglycinamide)
PNiPAM	poly(<i>N</i> -isopropylacrylamide)
PNiPAM@AuNR	PNiPAM stabilized gold nanorod
PS- <i>b</i> -PVP	poly(styrene- <i>block</i> -4-vinylpyridine)
PS- <i>b</i> -PVP@AuNP	PS- <i>b</i> -PVP stabilized gold nanoparticle
PVP	polyvinylpyridine

6. List of Abbreviations and Symbols

RAFT	reversible addition-fragmentation chain-transfer
SAXS	small-angle X-ray scattering
SAM	self-assembled monolayer
SEM	scanning electron microscopy
SERS	Surface-enhanced Raman spectroscopy
SPR	surface plasmon resonance
STM	scanning tunneling microscopy
TEM	transmission electron microscopy
TGA	thermal gravimetric analysis
TOAB	tetraoctylammonium bromide
TOPO	trioctylphosphine oxide
TPP	triphenylphosphine
TSPR	transverse surface plasmon resonance
UV-vis	Ultraviolet-visible
XPS	X-ray photoelectron spectroscopy
9-BBN	9-borabicyclo[3.3.1]nonane

7. Acknowledgement

At this moment, I want to give my sincerest thanks to all the people who have assisted me to finish this thesis.

The biggest thank goes to my supervisor **Prof. Dr. Andreas Greiner**. We first got to know each other in the lecture of polymer chemistry I, as I was a Bachelor student. He has been generously supporting me ever since. He guided me into the research field of nanocomposites and provided me this interesting and challenging topic. Without his efforts, patience, guidance, and encouragement, I could not have achieved so much in these years, such as winning the scholarship of the chemical industry, publishing two manuscripts in high-ranking journals, and being selected for McKinsey Workshops and so on. As a mentor of life, he gave me numerous valuable tips of social skills, broadened my horizon, and most important, taught me how to face and overcome failures. I appreciate his efforts and support from the depths of my heart.

Prof. Dr. Seema Agarwal is always very supportive of my thesis. I appreciate her patience and high efficiency while proofreading my manuscripts. She helped me to improve my presentation skills and develop a logic way of thinking. Not only her encouragement cheered me up, but also, her inspiration motivated me keeping optimizing my work. I am very impressed by her dedication to science and tender care for her students and the whole MC II group.

My sincere thanks go to **Dr. Moritz Tebbe** and **Prof. Dr. Andreas Fery** for their contribution concerning the gold nanorods and proofreading of the manuscript. Moritz offered me a large amount of gold nanorods for trial and error and shared his knowledge of nanoparticle preparation. I enjoyed working with him.

Many people have involved in the cage project. Here, I would like to thank **Dr. Holger Schmalz** for the scientific discussion and proofreading, **Dr. Melissa Köhn Serrano** for providing the block copolymer, **Dr. Xuelian Chen**, **Dr. Sabine Rosenfeldt** and **Prof. Dr. Stephan Förster** for SAXS measurements and scientific discussion, and **Matthias Burgard** for translating the manuscript into German. Without their contribution and team-working, this project could never have achieved this high level.

I would like to thank all the colleagues of MC II for their inspiring discussions and enjoyment during and after work. In particular, I want to thank former laboratory colleagues, Dr. Holger Pletsch, Dr. Melissa Köhn Serrano, and Dr. Peter Ohlendorf, for their intensive scientific

7. Acknowledgement

discussion and knowledge exchange of nanoparticle related topics. **Markus Langer**, **Dr. Shaohua Jiang**, **Gaigai Duan** and **Dr. Roland Dersch** assisted me with the SEM measurements and electrospinning. Besides, I have had a lot of fun working with **Tobias Moss** on the topic of catalysis pump and with **Steffen Reich** on the project of the spray dryer. I also would like to thank **Judith Sschöbel** for MALDI-TOF measurements and **Bianca Uch** for GPC. Moreover, our secretary **Gaby Rösner-Oliver** helped me with all the complex administrative work, which I very much appreciate. Thanks also go to **Dr. Markus Drechsler**, **Carmen Kunert**, and **Dr. Marina Krekhova** for solving TEM-related problems.

I could not have accomplished this thesis without the financial support from **Fonds der Chemischen Industrie**. My particular thanks go to **Elite Network of Bavarian** (ENB) for providing a series highly interest soft-skill workshops and scientific programs, which enriched my life experiences outside the lab. At this point, I would like to thank **Prof. Dr. Hans-Werner Schmidt** for not only enrolling me as a member of ENB but also for the recommendation for the internship in BASF Shanghai.

Without my friends and family, my life would never be so colorful. Here, I would like to give many thanks to **Sara City**. She is not only a dance teacher for me. Her energy, strength and gratefulness helped me form a positive attitude towards frustration. Also my friends, **Oxana**, **Ana**, **Sonia**, bring me laughter and make my days even brighter.

I am thankful for the trust and unconditional support of **my mother and father**. Although they are far away in China, they never care less about me. When I was down, they shared my sorrow and did everything they could. No one was happier than them when I shared my success.

At last, I want to give my thanks to my husband **Wei and his family**. Without his understanding, patience, and kindness, I would never have gone this far. I am very grateful that I met him, went through a lot of toughness together and finally built a family. I appreciate his support and responsibility through all these years very much.

8. Eidesstattliche Erklärung

(§ 8 S. 2 Nr. 6 PromO)

Hiermit erkläre ich mich einverstanden, dass die elektronische Fassung der Dissertation unter Wahrung meiner Urheberrechte und des Datenschutzes einer gesonderten Überprüfung hinsichtlich der eigenständigen Anfertigung meiner Dissertation unterzogen werden kann.

(§ 8 S. 2 Nr. 8 PromO)

Hiermit erkläre ich eidesstattlich, dass ich diese Dissertation selbständig verfasst und keine anderen als die von mir angegebenen Quellen und Hilfsmittel benutzt habe.

(§ 8 S. 2 Nr. 9 PromO)

Ich habe die Dissertation nicht bereits zur Erlangung eines akademischen Grades anderweitig eingereicht und habe auch nicht bereits diese oder eine gleichartige Doktorprüfung endgültig nicht bestanden.

(§ 8 S. 2 Nr. 10 PromO)

Hiermit erkläre ich, dass ich keine Hilfe von gewerblichen Promotionsberatern bzw. –vermittlern in Anspruch genommen habe und auch künftig nicht nehmen werde.

.....

(Ort, Datum, Unterschrift)